GAE/MC/75-4

(1)

A034877

(6) THERMAL STRESSES AS A LASER HEATING DAMAGE MECHANISM

(9) Master's thesis

THESIS

(14) GAE/MC/75-4

(19) Jan N. Garrison

(11) Nov 76

(12) 159 p.

Approved for public release; distribution unlimited

GAE/MC/7! -4

THERMAL STRESSES AS A LASER HEATING DAMAGE MECHANISM

THESIS

Presented to the Faculty of the School of Engineering
of the Air Force Institute of Technology
Air University
in Partial Fulfillment of the
Requirements for the Degree of
Master of Science

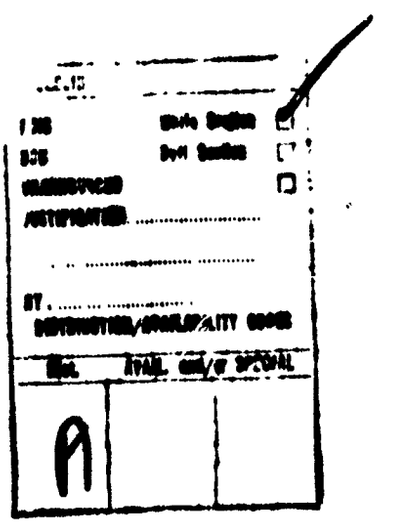

by

Jan N. Garrison, B.S.

Graduate Aerospace Engineering

1976

Approved for public release; distribution unlimited

Preface

I wish to acknowledge my deep appreciation to my thesis advisor, Dr. Peter J. Torvik, for his contributions to the accomplishment of this investigation. Especially appreciated is his understanding and patience in addition to his scientific and academic guidance throughout the study. I am particularly grateful for his guidance to me in studying the necessary fundamental subjects of heat conduction and thermoelasticity. My gratitude is also extended to Major Gil Camburn for his technical advice and assistance based on his practical experience in the area of laser heating effects on metal targets. A special acknowledgment is extended to Mr. Gordon Negaard for the extensive time and effort he contributed toward getting the transient thermal analysis portion of the NASTRAN (NASA Structural Analysis) finite element computer program operational.

A very special thanks goes to my family for their understanding, patience and sacrifices, and especially to my wife for her contributions to the preparation of this thesis.

Jan N. Garrison

Contents

List of Figures

List of Symbols

Symbol	Mnemonic	Definition	Typical Units
a	RFAIL or RMELT	radius of hole or failed area	cm
a_1		radius of heated disk	cm
b	B	radius of target plate	cm
c, c_p, C_p	CP	specific heat	joule/gm-°C
D	D	laser beam diameter	cm
E	E	modulus of elasticity	n/cm^2
F_{co}	COMPYLD	room temperature compressive yield strength	n/cm^2
F_{cy}	COMPLYD1	elevated temperature compressive yield strength	n/cm^2
F_{pa}	FLNCPK	peak absorbed fluence	$joules/cm^2$
F_{so}	ULTSHR	room temperature ultimate shear strength	n/cm^2
F_{su}	ULTSHR1	elevated temperature ultimate shear strength	n/cm^2
F_{to}	ULTENS	room temperature ultimate tensile strength	n/cm^2
F_{tu}	ULTEN1	elevated temperature ultimate tensile strength	n/cm^2
h		plate thickness	cm
I(r)		local absorbed heat flux density at radius, r	$joules/cm^2$-sec
$I_{pa}=\phi_0$	PKABSI	peak absorbed heat flux density	$joules/cm^2$-sec
k	COND1	thermal conductivity	joules/sec-cm-°C
ℓ	EL	plate thickness	cm

Symbol	Mnemonic	Definition	Typical Units
L_m	HFUSE	heat of fusion	joules/gm
P_a	PA	absorbed power	joules/sec
P_i	Q,QBEAM	incident power	joules/sec
$P_{\ell a}$	PLA	dimensionless power per unit thickness	(dimensionless)
r	R	radial coordinate	cm
Δr	DELR	numerical element radial width	cm
t	TIME	time	sec
Δt	DELT	computational time interval	sec
t_i	TI	melting time for one-dimensional axial heat flux	sec
t_D		time for complete thermal degradation	sec
T	TEMP	temperature (referenced to room temperature or stress free state)	°C
T_1		heated disk temperature	°C
T_D		complete thermal degradation temperature	°C
T_o	TI	reference temperature	°C
$T_m=T_\ell$	TMELT	lower melting temperature	°C
T_u	TUMELT	upper melting temperature	°C
x,y,z		cartesian coordinates	
r,θ,z		cylindrical coordinates	
α	ALPHAT	coefficient of thermal expansion	/°C

Symbol	Mnemonic	Definition	Typical Units
α_1	ALPHA1	material absorptivity	(dimensionless)
κ	CAPPA	thermal diffusivity	cm^2/sec
π	PI	geometric constant	(dimensionless)
ρ	RHO1	material density	gm/cm^3
σ_{rr}	SIGMAR(I)	radial stress component	n/cm^2
$\sigma_{\theta\theta}$	SIGMAA(I)	tangential stress component	n/cm^2
τ_{max}	TAUMAX(I)	maximum shear stress	n/cm^2
$\phi_0=I_{pa}$		peak absorbed heat flux density	$joules/cm^2$-sec

Abstract

The relative significance of thermal stresses as a laser heating damage mechanism is assessed by comparison with the damage mechanisms of melting and thermal degradation of structural strength properties. The limiting cases of one-dimensional axial and one-dimensional radial heat flux in a thin target plate whose plane is normal to the axis of a stationary, axially symmetric heat source, are investigated. A one-dimensional radial heat conduction numerical model of the linear thermoelastic stress field including the effects of melting and structural failure is developed. Residual tensile strength and damage size are presented as functions of the laser beam and target plate parameters.

THERMAL STRESSES AS A LASER HEATING DAMAGE MECHANISM

I. Introduction

The advent of the laser with its inherent potential capability of depositing very high intensity energy on a target has generated interest in possible applications of laser energy to cause structural damage to a target. This thesis presents the results of a study to assess the significance of laser induced thermal stresses as a damage mechanism in a metal target by comparison with the damage mechanisms of melting and thermal degradation of structural properties.

Statement of the Problem

The objective of this study is to determine whether thermal stresses are an efficient mechanism for causing structural damage to metal targets relative to the other laser heating induced damage sources of melting and thermal degradation of structural properties. The study is analytical and based primarily on the application of theoretical heat conduction and linear elasticity. A major goal is to develop analysis procedures which are relatively simple to apply (i.e., which do not require the use of large, expen-

sive to apply, computer programs) so that the procedures may be used to obtain rapid estimates of laser heating induced thermal stress fields under varying conditions.

Significance of the Problem

Most of the studies of laser heating damage conducted thus far have been experimental and concerned with target melting and/or material property degradation (Ref 12-18, 25, 30, 31). No known unclassified studies have been made to determine quantitatively the relative importance of thermal stresses as a source of damaging target materials. Thermal stresses are of interest because of the possibility that significant structural damage can be induced for lower laser beam power or peak intensities than for the other two damage sources under consideration. A need exists for an analytical procedure to rapidly assess the relative severity of damage to be induced by thermal stresses, melting, and thermal degradation in metal targets as functions of laser and target parameters. Experiments to obtain similar data, particularly concerning thermal stresses, can be expected to provide only minimal data in the near future because of the cost and time required to conduct sufficient tests over the wide range of parameters of interest, and due to the difficulty in adequately instrumenting numerous target specimens to obtain accurate thermal stress data. An analytical model thus could serve to provide such information in lieu of experiments and as a guide to planning efficient experiments in the future.

Physics of Heating Metals by Laser Radiation

The following description of the physical process by which laser light radiation is converted to heat energy in a metal target is adapted from Ref 1:2-7. When a laser beam is directed at a metal target, only a fraction of the initial beam energy is absorbed by the metal. A portion of the initial energy which is in the form of phctons may be attenuated by the intervening medium, usually air. A large fraction of the phctons incident on the metal target may be reflected. For the problem of interest, the assumptions are made that the photons absorbed by the metal are converted to heat essentially instantaneously and within a very thin layer (relative to the target thickness) at the surface of the metal. These assumptions have been shown to be valid for aircraft structural metals (aluminum, steel, titanium, magnesium) irradiated by continuous wave lasers (Ref 1:3-5).

Following the conversion of the light energy to thermal energy, heat is transferred from the metal surface by four mechanisms. The only one of these mechanisms to be considered in the present study is that of heat conduction within the metal. The three mechanisms being neglected here are radiation from the metal surface, convection in the adjacent medium, and removal by gravity or airflow of any melted (liquid) portion of the metal. Only the latter mechanism (melt removal) affects a comparison of the relative significance of the damage modes of interest. The efficiency of the melting mechanism obviously is dependent on the behavior

of the melt at the metal surface. For this study, the assumption is made that any melt formed is removed instantaneously by an unspecified mechanism so that the most efficient mode of the melting mechanism is considered. Studies of melt removal are contained in References 1, 22, 23, 25, 31.

Scope of Study

Limiting cases of laser heating induced damage were studied by considering the limiting heat conduction cases of one-dimensional axial (through-the-thickness) and one-dimensional radial conduction. The study is theoretical, based on the quasi-static, uncoupled thermoelasticity theory. The problem is that of a finite, stationary heat source normally incident at the center of a large, thin plate. The plate material is assumed to be a homogeneous, isotropic, linearly elastic material. The plate material properties are assumed to be temperature independent with the exception of the strength properties. Heat losses to all sources are neglected.

For the axial heat conduction problem, analytical solutions are applied to obtain temperature distributions for input to the thermal stress problem. Numerical integration of the thermoelasticity equations is used to obtain the thermal stress distributions. For the radial heat conduction case, a numerical model of the heat flux based on the Fourier heat conduction equation is applied.

Melting and thermal degradation of the plate material

structural properties are modeled for comparison with thermal stresses as damage mechanisms. Damage due to the combined effects of these mechanisms is also considered. Measures of plate damage used are residual tensile strength and material failure.

II. Outline of Study

The primary objective of this effort was to determine the relative efficiency of thermal stresses as a damage mechanism due to heating a target material with a stationary continuous wave (CW) laser beam. The problem basically consists of applying the concepts of both heat transfer and thermoelasticity. In the basic theory for describing, mathematically, the behavior of elastic, isotropic solid media under the combined action of heating and external loading, the problem is one of a coupled thermal/mechanical boundary value problem (Ref 5:3). For most applications, useful solutions to the problem require that certain simplifications be made to the coupled theory. The usual simplifications result in eliminating the thermal/mechanical coupling and inertia terms. Elimination of the coupling between mechanical and thermal effects enables the thermodynamic and mechanical parts of the problem to be analyzed separately. If the inertia effects are negligible, the mechanical part of the problem reduces to one of static thermoelasticity.

The subject study began with an investigation to determine a suitable form of the thermal/mechanical theory for the present application, as discussed in Section III. Solutions to the thermal and mechanical equations were then investigated to describe the heat transfer and thermal

stress fields for the specific problem at hand, laser beam heating of thin plates. The models thus developed are discussed in Sections IV and V. Section VI describes the models used to characterize the melting and thermal degradation mechanisms for comparisons with the thermal stress damage source. Section VII contains the analysis of the damage mechanisms, input parameter sensitivity and relative efficiencies based on the one-dimensional axial and radial heat conduction models. Study results and conclusions are presented in Section VIII.

Appendix A is a listing of the one-dimensional radial flux numerical model developed as part of the study. A sample output listing is given following the program listing. Appendix B describes the algorithms used in the radial flux numerical code. Appendix C presents the analysis conducted to validate the radial flux code.

The damage effects of laser heating were determined for the ranges of laser beam and target parameters listed below.

1. Absorbed laser beam powers up to about 30,000 joules/sec
2. Laser beam diameters between 5 and 15 cm.
3. Target plate thicknesses of 0.1 to 0.65 cm.
4. Large plate diameters relative to beam diameter

A single target material was considered, 2024-T3 aluminum, with a constant absorptivity of 0.5. The target plate was assumed to be heated in the absence of external mechanical loading.

III. Theory Development

This background discussion of the fundamental mathematical theory for the behavior of a homogeneous, isotropic, elastic solid under the combined action of heat and external loading is adapted from Ref 5. This behavior is uniquely described by the following four equations together with proper initial and boundary conditions:

$$kT_{,ii} = \rho c_E \dot{T} + (3\lambda+2\mu)\alpha T_o \dot{\varepsilon}_{kk} \tag{1}$$

$$\sigma_{ij,j} = \rho \ddot{u}_i \tag{2}$$

$$\varepsilon_{ij} = \tfrac{1}{2}(u_{i,j}+u_{j,i}) \tag{3}$$

$$\sigma_{ij} = \lambda\delta_{ij}\varepsilon_{kk} + 2\mu\varepsilon_{ij} - (3\lambda+2\mu)\alpha\delta_{ij}(T-T_o) \tag{4}$$

where

k = thermal conductivity

T = temperature (absolute)

T_o = reference temperature (absolute) at which material is stress free

ρ = material density

c_E = specific heat at constant deformation

λ = Lame constant = $\dfrac{\nu E}{(1+\nu)(1-2\nu)}$

μ = Lame constant = G

ν = Poisson's ratio

E = Young's modulus

G = shear modulus

ε = linear strain

σ = stress

u = displacement

α = coefficient of thermal expansion

δ_{ij} = Kronecker delta $\begin{cases} = 1 \text{ if } i=j \\ = 0 \text{ if } i \neq j \end{cases}$

Indicial notation (Ref 7:24-27) is used here for brevity, however familiarity with this notation is not necessary for understanding the material which follows. A brief outline of the notation is given here to clarify the subsequent discussion.

Subscript indices are used to refer to the three rectangular cartesian coordinate axes. The range of each index is therefore three. For example, the three coordinate axes x_1, x_2, x_3 can be expressed as x_i where i takes on the values 1,2,3. An indicial equation with a single index on each term then represents three equations. A summation convention is employed where repeated indices in a term imply summation over the range of the repeated index. A comma between indices denotes partial differentiation with respect to one of the coordinates, i.e.

$$f_{i,j} = \frac{\partial f_i}{\partial x_j} \tag{5}$$

Returning to the subject equations, the first equation is the energy equation for the linear thermoelastic theory. Equation (2) represents the equations of motion which reduce to the static equilibrium equations of elasticity theory

when the inertia term, $\rho\ddot{u}_i$, is zero. Equation (3) is the strain-displacement relationship and equation (4) is the stress-strain or constitutive equation for an isotropic solid.

The boundary value problem governed by these equations is very difficult to solve in general (Ref 5:41). For most engineering applications, two simplifying assumptions are made which reduce the problem to one in which the heat conduction and thermoelasticity equations are not coupled. This allows the two separate problems to be solved independently. The two simplifications are that the thermal/mechanical coupling defined by equation (1) and the inertia term ($\rho\ddot{u}_i$) in equation (2) may be neglected. Using the terminology in Ref 5, the basic theory represented by equations (1) through (4) is called the coupled theory; neglecting the strain rate term ($\dot{\varepsilon}_{kk}$) in equation (1) results in the uncoupled theory; and neglecting both the strain rate and inertia terms produces the uncoupled quasi-static theory. Whether either or both of these simplifications are appropriate to the present study is the subject of the remaining discussion in this section.

A review of the mathematical problem quickly led to the conclusion that only the uncoupled quasi-static theory presented reasonable expectation for a successful application to the subject problem within the temporal constraints existing. Hence, the studies described herein are based on that theory. However, the implications on the results of

neglecting the inertia effects may be significant. It is shown in (Ref 5:43) that for most metals (and particularly for aluminum which is of prime interest for this study) the mechanical coupling term (strain rate term, $\dot{\varepsilon}_{kk}$) in equation (1) is negligible if

$$\frac{\dot{\varepsilon}_{kk}}{\alpha \dot{T}} << 60 \qquad (6)$$

An intuitive argument is used to indicate that the strain rate should be of the same order of magnitude as the time rate of change of the temperature if there are no sharp variations in the temperature time histories. Since the strain rates are related directly to displacement time histories, the question of whether mechanical coupling is negligible is related to the magnitude of the inertia effects.

It is further concluded (Ref 5:50) that the mechanical coupling and inertia terms are negligible if the rate of heat application is not too great. Quantitative limits on the application of the uncoupled, quasi-static theory must be determined for each problem of interest. Based on a review of example analyses (Ref 5:339, 406) it was decided that such an analysis was beyond the scope of the present study. However, it is probable that for at least the higher heating rates and shorter times of interest in the present study, the use of the uncoupled quasi-static theory is questionable and should be the subject of a subsequent study of laser beam generated thermal stresses.

IV. Thermal Models

The basic situation to be modeled is that of a stationary laser beam normally incident on a flat plate. The incident beam is considered to be axially symmetric so that only heat flux in the axial and radial directions occurs. That is, the heat flux is assumed to be two-dimensional in cylindrical coordinates with no heat transfer in the circumferential direction. The effects of the medium between the laser beam source and the plate are not included as these effects do not contribute to the physical processes of interest for this study. The concern of this study beoins with the incidence of the beam energy on the plate surface.

Attempts were made to obtain a closed form solution to the problem without success. Various approximate solutions are given in Ref 4, some of which are discussed and applied in this study. Other approximate solutions and methods (Ref 26-29) were reviewed but all involve computational difficulties or complexities which are contrary to the objective of obtaining solutions that are relatively simple to apply.

To present readily tractable problems for the subsequent stress analyses, the heat transfer problem was restricted to modeling the two limiting cases of axial and radial flux separately. A one-dimensional axial flux model was developed for application to cases of relatively short heating times

and/or thick plates. The other limiting case associated with long heating times and thin plates is thermally modeled by a one-dimensional numerical radial heat flux model. As discussed in Section VII, quantitative definitions of these bounding conditions were to be obtained from NASTRAN (NASA Structural Analysis), (Ref 2) a large finite element program developed by the National Aeronautics and Space Administration (NASA). This goal was not achieved completely because of the fairly excessive amount of time required to run all of the cases necessary to determine the combinations of heating rates, heating times and plate thicknesses which could be modeled accurately by either an axial or radial flux model.

The effects of heat losses from the heated plate, regardless of the mechanism, also have been neglected in the present study in that they are not expected to have sufficient impact on the results to justify the additional complexity of including realistic radiation and convection loss conditions.

Incident Flux Models

In general, the spatial distribution of the incident beam is represented as a Gaussian distribution which is generally accepted as being representative in analytical studies of laser heating effects (Ref 3:13, 75). A uniformly distributed beam was considered in the axial flux cases to simplify the stress analysis. For the Gaussian beam the

heat flux density absorbed at the plate surface is given by

$$I(r) = I_{pa} e^{-r^2/2\sigma^2} \tag{7}$$

where I_{pa} is the peak absorbed flux density at the beam axis, r is the radial distance from the beam axis and σ is the standard deviation. It is convenient to define the beam radius as

$$a = 2\sigma \tag{8}$$

Therefore, the flux density becomes

$$I(r) = I_{pa} e^{-2r^2/a^2} \tag{9}$$

where for a Gaussian distribution 86.5% of the beam energy is contained within the beam diameter(2a). The total absorbed power under a Gaussian beam is given by

$$P_a = 2\pi I_{pa} \int_0^\infty re^{-r^2/2\sigma^2} dr \tag{10}$$

$$P_a = 2\pi I_{pa}\sigma^2 \tag{11}$$

$$I_{pa} = \frac{2P_a}{\pi a^2} \tag{12}$$

The portion of the incident beam power (P_i) which is absorbed at the plate surface is given by the absorptivity

$$\alpha_1 = \frac{P_a}{P_i} \tag{13}$$

Hence,

$$I_{pa} = \frac{2\alpha_1 P_i}{\pi a^2} \tag{14}$$

and

$$I(r) = \frac{2\alpha_1 P_i}{\pi a^2} e^{-2r^2/a^2} \tag{15}$$

Heat Conduction Models

The purpose of the heat conduction models is to determine temperature distributions to which thermal stress, melting, and thermal degradation models may be applied. Analytical models for various classes of axial heat flux conditions were investigated and a numerical finite thermal element model was applied for the radial flux case.

Axial Heat Flux Models. Analytical temperature distribution models are presented as solutions to the differential equation of heat conduction in an isotropic solid (Ref 4:10):

$$\rho c \frac{\partial T}{\partial t} = \frac{\partial}{\partial x}\left(k\frac{\partial T}{\partial x}\right) + \frac{\partial}{\partial y}\left(k\frac{\partial T}{\partial y}\right) + \frac{\partial}{\partial z}\left(k\frac{\partial T}{\partial z}\right) + q \tag{16}$$

where

ρ = material density

c = specific heat

T = temperature

t = time

k = thermal conductivity

q = rate of heat gain per unit volume

For homogeneous solids such that thermal conductivity does not vary with position, the heat conduction equation reduces to

$$\kappa \nabla^2 T + \frac{q}{\rho c} = \frac{\partial T}{\partial t} \tag{17}$$

where

$\kappa = k/\rho c$ = thermal diffusivity

∇ = Laplacian operator

$$\nabla^2 T = \frac{\partial^2 T}{\partial x^2} + \frac{\partial^2 T}{\partial y^2} + \frac{\partial^2 T}{\partial z^2} \tag{18}$$

Isotropic, homogeneous solids were the only type considered in this study. An additional restriction applied throughout the heat transfer analyses is that the material heat transfer properties are not functions of temperature. The justification for this restriction is that the complexities introduced into the analyses by including variable thermal properties were not believed to be necessary for this initial study.

Closed form analytical solutions for several one-dimensional axial heat flux cases were reviewed for possible application. For the case of a semi-infinite solid with uniform flux into one surface and insulated on the opposite surface, as shown in the following sketch, the temperature distribution is given by (Ref 4:112)

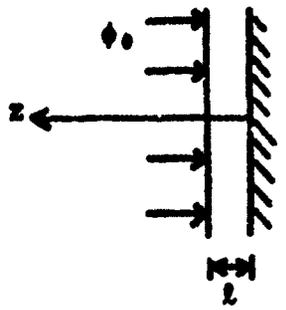

$$T(z,t) = T_o + \frac{\phi_0 t}{\rho c \ell} + \frac{\phi_0 (3z^2 - \ell^2)}{6k\ell}$$

$$- \frac{2\phi_0 \ell}{k\pi^2} \sum_{n=1}^{\infty} \frac{(-1)^n}{n^2} \cos\left(\frac{n\pi z}{\ell}\right) e^{-\kappa t n^2 \pi^2/\ell^2} \qquad (19)$$

where

ϕ_0 = absorbed heat flux density

T_o = initial uniform temperature throughout slab

For thermally thin plates or long enough heating times such that $\kappa t/\ell^2 > 1$, the series term becomes negligibly small and the thermal model reduces to

$$T(z,t) - T_o = \frac{\phi_0}{6k\ell}(6\kappa t + 3z^2 - \ell^2) \qquad (20)$$

Applications of these models to the general problem of laser heating of solid plates is discussed in Section VII.

Radial Heat Flux Model. For relatively low heating rates and thin target plates the heat flux might be expected to become essentially radial after some initial period in which the flux is primarily axial and the plate volume under

the beam becomes heated to an essentially uniform temperature through-the-thickness. One-dimensional radial flux develops a plane stress state which is particularly amenable to analysis, as discussed in Section V. For this case, a numerical finite thermal element model was developed. The numerical model also allows the Gaussian beam profile to be considered. Figure 1 is a schematic illustration of the numerical model which is obtained by dividing the plate into concentric cylindrical elements.

The numerical model is used to solve the Fourier heat conduction equation for each element:

$$q_c = -k\frac{\partial T}{\partial r} \tag{21}$$

where

q_c = rate of heat flux per unit area

Heat is transferred between any two points in a solid body only by conduction and equation (21) is the law of heat conduction for isotropic bodies (Ref 5:137). A finite difference version of equation (21) is applied to the heat flow between adjacent concentric elements as indicated in the following sketch:

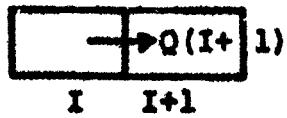

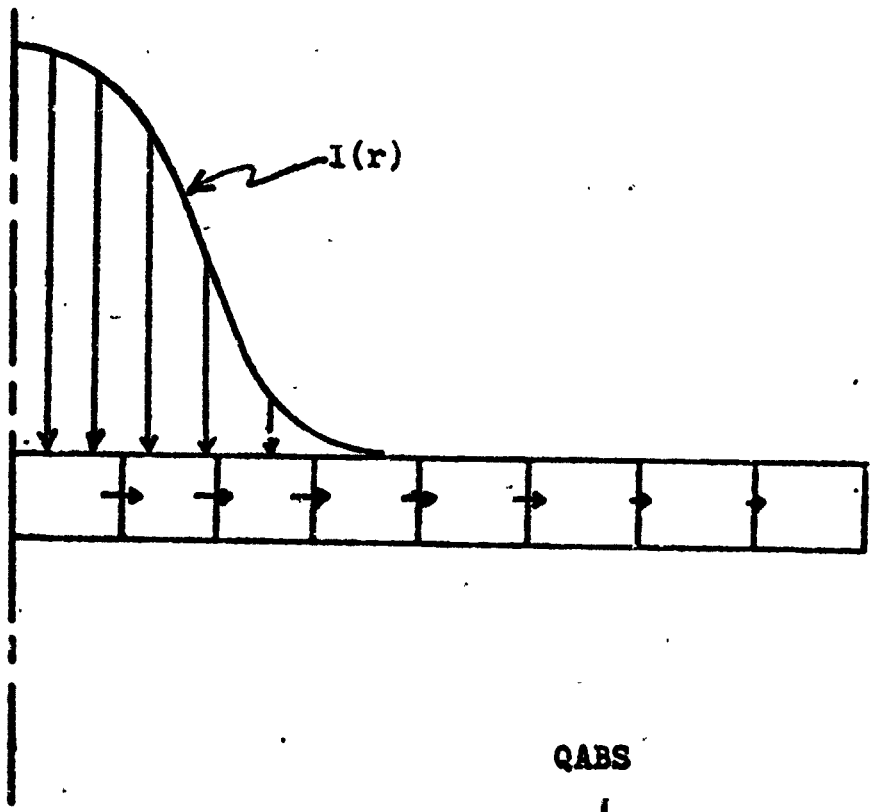

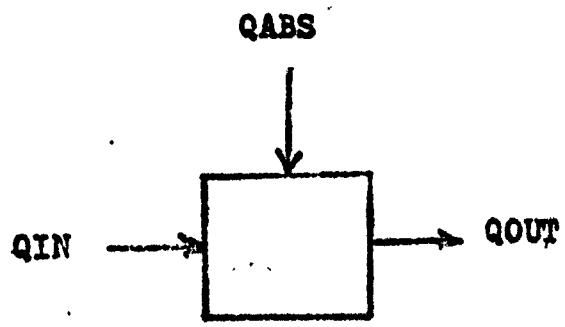

Fig. 1 One-Dimensional Radial Heat Flux Numerical Model

where $Q = q_c A$ = total flux into element (I + 1)

Hence, applying equation (21) at the interface between two elements

$$\frac{Q(I+1)}{A(I+1)} = \left[\frac{k(I+1) + k(I)}{2}\right] [T(I) - T(I+1)] \Big/ \left[\frac{\Delta r(I+1) + \Delta r(I)}{2}\right] \quad (22)$$

where

$$A(I+1) = 2\pi R\ell$$

R = inner radius of element (I + 1)

ℓ = plate thickness

The conductivity and incremental radius terms in brackets represent averages of the respective quantities taken between the two elements.

For the present study, the concentric cylinders all have the same width (Δr = constant) and the thermal conductivity is assumed to be independent of position and temperature. Thus equation (22) reduces to

$$Q(I+1) = k[T(I) - T(I+1)]2\pi R\ell/\Delta r \quad (23)$$

or, in FORTRAN code

```
QIN(I + 1) = COND*(TEMP(I)
   -TEMP(I + 1))*2*PI*R*EL/DELR        (24)
```

The temperature of each element is determined by itera-

tion over small time increments of an energy balance equation for each element, as indicated in the following sketch.

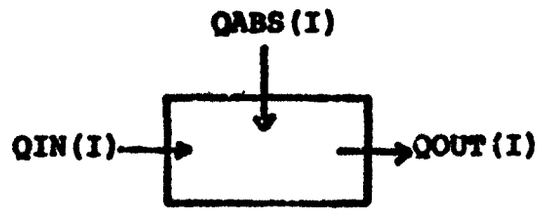

where

QABS(I) = heat energy absorbed into element (I) per unit time

QOUT(I) = QIN(I + 1)

Hence, the net increase in heat energy per unit time is

$$QABS(I) + QIN(I) - QIN(I + 1)$$

This increase in heat energy results in a corresponding increase in the internal heat energy of the element. Assuming constant density and specific heat, the incremental increase in internal heat energy per unit volume is given by $\rho c\frac{\Delta T}{\Delta t}$. Hence, the energy balance gives

$$QABS(I) + QIN(I) - QIN(I + 1) = RHO*CP*VOL*DELTEMP(I)/DELT \quad (25)$$

where

RHO = ρ = density

CP = c = specific heat

DELTEMP(I) = ΔT = change of temperature in time increment Δt

DELT = Δt = time increment

VOL = volume of element (I) = PI*EL*(2*I - 1)*DELR**2

DELTEMP is the incremental temperature change in element (I). This may be expressed as

$$DELTEMP(I) = TEMP(I)_2 - TEMP(I)_1 \qquad (26)$$

where

$TEMP(I)_2$ = current temperature of element (I)

$TEMP(I)_1$ = previous temperature of element (I)

Hence, equation (25) may be solved for the current temperature:

$$TEMP(I)_2 = TEMP(I)_1 + DELT*(QIN(I) + QABS(I) - QIN(I + 1))/(CP*RHO*PI*EL*(2*I - 1)*DELR**2) \qquad (27)$$

Equations (24) and (27) are solved for each thermal element at each time increment to give the radial flux temperature distribution. This model is Subroutine TEMPRAD in the TSTRESS program listed in Appendix A.

To maintain heat flow stability in such a numerical, incremental time model, the time increment must be kept below a certain limit. If the time increment becomes large enough, sufficient heat would flow between adjacent elements to cause the temperature of the initially cooler element to

become larger than the initially hotter element causing the heat flow to become reversed. To maintain heat flow stability the computational time increment for the one-dimensional radial flux model must be restricted to (Ref 6:12)

$$\Delta t \leq \frac{\Delta r^2}{2\kappa} \tag{28}$$

As a check and to be slightly conservative, the TSTRESS code limits the time increment to ninety percent of the value defined in eqn (28).

V. Thermal Stress Models

In the uncoupled quasi-static theory the thermal stress problem is solved in sequence after the heat conduction problem is solved for the temperature distributions. The thermal stress problem is uniquely defined by the static thermoelasticity equations

$$\sigma_{ij,j} = 0 \tag{29}$$

$$\epsilon_{ij} = 1/2(u_{i,j} + u_{j,i}) \tag{30}$$

$$\sigma_{ij} = \lambda\delta_{ij}\epsilon_{kk} + 2\mu\epsilon_{ij} - (3\lambda + 2\mu)\alpha\delta_{ij}(T - T_o) \tag{31}$$

along with proper boundary conditions. For the case when the heat flow in the plate is primarily axial (i.e. through-the-thickness), the only portion of the plate being heated significantly is that directly under the beam. For a uniformly distributed beam the temperature variation will be through-the-thickness only. Near the beam axis the thermal stress field can be approximated by that for a semi-infinite plate of thickness 2h:

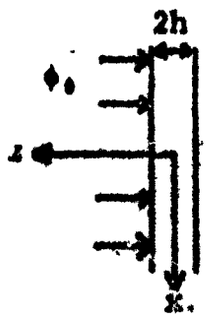

Since there are no surface tractions on the edges of the plate and the temperature is a function of z only, and due to axial symmetry, it is expected that

$$\sigma_{xx} = \sigma_{yy} = f(z) \tag{32}$$

at any time. Since the temperature is uniform in the x - y plane, no shear stresses are generated:

$$\sigma_{xz} = \sigma_{yx} = \sigma_{zy} = 0 \tag{33}$$

Also since no constraints on expansion in the z - direction exist,

$$\sigma_{zz} = 0 \tag{34}$$

All of the boundary conditions are seen to be in terms of stresses only. For thermoelasticity problems of this type, the solution is facilitated by reformulating the thermoelasticity equations in terms of stresses alone. That is, the displacements and strains are eliminated. This is done through the use of the strain compatibility equations (Ref 7: 124) which are mathematical constraints that insure the integrability of equations (30) to obtain the displacements.

In the stress formulation of the problem, the equilibrium equations (29) are unchanged, but stress-strain equations (31) and the strain-compatibility equations are re-

placed by the so-called stress compatibility equations (Ref 5:89):

$$(1 + \nu)\sigma_{ij,kk} + \sigma_{kk,ij} + \alpha E\left[\delta_{ij}\left(\frac{1+\nu}{1-\nu}\right)T_{,kk} + T_{,ij}\right] = 0 \qquad (35)$$

For the present problem, the equilibrium equations (29) are identically satisfied and equations (35) are satisfied if

$$\frac{d^2}{dz^2}\left[\sigma_{xx} + \left(\frac{\alpha E}{1-\nu}\right)T\right] = 0 \qquad (36)$$

Integration of (36) yields

$$\sigma_{xx} = -\left(\frac{\alpha E}{1-\nu}\right)T + c_1 + c_2 z \qquad (37)$$

where it is recalled that $T = T(z,t) - T_o$. To obtain a non-trivial solution, Saint Venant's principle (Ref 5:270) may be applied. That is, the requirement for zero surface tractions at the edges of the plate is replaced by the statically equivalent requirement that the net force and moment produced by some σ_{xx} distribution on the edge be zero. These boundary conditions expressed for net force and moment per unit length of the plate edge become, respectively

$$\int_{-h}^{h} \sigma_{xx} dz = 0 \qquad (38)$$

and

$$\int_{-h}^{h} \sigma_{xx} z dz = 0 \tag{39}$$

Substituting (37) into (38) and (39) gives

$$c_1 = \frac{3}{2h^3}\left(\frac{\alpha E}{1-\nu}\right)\int_{-h}^{h} Tz dz \tag{40}$$

and

$$c_2 = \frac{1}{2h}\left(\frac{\alpha E}{1-\nu}\right)\int_{-h}^{h} T dz \tag{41}$$

Hence, from equation (37)

$$\sigma_{xx} = \sigma_{yy} = \frac{\alpha E}{1-\nu}\left[-T + \frac{1}{2h}\int_{-h}^{h} T dz + \frac{3z}{2h^3}\int_{-h}^{h} Tz dz\right] \tag{42}$$

The application of equation (42) to the present study along with suitable thermal models is discussed in Section VII. This result is given in (Ref 5:278).

The other thermal stress models of interest are associated with conditions when the temperature distributions in the heated plate are primarily radial only, i.e. constant through-the-thickness. For a thin cylindrical plate with with diameter >> thickness and no surface tractions, the problem is one of plane stress such that the only non-zero stresses are

$$\sigma_{rr} = f_1(r) \tag{43}$$

$$\sigma_{\theta\theta} = f_2(r) \tag{44}$$

using cylindrical coordinates.

The only equilibrium equation (Ref 5:248) which is not identically zero is

$$\frac{\partial \sigma_{rr}}{\partial r} + \frac{\sigma_{rr} - \sigma_{\theta\theta}}{r} = 0 \tag{45}$$

From the stress-strain equations (Ref 5:245)

$$E\varepsilon_{rr} = \sigma_{rr} - \nu\sigma_{\theta\theta} + E\alpha T \tag{46}$$

$$E\varepsilon_{\theta\theta} = \sigma_{\theta\theta} - \nu\sigma_{rr} + E\alpha T \tag{47}$$

and from the strain-displacement equations

$$\varepsilon_{rr} = \frac{\partial u}{\partial r} \tag{48}$$

$$\varepsilon_{\theta\theta} = \frac{u}{r} \tag{49}$$

Eliminating $\sigma_{\theta\theta}$ between (46) and (47) and substituting (48) and (49) gives

$$\sigma_{rr} = \frac{E}{1 - \nu^2}\left(\frac{\partial u}{\partial r} + \nu\frac{u}{r}\right) - \frac{E\alpha T}{1 - \nu} \tag{50}$$

Similarly, eliminating σ_{rr} in (46) and (47) gives

$$\sigma_{\theta\theta} = \frac{E}{1 - \nu^2}\left[\nu\frac{\partial u}{\partial r} + \frac{u}{r} - \alpha T(1 + \nu)\right] \tag{51}$$

Substituting (50) and (51) into (45) results in

$$\frac{d}{dr}\left[\frac{1}{r}\frac{d(ru)}{dr}\right] = (1+\nu)\alpha\frac{dT}{dr} \tag{52}$$

Integrating and solving for the radial displacement

$$u = \frac{(1+\nu)\alpha}{r}\int_a^r Trdr + c_1\frac{r}{2} + \frac{c_2}{r} \tag{53}$$

Substituting back into (50) gives

$$\sigma_{rr} = \frac{E}{1-\nu^2}\left[-\frac{(1-\nu^2\alpha}{r^2}\int_a^r Trdr + (1+\nu)\frac{c_1}{2} - (1-\nu)\frac{c_2}{r^2}\right] \tag{54}$$

By substituting the boundary conditions of zero tractions ($\sigma_{rr} = 0$) on the inner (r = a) and outer (r = b) radii of the cylinder, the constants, c_1, and c_2 are determined. Hence, (Ref 5:290),

$$\sigma_{rr} = \frac{\alpha E}{r^2}\left[\frac{(r^2-a^2)}{(b^2-a^2)}\int_a^b Trdr - \int_a^r Trdr\right] \tag{55}$$

$$\sigma_{\theta\theta} = \frac{\alpha E}{r^2}\left[\frac{(r^2+a^2)}{(b^2-a^2)}\int_a^b Trdr + \int_a^r Trdr - Tr^2\right] \tag{56}$$

For the particular case of a solid plate, a = 0 and

$$\sigma_{rr} = \alpha E\left[\frac{1}{b^2}\int_0^b Trdr - \frac{1}{r^2}\int_0^r Trdr\right] \tag{57}$$

$$\sigma_{\theta\theta} = \alpha E\left[\frac{1}{b^2}\int_0^b Trdr + \frac{1}{r^2}\int_0^r Trdr - T\right] \tag{58}$$

Another particular case of interest is a solid cylin-

drical plate of which only a finite inner cylindrical portion is heated appreciably. If it is assumed that this heated core ($r = a_1$) is at a uniform temperature ($T = T_1$) with $T = 0$ for $r > a_1$, then from (57) and (58) respectively, for $r \leq a_1$,

$$\sigma_{rr_1} = \sigma_{\theta\theta_1} = \frac{\alpha E T_1}{2}\left(\frac{a_1^2}{b^2} - 1\right) \tag{59}$$

and for $r \geq a_1$,

$$\sigma_{rr_2} = \frac{\alpha E T_1 a_1^2}{2}\left(\frac{1}{b^2} - \frac{1}{r^2}\right) \tag{60}$$

$$\sigma_{\theta\theta_2} = \frac{\alpha E T_1 a_1^2}{2}\left(\frac{1}{b^2} + \frac{1}{r^2}\right) \tag{61}$$

The stresses in the heated core are seen to be compressive. The peak tensile stress occurs just outside the heated core and is

$$\sigma_{\theta\theta_2} = \frac{\alpha E T_1}{2}\left(\frac{a_1^2}{b^2} + 1\right), \quad r = a_1 \tag{62}$$

The maximum shear stress (τ_{max}) in the case of a biaxial stress field occurs on planes at ± 45 degrees to the principal stress axes and is

$$\tau_{max} = \frac{\sigma_{rr_1}}{2} \tag{63}$$

in the heated core. Outside the heated core the maximum

shear stress is given by

$$\tau_{max} = \frac{\sigma_{rr_2} - \sigma_{\theta\theta_2}}{2} = -\frac{\alpha E T_1}{2}\left(\frac{a_1}{r}\right)^2, \quad r \geq a_1 \qquad (64)$$

Applications of these thermal stress models to the laser heating problem are discussed in Section VII.

VI. Melting and Thermal Degradation Models

To assess the relative effects of thermal stresses as damage mechanisms from laser heating of metal targets, the melting and thermal degradation damage mechanisms were selected for purposes of comparison. Other damage modes such as explosive boiling, explosive vaporization, and thermoelastic shock waves (Ref 12) occur at generally higher heating rates than the mechanisms of interest in this study. Since the concern is with determining efficiencies of the damage mechanisms, only those believed to occur at the relatively lower beam powers were considered.

Melting. The analytical model used to predict melting effects follows that of (Ref 8:18). Melting is assumed to occur over a range of temperatures, T_l to T_u, where T_l is the temperature below which the material behaves as a solid and T_u is the temperature above which the material behaves as a liquid. For the present study, the melted material is assumed to be removed immediately upon reaching T_u so that the effects of melt retention are not considered.

During the phase change from solid to liquid an effective specific heat, c_{pe} is assumed such that the heat of fusion over the melting range is

$$c_{pe} = c_p + L_m/(T_u - T_l) \text{ for } T_l < T < T_u \qquad (65)$$

where

c_p = specific heat of solid phase ($T < T_1$)

L_m = heat of fusion

Once any portion of the heated target reaches the upper melting point, that portion of the target is assumed to be instantaneously removed and is no longer considered in subsequent computations. Damage due to melting is then defined by the reduction in target strength due to the reduced load carrying area.

Thermal Degradation. The definition of thermal degradation as applied in this study is the reduction in structural strength properties with increasing temperature of thin plates as described in Ref 9. Although, as discussed in Section VII, the primary measure of damage being used for this study is the residual tensile strength in a uniaxial loaded panel, the effects of thermal degradation on tensile, compressive and shear strength properties are considered.

The only material considered is 2024-T3 aluminum. Ref 9 contains data for the effects of temperature on material strength as a function of time at temperature. The particular data used here is contained in Figures 3.2.3.1.1(a)., 3.2.3.1.2(a)., and 3.2.3.1.2(b). of Ref 9 for ultimate tensile strength, compressive yield strength, and ultimate shear strength, respectively. These figures are reproduced here as Figures 2, 3, and 4.

It was decided to use the half-hour exposure data in Ref 9 after reviewing available data on the more rapid heating effects associated with high power laser heating. Such

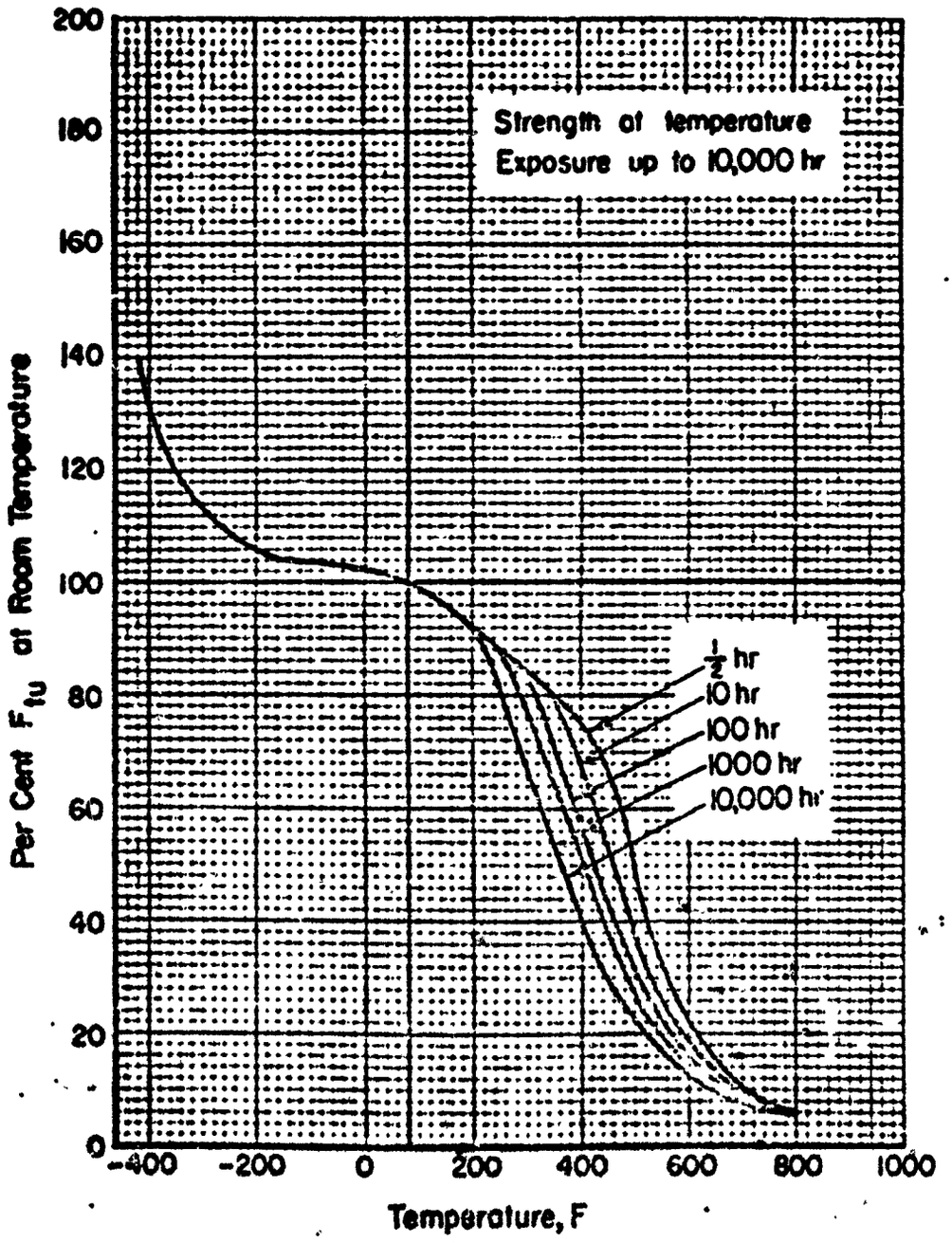

Fig. 2 Thermal Degradation of Ultimate Tensile Strength for 2024-T3 Aluminum

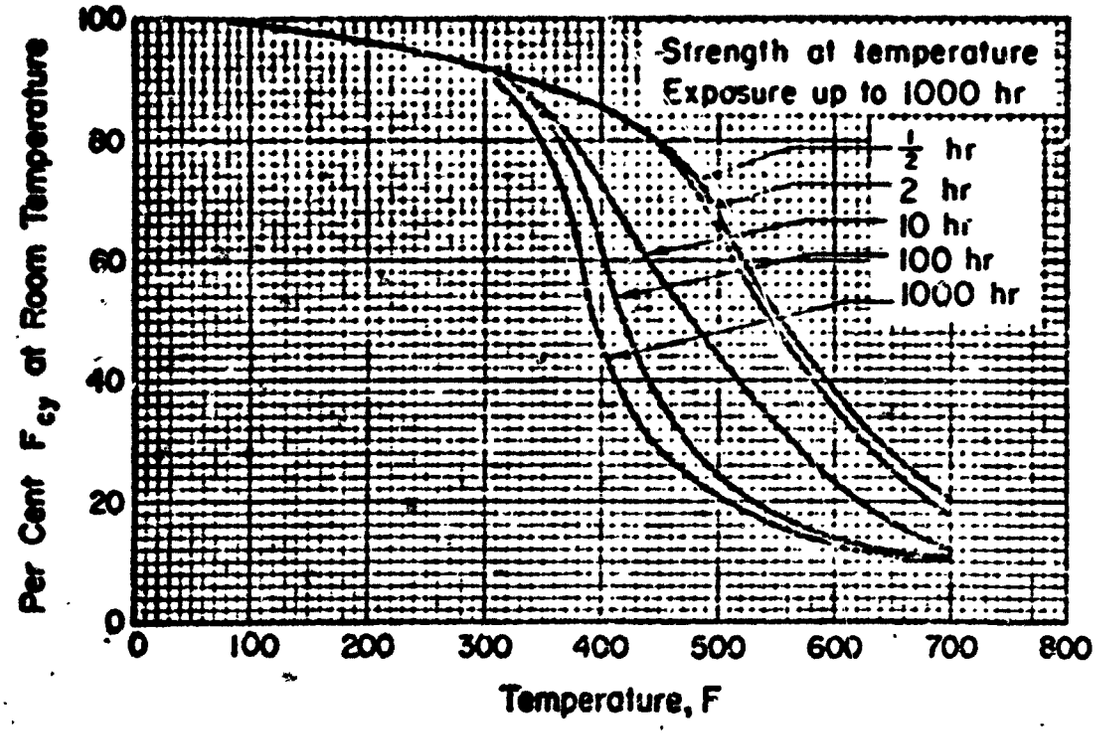

Fig. 3 Thermal Degradation of Compressive Yield Strength for 2024-T3 Aluminum

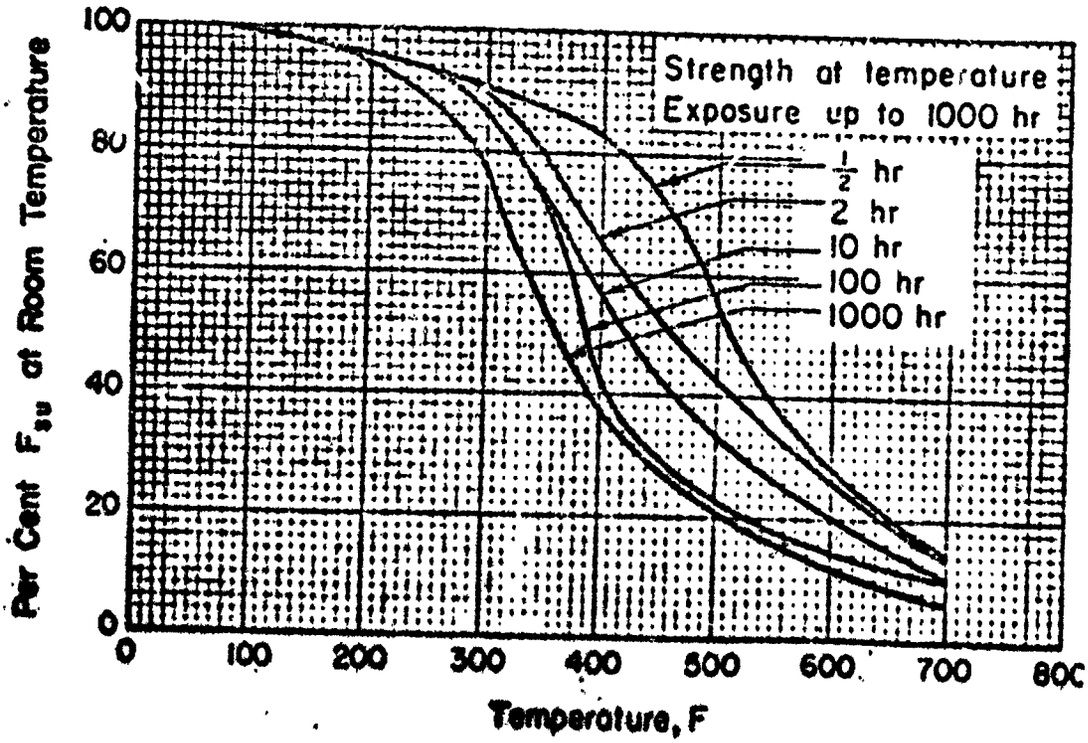

Fig. 4 Thermal Degradation of Ultimate Shear Strength for 2024-T3 Aluminum

data are contained in Ref 13 through 18. Due to data scatter, variations in test methods, inconsistent test parameters, etc., these data do not present a clearly defined relationship between strength and exposure time. Additionally the data for the material of interest, 2024-T3 aluminum, are concerned only with tensile properties. For the present study, degradation of compression and shear strengths were also of interest. The thermal data of Ref 9 provides the necessary tensile, compressive and shear degradation relationships for consistent conditions. Although the data for the much shorter heating times presented in Ref 13 through 18 indicate that strength properties for the short heating times associated with laser heating can vary appreciably from the half-hour exposure data, it was decided to use the latter data for the present study based on the presumption that these data are suitable first-approximations and they are of standardized validity, complete, and consistent which at least partially compensates for possible detailed discrepencies with the shorter heating time effects.

Based on the half-hour exposure curve of Fig. 2, for computational convenience it was decided to approximate the ultimate tensile strength by two straight lines such that

$$F_{tu} = F_{to} - 55T \qquad 0 < T < 200°C \qquad (66)$$

$$F_{tu} = 0.75F_{to} - 200(T-200) \qquad 200°C < T < 370°C \qquad (67)$$

$$F_{tu} = 0 \qquad T > 370°C \qquad (68)$$

where

F_{tu} = ultimate tensile strength at temperature $T(n/cm^2)$

F_{to} = ultimate tensile strength at room temperature = 44,820 n/cm^2 for 2024-T3

T = temperature, °C above room temperature

Similarly, the half-hour exposure compressive yield strength was modeled as

$$F_{cy} = F_{co} - 25T \qquad 0 < T < 232°C \qquad (69)$$

$$F_{cy} = 0.75F_{co} - 140(T-232) \qquad 232°C < T < 370°C \qquad (70)$$

$$F_{cy} = 0 \qquad T > 370°C \qquad (71)$$

where

F_{cy} = compressive yield strength at temperature $T(n/cm^2)$

F_{co} = room temperature compressive yield strength = 23,440 n/cm^2 for 2024-T3

The ultimate shear strength was modeled analytically as

$$F_{su} = F_{so} - 29T \qquad 0 < T < 216°C \qquad (72)$$

$$F_{su} = 0.75F_{so} - 132(T-216) \qquad 216°C < T < 370°C \qquad (73)$$

$$F_{su} = 0 \qquad T > 370°C \tag{74}$$

where

F_{su} = ultimate shear strength at temperature T(n/cm^2)

F_{so} = ultimate shear strength at room temperature = 25,510 n/cm^2 for 2024-T3

VII. Laser Heating Effects

One-Dimensional Heat Flux Model Limits

Since the present study was concerned with the limiting cases of axial and radial heat flux conditions, an initial question to be answered was under what conditions were the assumptions of one-dimensional axial or radial flux valid. It was originally planned that the ranges of input parameters for which the heat flow could be considered to be essentially one-dimensional (either axial or radial) were to be determined by comparing temperature and stress distributions from the one-dimensional models to those obtained from a large two or three-dimensional analysis finite element computer program.

Initially, the MARC (Ref 10) three-dimensional transient thermal stress code was to be used but was abandoned when access to the program was terminated by non-renewal of a lease contract between the Air Force Flight Dynamics Laboratory and Control Data Corporation. Efforts were then made to apply the NASTRAN (Ref 2) program using the Navy thermostructural analysis additions and modifications (Ref 11). Considerable time was expended in getting this program to function properly due to lack of familiarity with NASTRAN and due to insufficient documentation in Ref 11. As a consequence of these and other difficulties with the program, it was decided to eliminate this approach to defining the

one-dimensionality limits. As discussed later in this section, NASTRAN was used to validate the numerical one-dimensional radial flux computations for temperatures and thermal stresses.

An alternate approach was used to define the limits of the one-dimensional axial and radial flux thermal stress models based on the results of the studies presented in Ref 8 and 19. There is reported the development of a single parameter which is shown to determine the limits on the one-dimensionality of heat flux for the stationary beam melting problem. The parameter is a dimensionless absorbed power per unit thickness defined by

$$P_{\ell a} \quad \frac{P_a}{\ell \kappa \rho \left[C_p (T_m - T_o) + L_m \right]} \tag{75}$$

where

ℓ = plate thickness

T_m = melting temperature

L_m = heat of fusion

In Ref 19 it is shown that melt-through times based on the assumption of one-dimensional axial conduction closely predict those from a two-dimensional numerical analysis for values of $P_{\ell a}$ greater than about 70. Values of $P_{\ell a}$ less than about 5 are shown to indicate that the flux is primarily radial. In (Ref 20) an "effective" dimensionless power per unit thickness is developed for correlation with melt-

through times which includes an approximate allowance for the temperature dependence of C_p.

Although these one-dimensionality limits are based on the melting problem, it is reasoned here that the assumption that these limits would also apply for the thermal stress problem, at least for heating times up to melting, is consistent with the earlier assumption (Section III) that the strain rate is of the same order of magnitude as the time rate of change of temperature. That is, it seems reasonable to assume that the one-dimensionality limits for the heat conduction problem (based on melting times) should be about the same as for the thermal stress problem if the strain rates closely follow the temperature time rates. Consequently, the above noted limits on one-dimensional axial and radial flux are applied in the present study.

For the material considered in this study, 2024-T3 aluminum, the one-dimensionality limits based on $P_{\ell a}$ can be reduced to limits on laser beam power and target thickness. For 2024-T3 aluminum,

$$\kappa = 0.514 \text{ cm}^2/\text{sec}$$

$$\rho = 2.78 \text{ gm/cm}^3$$

$$C_p = 1.05 \text{ joule/gm-°C}$$

$$T_m = 502°C$$

$$T_o = 24°C$$

$$L_m = 375 \text{ joule/gm}$$

$$P_{\ell a} = \frac{E_a}{1222\ell} \qquad (76)$$

Hence, for one-dimensional axial conduction $P_{\ell a} \geq 70$ and

$$\frac{P_a}{\ell} \geq 8.55 \times 10^4 \qquad \text{(axial flux)} \qquad (77)$$

Similarly, for one-dimensional radial conduction, $P_{\ell a} \leq 5$ and

$$\frac{P_a}{\ell} \leq 6.11 \times 10^3 \qquad \text{(radial flux)} \qquad (78)$$

Axial Flux Analyses

For relatively high heating rates, the initial heating of a plate with the beam incidence normal to the plate mid-plane would be expected to be primarily axial through-the-thickness of the plate. Since the only area being heated significantly is that directly under the beam, the thermal model of equation (19) gives the temperature distribution through-the-thickness. To obtain a closed form analytical solution to the thermal stress problem, the approximation for thermally thin plates ($\kappa t/\ell^2 > 1$) is applied so that the temperature distribution is given by equation (20). If this thermal model is applied to the thermal stress model of equation (42), the in-plane normal stresses near the beam axis are given by

$$\sigma_{xx} = \sigma_{yy} = \frac{\alpha E \phi_o}{12(1-\nu)kh}(h^2 - 3z^2) \qquad (79)$$

where the coordinate system of Section V is used. This sol-

ution is seen to be independent of time once the initial restriction that $\kappa t/\ell^2 > 1$ is met. The maximum tensile stress occurs at $z = 0$. The stress distribution through the plate is shown in Fig. 5.

An intermediate thermal situation can be hypothesized which might approximate the peak stresses during transition from a predominantly axial flux case to one in which the flux becomes essentially radial. After the core area under the beam is heated for some time by axial flux, this heated core will become heated to an essentially uniform temperature. At this time and prior to the development of significant radial flux, the thermal stress problem can be considered as one of a heated center disk surrounded by an unheated elastic cylinder. Equations (59) through (64) thus provide the thermal stress model for this problem. An initial assessment of the stresses generated for this case is obtained from equation (62) for the peak tensile stress

$$\sigma_{\theta\theta_2} = \frac{\alpha E T_1}{2}\left(\frac{a_1^2}{b^2}+1\right), \quad r = a_1 \tag{80}$$

T_1 is the uniform temperature of the heated core as developed from equation (20),

$$T(z,t) - T_o = \frac{\phi_s}{6k\ell}[6\kappa t+3z^2-\ell^2], \quad \kappa t/\ell^2 > 1 \tag{81}$$

Arbitrarily, to define the heating time when the flux vector would be expected to be primarily radial let it be

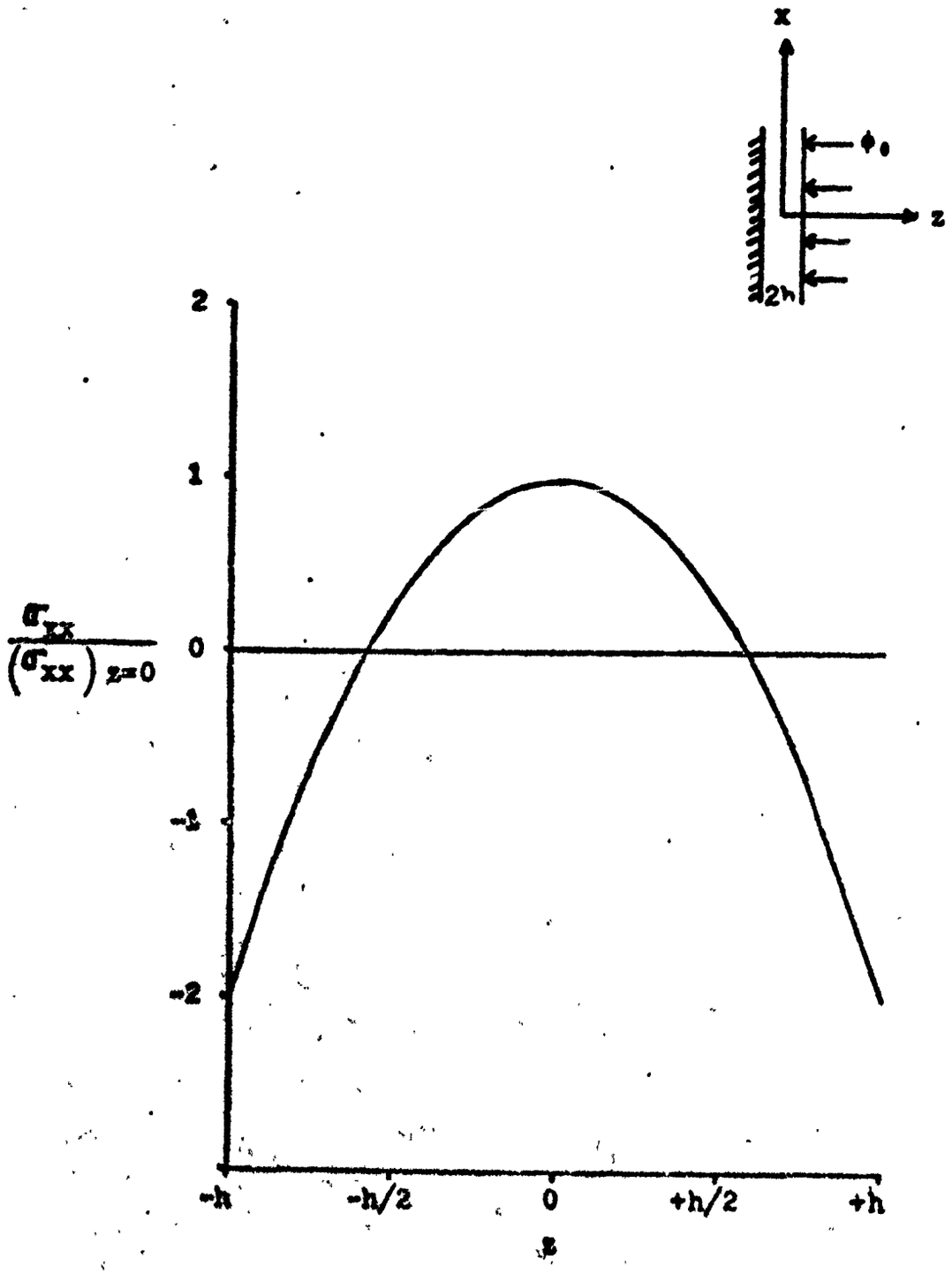

Fig. 5 Steady-State ($\kappa t/z^2 \gg 1$) Thermal Stress Distribution for One-Dimensional Axial Heat Flux

required that the front-to-back surface temperature variation be restricted to 10% or less of the front surface (z = ℓ) temperature. From equation (81) above

$$T(\ell,t) - T_0 = \frac{\phi_0}{3k\ell}(3\kappa t+\ell^2) \tag{82}$$

The back surface (z=0) temperature is

$$T(0,t) - T_0 = \frac{\phi_0}{6k\ell}(6\kappa t-\ell^2) \tag{83}$$

Subtracting (83) from (82) gives the front-to-back temperature variation, ΔT_{F-B}

$$\Delta T_{F-B} = \frac{\phi_0 \ell}{2k} \tag{84}$$

Requiring that

$$\Delta T_{F-B} \leq 0.1[T(\ell,t)-T_0] \tag{85}$$

results in

$$\frac{\phi_0 \ell}{2k} \leq \frac{\phi_0}{30k\ell}(3\kappa t+\ell^2) \tag{86}$$

which reduces to

$$\frac{\kappa t}{\ell^2} \geq 4.67 \tag{87}$$

This result is seen to be an increase in the thermal model restriction of $\kappa t/\ell^2 > 1$.

The solutions for axial flux problems given thus far apply to long heating times and/or thin plates ($\kappa t/\ell^2 > 1$). For earlier heating times (or thicker plates) the thermal model of eqn (19) gives the temperature distribution through-the-thickness of the plate. The thermal stresses can then be determined by numerical integration of the stress model given as eqn (42). Fig. 6 summarizes the results of such an analysis. It was initially found empirically that the in-plane stress is given uniquely by the value of $\kappa t/\ell^2$ at any depth (z/ℓ) in the plate as shown in Fig. 6. This was subsequently confirmed analytically by factoring ($\phi_o \ell$) out of the thermal model equation giving

$$T(z,t) - T_o = \frac{\phi_o \ell}{k}\left[\frac{\kappa t}{\ell^2}+\frac{1}{2}\left(\frac{z}{\ell}\right)^2-\frac{1}{6}\right.$$

$$\left.-\frac{2}{\pi^2}\sum_{n=1}^{\infty}\frac{(-1)^n}{n^2}\cos\left(\frac{n\pi z}{\ell}\right)e^{-\kappa t n^2\pi^2/\ell^2}\right] \qquad (88)$$

The combined factor $\frac{\phi_o \ell}{k}$ has the dimensions of temperature and the terms inside the brackets are dimensionless. Examination of the thermal stress equation (42)

$$\sigma_{xx} = \sigma_{yy} = \frac{\alpha E}{1-\nu}\left[-T+\frac{1}{2h}\int_{-h}^{h} T dz+\frac{3z}{2h^3}\int_{-h}^{h} T x dx\right] \qquad (89)$$

shows that $\frac{\phi_o \ell}{k}$ also factors out of each of these terms. Hence, the thermal stresses are seen to be directly propor-

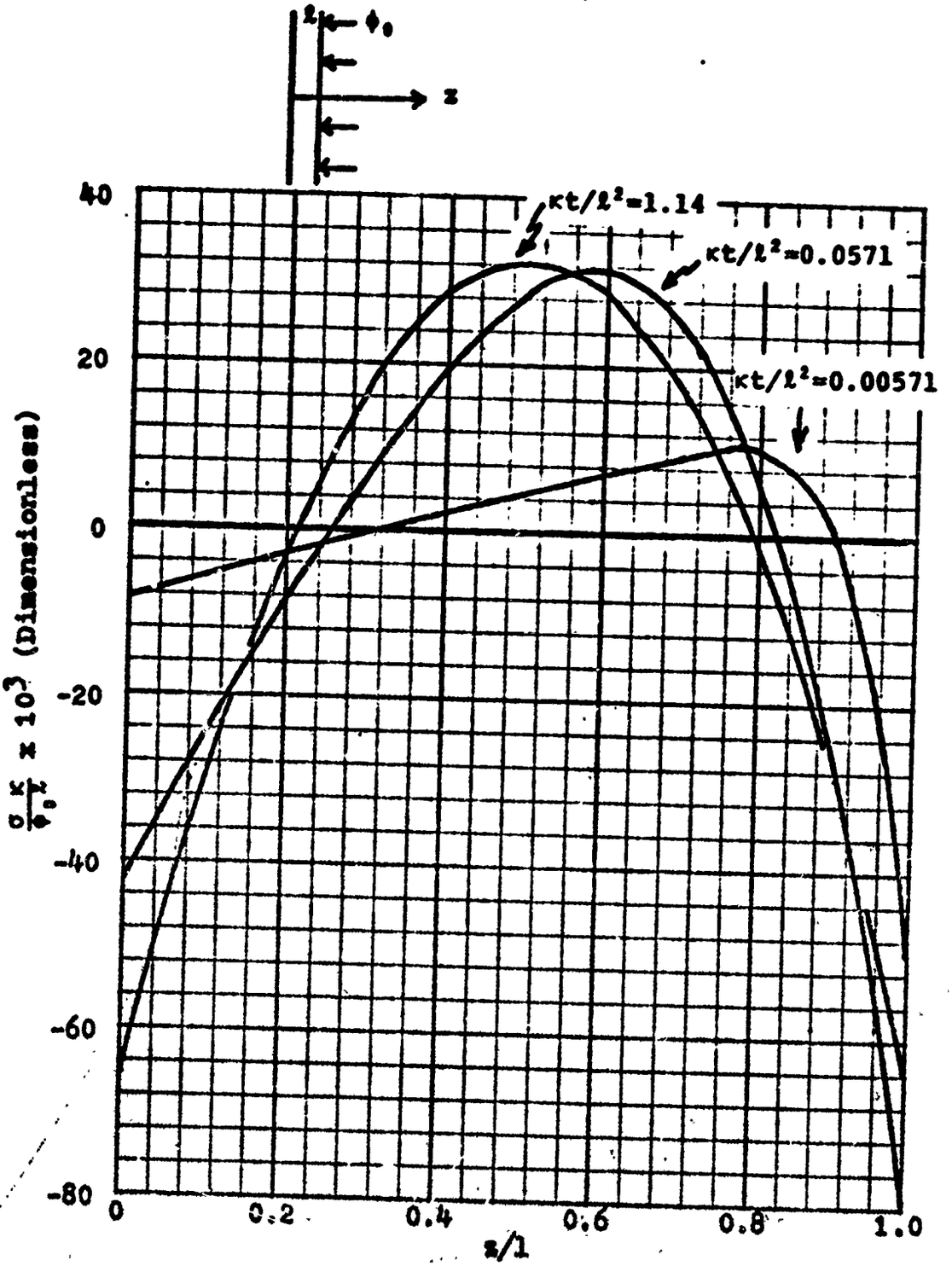

Fig. 6 Transient Thermal Stress Distributions for One-Dimensional Axial Heat Flux (2024-T3 Aluminum)

tional to the flux density, ϕ_0, and the plate thickness, l. When expresses in a consistent set of units, the parameter $\frac{\sigma}{\phi_0 l}$ has the inverse dimensions of thermal diffusivity. Hence, multiplying both sides of eqn (89) by $\frac{\kappa}{\phi_0 l}$ results in a non-dimensionalized stress parameter

$$\frac{\sigma_{xx}\kappa}{\phi_0 l} = \frac{\alpha E}{\rho C_p(1-\nu)}\left[-T^*+\frac{1}{2h}\int_{-h}^{h} T^* dz+\frac{3z}{2h^3}\int_{-h}^{h} T^* z dz\right] \qquad (90)$$

where

$$T^* = \frac{\kappa t}{l^2} + \frac{1}{2}\left(\frac{z}{l}\right)^2 - \frac{1}{6}$$

$$- \frac{2}{\pi^2}\sum_{n=1}^{\infty}\frac{(-1)^n}{n^2}\cos\left(\frac{n\pi z}{l}\right) e^{-\kappa t n^2\pi^2/l^2} \qquad (91)$$

It should be noted that eqn(90) and eqn (91) are expressed in terms of the thermal stress and heat conduction coordinate systems, respectiveiy. Eqn (90) is plotted in Fig. 6 for 2024-T3 aluminum. If the material property parameters outside the brackets in eqn (90) were transposed to the other side of the equation, another dimensionless stress parameter would be defined, which is independent of material within the general class (homogeneous, isotropic) of interest.

In Fig. 6 the curve for $\kappa t/l^2 = 1.142$ represents the steady state stress distribution which remains constant for all $\kappa t/l^2 > 1$. This curve is the same as that shown in Fig. 5 which is based on the analytical approximation given by eqn (79). For earlier times, the development of the thermal

stresses is shown by the other curves in Fig. 6. Initially, as shown by the curve for $\kappa t/\ell^2 = .00571$, only the plate volume near the heated surface is heated appreciably and relatively large compressive stresses are quickly generated at this surface. As the temperature drops to near zero beyond this heated layer, the expansion of the heated layer creates tensile stresses in the unheated area which reach a peak near the front of the relatively unheated zone, then gradually decay becoming compressive again at the unheated surface.

Both the compressive and tensile maximum stresses increase with time, attaining peak values prior to reaching the steady state values. The peak tensile stress is only slightly larger than the steady value, which occurs at $z/\ell = 0.5$. However, the peak compressive stress (at the heated surface) is approximately 20 percent larger than the steady state value. Fig. 6 also shows that the peak compressive stress occurs at an earlier time than the peak tensile stress.

The temporal development of the peak tensile and compressive stresses is shown in Figure 7. The vertical dashed line at $\kappa t/\ell^2 = 4.67$ represents the time at which the temperature variation through-the-thickness of the plate becomes less than 1/10 that of the heated surface temperature. This is arbitrarily taken as an appriximation of the time when the flux vector is no longer primarily axial since the radial thermal gradients at the outer diameter of the beam

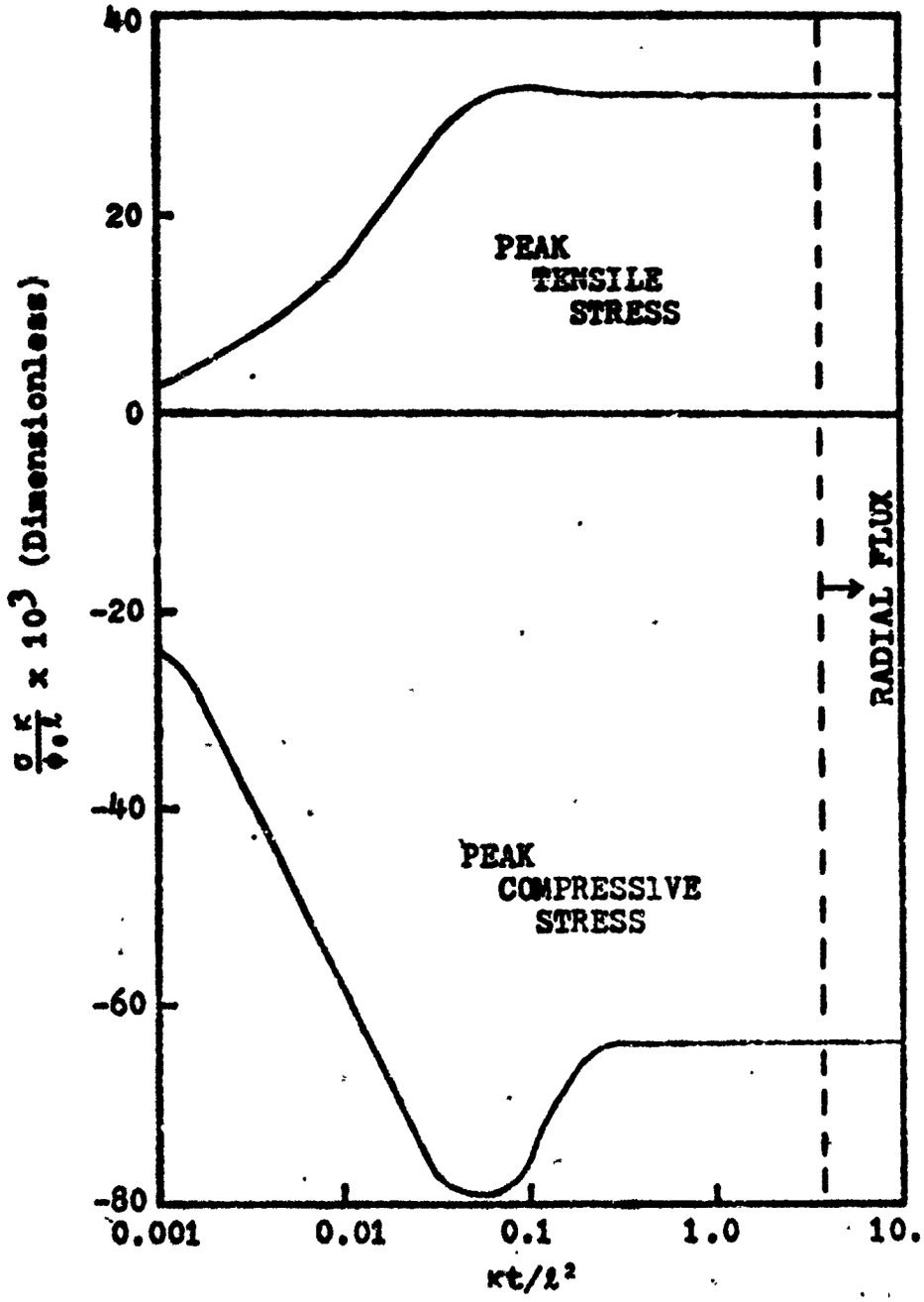

Fig. 7 Peak Thermal Stress versus Dimensionless Heating Time for One-Dimensional Axial Heat Flux (2024-T3 Aluminum)

would be expected to be large relative to the axial gradients under the beam.

The slight peak in the tensile stress near $\kappa t/\ell^2 = 0.1$ is apparent. The peaking of the compressive stress is seen to be much more significant and extending over a larger period of time. It is concluded that the maximum thermal stresses produced by one-dimensional axial heating occur just prior to attaining steady state heat conduction, and that these stresses are defined by the following equations as derived from Fig. 7.

$$\left(\frac{\sigma_{xx}^{K}}{\phi_o \ell}\right)_{\substack{\max \\ \text{tensile}}} = 3.30 \times 10^{-2} @ \kappa t/\ell^2 = 0.1 \qquad (92)$$

$$\left(\frac{\sigma_{xx}^{K}}{\phi_o \ell}\right)_{\substack{\max \\ \text{compressive}}} = -7.94 \times 10^{-2} @ \kappa t/\ell^2 = 0.06 \qquad (93)$$

To assess the relative importance of the melting and thermal degradation damage mechanisms for comparison with thermal stresses for the axial flux case, the times required for complete melt-through and for complete thermal degradation are useful. The time required for complete melt-through, assuming one-dimensional axial flux, temperature independent properties, and immediate melt removal, is given by (Ref 19:2)

$$t_1 = \frac{\rho \ell}{I_{pa}}[C_p(T_m - T_o) + L_m] \qquad (94)$$

As defined in Section VI, thermal degradation is a

function of temperature only, with essentially zero strength remaining if local temperatures exceed 370°C. Analogous to the one-dimensional axial flux melt-through time, t_1, a heating time for complete thermal degradation can be defined by

$$t_D = \frac{\rho \ell}{I_{pa}} C_p (T_D - T_o) \tag{95}$$

where

t_D = heating time for complete thermal degradation of structural strength (sec)

T_D = temperature above which material has essentially zero strength
= 370°C

Dividing by t_1 gives

$$\frac{t_D}{t_1} = \frac{T_D - T_o}{(T_m - T_o) + L_m/C_p} \tag{96}$$

It is seen that t_D is always less than t_1 for structural metals since T_m is generally greater that T_D. For 2024-T3 aluminum, assuming $T_o = 0$,

$$t_D = 0.43\ t_1 \tag{97}$$

Hence, complete thermal degradation of the structural strength properties of the plate would be expected to occur prior to complete melt-through.

Although not directly pertainent to the present study,

the heating time to complete thermal degradation for other structural materials was investigated briefly. Based on extrapolation of the thermal degradation data in Ref 9, the following table presents t_D/t_1 as calculated from eqn (96). Thermal properties are taken from Ref 32.

Material	T_m(°C)	T_D(°C)	L_m(j/gm)	C_p(j/gm°C)	t_D/t_1
AZ-31B Magnesium	605	425	338	1.21	0.48
301 Stainless Steel	1400	870	290	0.42	0.42
6Al-4V Titanium	1600	870	390	0.77	0.41

Hence, it appears that complete thermal degradation precedes melting for most structural metals.

A qualitative comparison of the thermal degradation and thermal stress damage mechanisms for the axial flux case can be obtained by examining the ratio of heating time to complete thermal degradation time and comparing it to the ratio of maximum compressive thermal stress to room temperature compressive yield strength. This comparison is made in Fig. 8 for a particular value of absorbed heat flux density. Since both of these dimensionless ratios are linear functions of the absorbed heat flux density (see eqns (90) and (95)), changes in this parameter do not affect the relative positions of the two curves.

The solid curves apply when $\kappa t/\ell^2 = 0.06$ which corres-

$I_{pa} = 1500\ W/CM^2$

——— $\kappa t/\ell^2 = 0.06$

– – – $\kappa t/\ell^2 = 0.01$

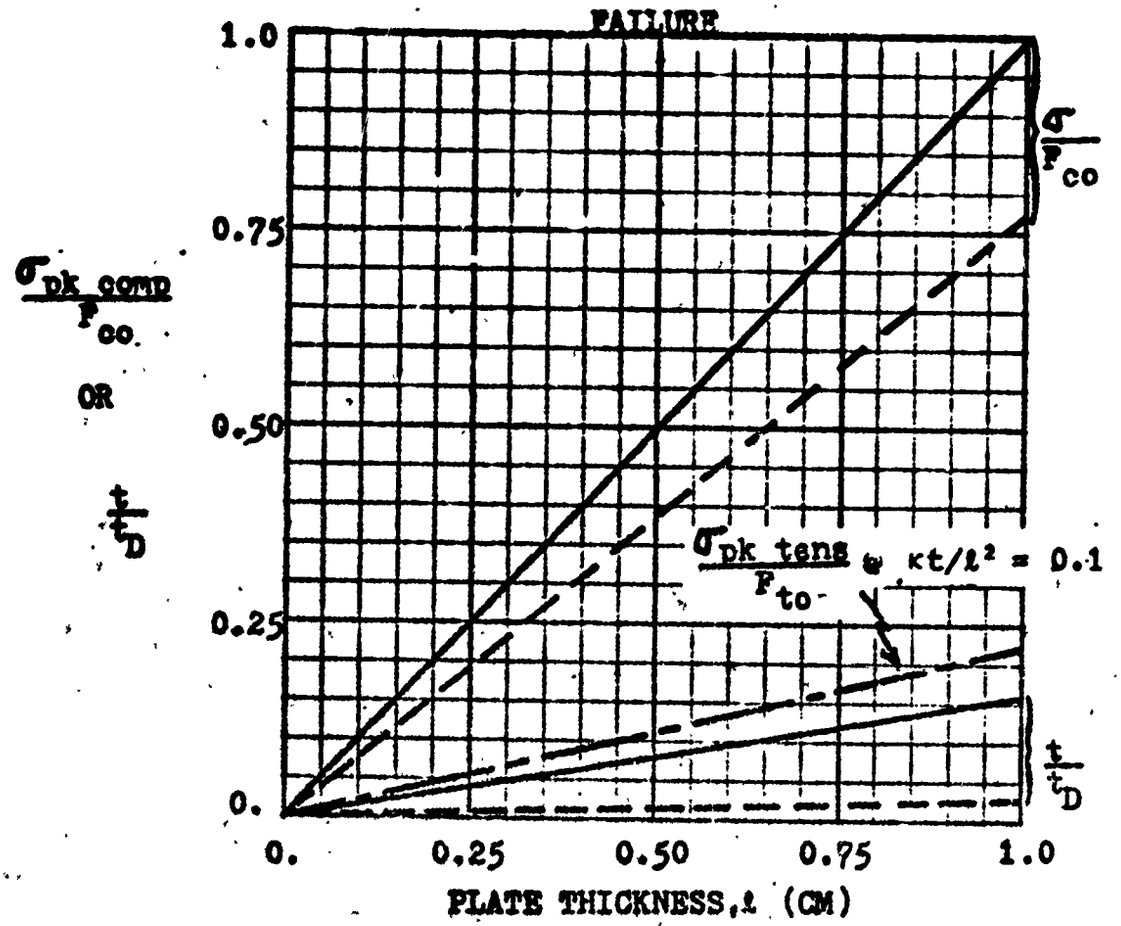

Fig. 8 Comparisons of Peak Thermal Stresses and Thermal Degradation Heating Time for One-Dimensional Axial Heat Flux (2024-T3 Aluminum)

ponds to the maximum value of the peak compressive stress (see Fig. 7). The stress ratio is computed from eqn (93) by substituting the material property values for 2024-T3 aluminum and $I_{pa} = 1500$ w/cm^2 which is approximately the maximum value of interest for this study. The following relationship is obtained.

$$\left(\frac{\sigma_{xx}}{F_{co}}\right)_{\substack{\max \\ comp.}} = 0.989(1/cm)\ell\sqrt{\kappa t/\ell^2} = 0.06 \qquad (98)$$

Similarly, eqn (95) gives

$$\frac{t}{t_D} = 1.39(cm/sec)\frac{t}{\ell} \qquad (99)$$

from $\kappa t/\ell^2 = 0.06$,

$$t = 0.117\ell^2(sec) \qquad (100)$$

Substituting (100) into (99) results in

$$\frac{t}{t_D} = 0.162(1/cm)\ell \qquad (101)$$

Eqns (98) and (101) are plotted as solid curves in Fig. 8. The initial conclusion drawn from this comparison is that the damage from these two sources is of the same order of magnitude at times defined by $\kappa t/\ell^2 = 0.06$. This is a qualitative conclusion in that peak thermal stresses represent the onset of material failure rather than through-the-thick-

ness failure represented by the thermal degradation ratio. Even though the stress ratio exceeds the thermal degradation ratio by about a factor of six, consideration of the additional time required to completely fail the plate through-the-thickness by both compressive and tensile thermal stresses would likely compensate for this difference and might reverse the relationships.

For comparison to the maximum compressive stress, the corresponding stress ratio for maximum tensile thermal stresses is shown on Fig. 8 as derived from eqn (92). Tensile stresses are concluded to be a relatively insignificant contributor to damage for axial flux heating.

Also shown in Fig. 8 are the corresponding relationships for an earlier time, $\kappa t/\ell^2 = 0.01$. In this case the stress ratio is determined from Fig. 7. Since t/t_D is linear in time and the peak compressive stress is a logarithmic function of time, the stress ratio exceeds the thermal degradation ratio by an even larger factor. Consequently the relative significance of thermal degradation increases with time. Since the heating conditions for the solid curves in Fig. 8 generate the maximum thermal stresses for the range of beam/target parameters considered, it is seen that the maximum value for the compressive stress ratio is about 0.65 (at the maximum plate thickness of interest, $\ell = 0.65$ cm).

Hence, for the axial flux conditions considered, peak thermal stresses do not reach material failure values.

Complete thermal degradation occurs at $t/\ell = 0.719$ sec/cm as determined from eqn (99). This corresponds to

$$\frac{\kappa t}{\ell^2} = \frac{0.370}{\ell} \tag{102}$$

which varies between 0.57 and 3.70 for the range of plate thicknesses considered ($0.1>\ell>0.65$cm). That is, complete thermal degradation does occur for the axial heat flux case within the range of beam/target parameters of interest. Since the range of $\kappa t/\ell^2$ in which complete degradation can occur exceeds the $\kappa t/\ell^2$ values for maximum thermal stresses, the actual failure mechanism is expected to be the combined actions of thermal stresses and thermal degradation. However, since the majority of the plate thickness under the beam is subjected to tensile stresses (Fig. 5), and these tensile stresses do not become significant relative to room temperature ultimate tensile strength for the range of heating parameters considered, thermal degradation will contribute much more to complete through-the-thickness failure than thermal stresses. It is concluded that the heating time to complete thermal degradation, t_D, provides a reasonable approximation to the time required for through-the-thickness material failure under the combined actions of thermal stresses and degradation for the case of axial flux heating.

Comparisons of thermal stresses generated during

one-dimensional axial heat conduction to those associated with one-dimensional radial conduction are discussed in later paragraphs of this section.

Radial Flux Analyses

The numerical radial flux computer program is based on the numerical thermal model described in Section IV. The total program is named TSTRESS and is listed in Appendix A along with sample program outputs. The radial thermal model described in Section IV is subroutine TEMPRAD in Appendix A. Based on the radial temperature distributions output from TEMPRAD, numerical integration of thermal stress equations (55) & (56) is accomplished by subroutine STRESSR to determine the radial flux stress components. A separate algorithm (see Appendix B) was developed to compute stresses near r = 0 as equations (55) & (56) are indeterminate there.

The one-dimensional radial heat conduction model implies that the plate is circular in planform. However, for those cases where the plate diameter is large enough that the plate size no longer significantly affects the heat conduction or thermal stresses, the plate can be considered to be rectangular with width equal to the circular plate diameter. The length of the rectangular plate can be considered to be any length equal to or greater than the circular plate diameter. The residual tensile strength of the rectangular plate in the lengthwise direction can then be used as a measure of the damage inflicted by the mechanisms

of thermal degradation of structural properties, thermal stresses, and melting.

Subroutine STRONG computes the radially averaged residual tensile strength of the plate (RESDEG) due to thermal degradation, based on the radial temperature distribution and the half-hour exposure, thermal degradation of ultimate tensile strength data for 2024-T3 aluminum given in Ref 9. These data are approximated by the analytical functions given in Section VI. This subroutine provides a measure of the damage caused by thermal degradation of tensile strength.

Other damage measures are computed in subroutine RESTRNG. Residual tensile strength due to thermal stresses (RESTRSS) is computed based on thermal tensile stress distribution by assuming ultimate tensile stress remains at the room temperature value. Residual strength due to the combined action of thermal stresses and thermal degradation is computed as RESTRS2. Structurally failed areas due to thermal stresses alone (RFS), thermal degradation alone (RFD), and in combination (RFDS) are calculated in subroutine RADFAIL. Failed radius due to melting a hole (RMELT) is computed in the main program (beginning at line 153).

A parallel calculation of the effect of stress concentration is made in subroutine RADSC. This calculation is based on holes caused by thermal stresses and degradation in combination (RFDS) as it is assumed that hole stress concentrations associated with melted holes are negligible

due to relief provided by plastic flow associated with high temperatures.

Structural failure may be caused by thermal stresses or degradation, or their combined actions. Two alternative treatments of structurally failed areas were used. In one case, the failed area is assumed to be immediately removed from the plate, thus forming a hole. In the other case, the failed area is assumed to remain in the plate and continue to absorb and conduct heat.

In the case where the failed area is retained in the plate, melting is the only mechanism which can generate a hole. At each time increment, thermal stresses, residual strengths and failed areas are all computed based on the assumption that the current failed area has zero strength, that is only the temperature distribution outside the failed area is considered. The temperature distribution is based on the heat flux into the plate outside the melted hole. The failed area will either be equal to or greater than the melted hole.

In the case where the failed area is assumed to be immediately removed (by an unspecified source such as aerodynamic pressure), the actual hole size at any time is the larger of the melted hole and the failed area. Temperatures, thermal stresses, residual strengths and failed areas are computed based on this actual hole size.

Fig. 9 (solid curves) shows a typical comparison of the respective hole sizes for the above described alterna-

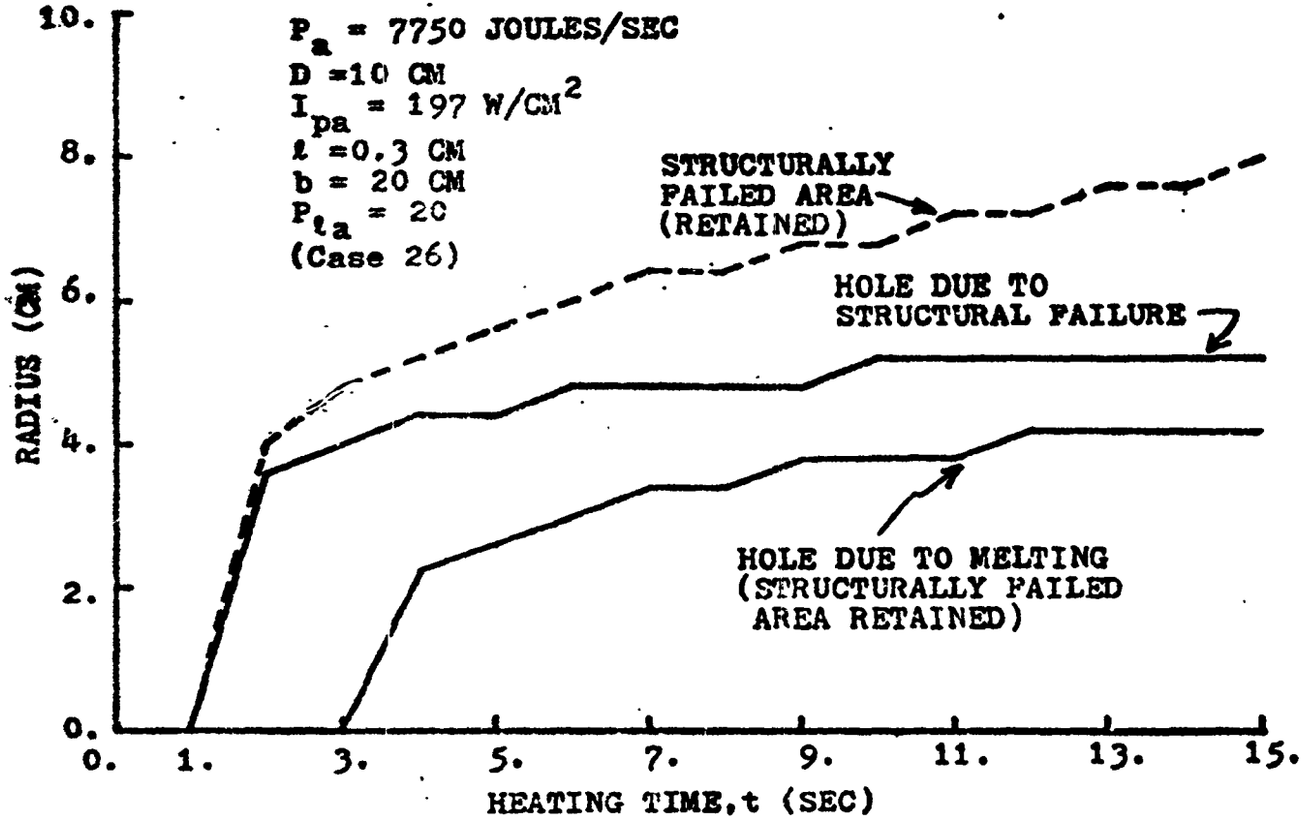

Fig. 9 Comparison of Damage Sizes due to Structural Failure and Melting, 1-D Radial Heat Flux

tive failure modes. The plots are based on data output from the TSTRESS program at one second time intervals. The data are connected by straight lines which results in the incremental characteristic of the plots. The bottom solid curve is for the case in which only melting is considered to form a hole in the plate. For these conditions a failed area is generated by the combined actions of thermal stresses and thermal degradation and the radius of this failed area is given by the dashed curve. The failed area is assumed to remain in position in the plate. For the alternative situation in which the failed area is assumed to be immediately removed from the plate, the resulting hole radius is given by the upper solid curve in Fig. 9. These results are typical for the range of parameters studied in that the structurally failed area due to the combined action of thermal stresses and degradation is always larger than holes formed by melting, and that the failed area is generated prior to melting a hole.

It should be noted that although the one-dimensional radial flux code is strictly applicable only when the dimensionless power per unit thickness, P_{1a}, is less than 5, much of the data presented is based on heating conditions for which $P_{1a} > 5$. This is done to facilitate data presentation as the trends shown are the same for both conditions, but much longer computer run times are required to obtain structural failure and melting effects when $P_{1a} < 5$.

Fig. 10 is a typical plot of principal thermal stress

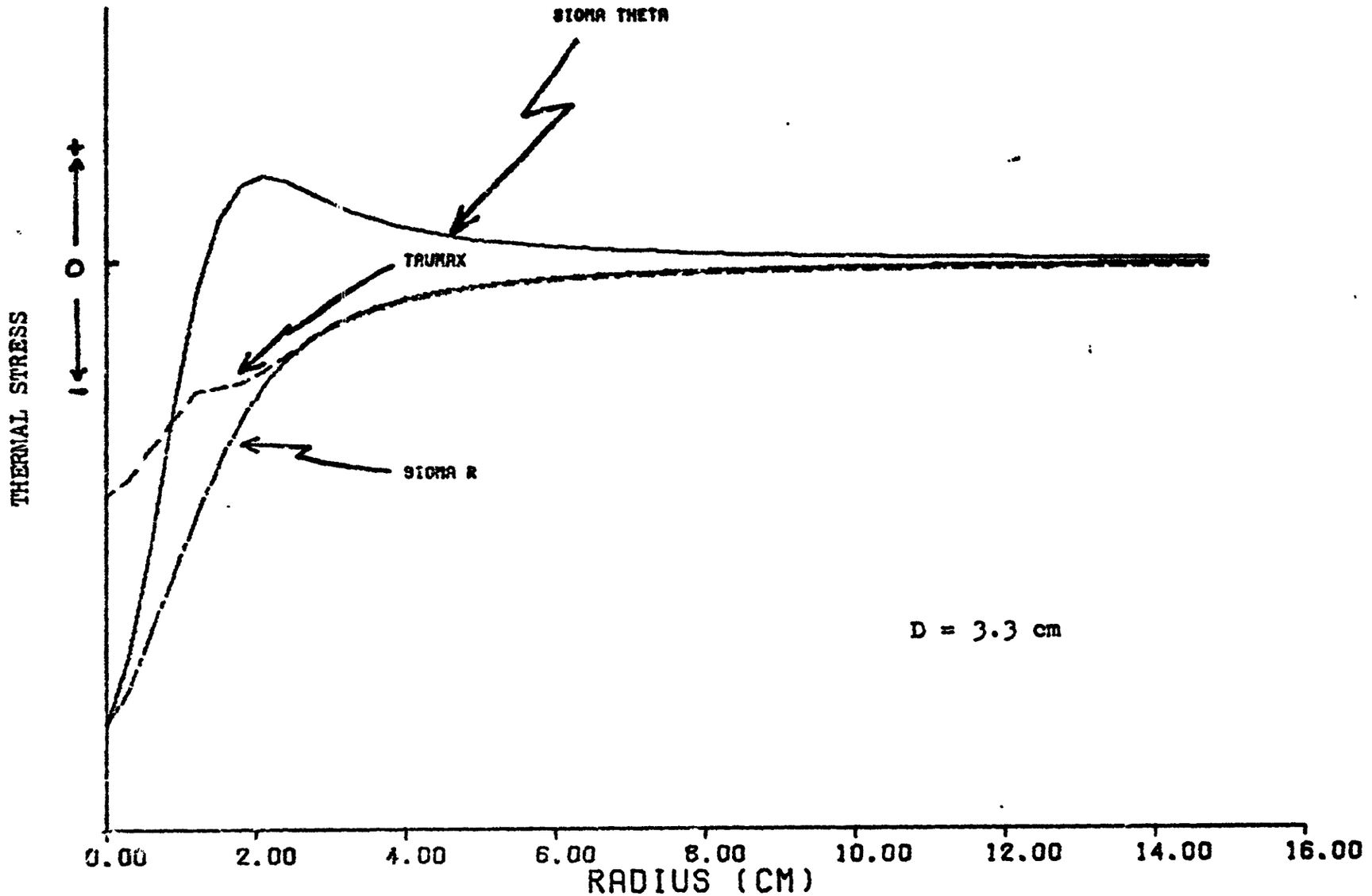

Fig. 10 Thermal Stress Distributions, 1-D Radial Heat Flux, Gaussian Heat Flux Density

distributions for a solid disk at some time prior to melting or structural failure. An understanding of thermal stress distributions prior and subsequent to hole formation is necessary to explain the relative damage modes. Fig. 10 shows that the radial (σ_r) and tangential (σ_θ) stresses are compressive near the plate and beam center. The radial stress becomes less compressive with increasing radius, becoming zero at the plate edge. The tangential stress becomes tensile just outside the heated cylinder, rapidly reaching a peak value before gradually decreasing to zero at the plate edge.

The maximum shear stress is equal to the one-half the maximum difference between any two of the three principal orthogonal stresses. In the case of plane stress, the stress component normal to the plane of the plate is zero. Inside the heated cylinder the maximum difference in stress components is between the radial and normal components. Outside the heated core, the maximum shear stress is determined by the difference between the radial and tangential components. This change in the maximum shear stress determination accounts for the inflection in the maximum shear stress distribution shown in the figure.

A typical temperature distribution at some time prior to formation of a hole is illustrated in Fig 11. Both melting and thermal degradation are direct functions of temperature (see Section VI), and knowledge of the general form of the temperature distribution aids in understanding the rela-

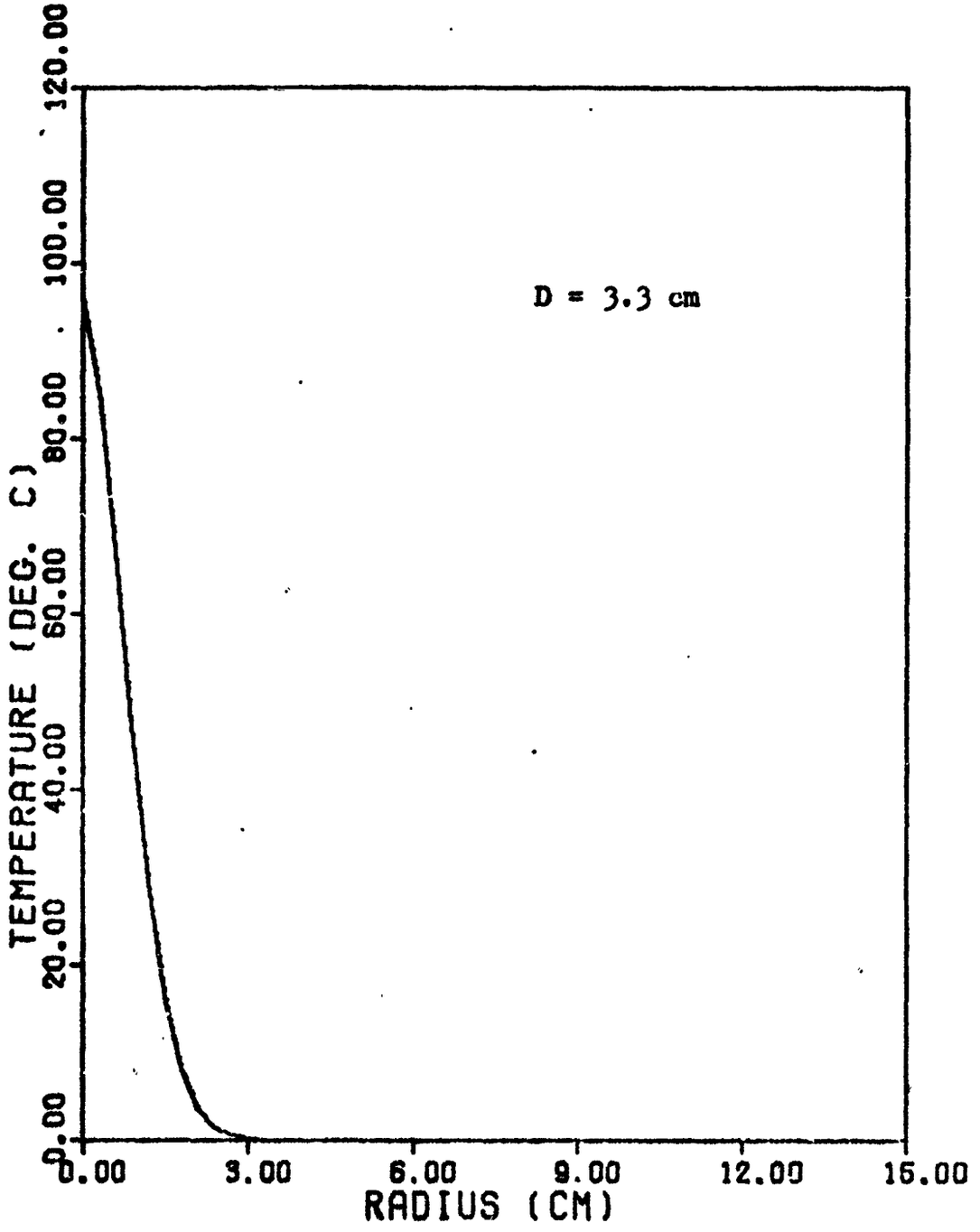

Fig. 11 Temperature Distribution, 1-D Radial Heat Flux, Gaussian Heat Flux Density

tive influence of these damage mechanisms. The figure shows the typically rapid decrease in temperature within the beam radius for a Gaussian distribution heat flux density.

Fig. 12 presents the residual tensile strength, normalized by the unheated ultimate tensile strength, as a function of heating time for each of the damage mechanisms. In this case, the failed area is assumed to be immediately removed, thus forming a hole. Since the failed area radius is always equal to or greater than any melted hole radius, no damage due to melting occurs.

The effect of assuming that the failed area remains in the plate but does not transmit stresses and that only melting generates a hole is shown in Fig. 13. Comparison with Fig. 12 shows that the assumption that the failed area remains in place results in slightly greater strength reduction, again due to the larger heat absorbing surface for this situation. Both figures show that the largest contributor to tensile strength reduction is the structurally failed area and that thermal stresses contribute more than thermal degradation. The respective radii of the melted hole and failed area for the heating conditions of Fig. 13 are given by the solid curves in Fig. 14. The dashed curve is for the alternative assumption that the failed area forms a hole.

The effect of varying laser beam diameter on residual tensile strength is shown in Fig. 15 for the situation of retained failed areas. For smaller beam diameters the peak

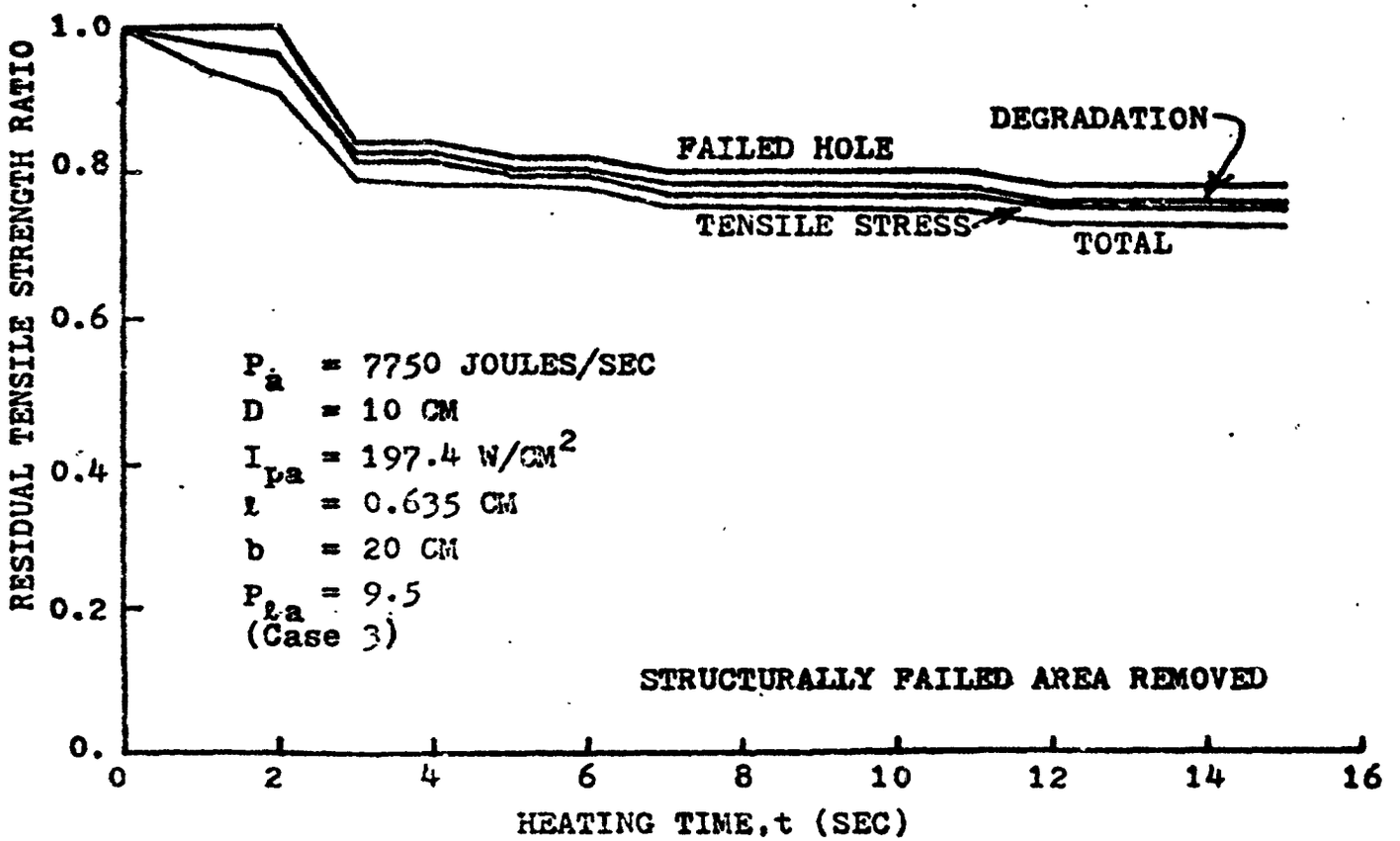

Fig. 12 Effect of Damage Mechanisms on Residual Tensile Strength, Structurally Failed Area Removed

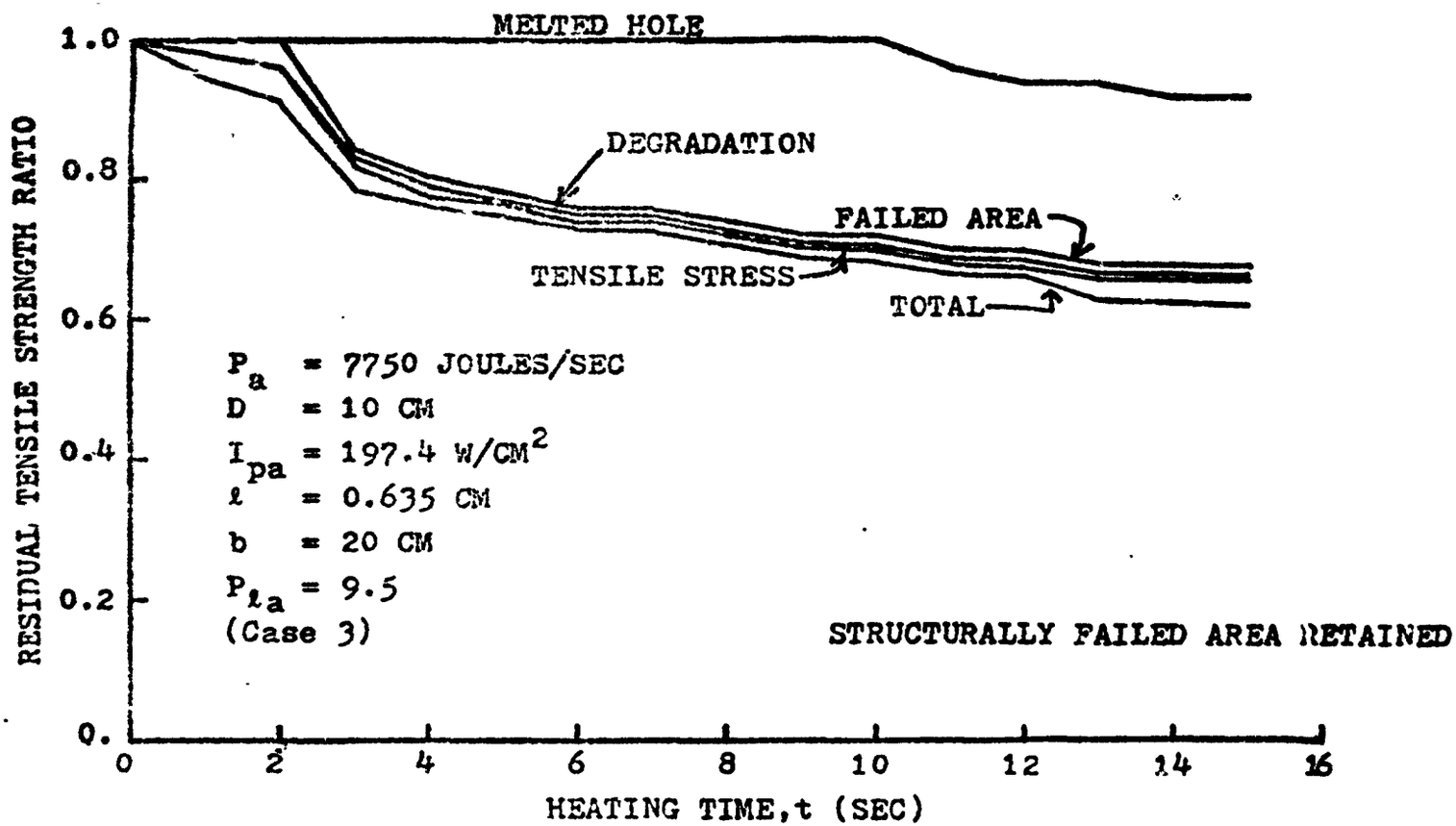

Fig. 13 Effect of Damage Mechanisms on Residual Tensile Strength, Structurally Failed Area Retained

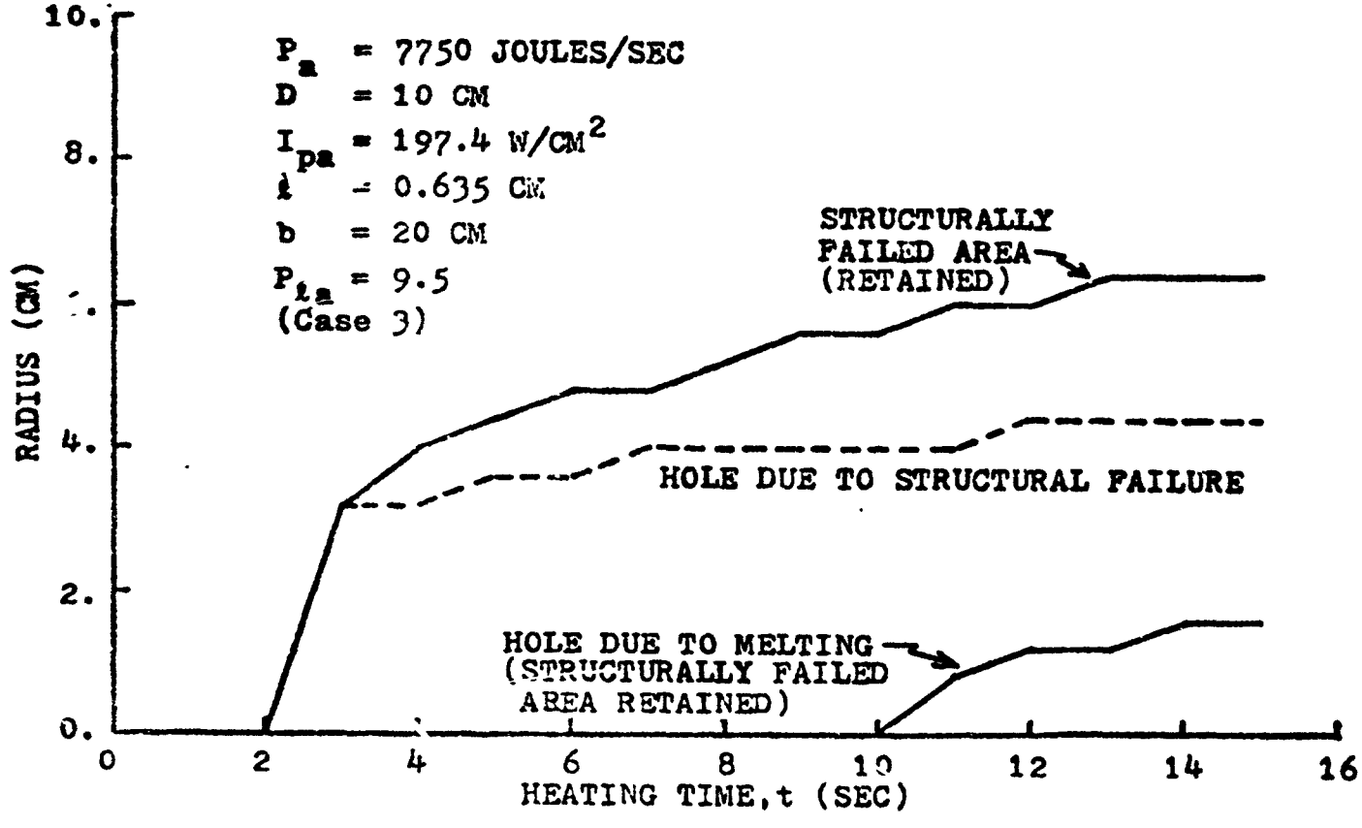

Fig. 14 Radii of Melted and Structurally Failed Regions for Heating Conditions of Figure 13

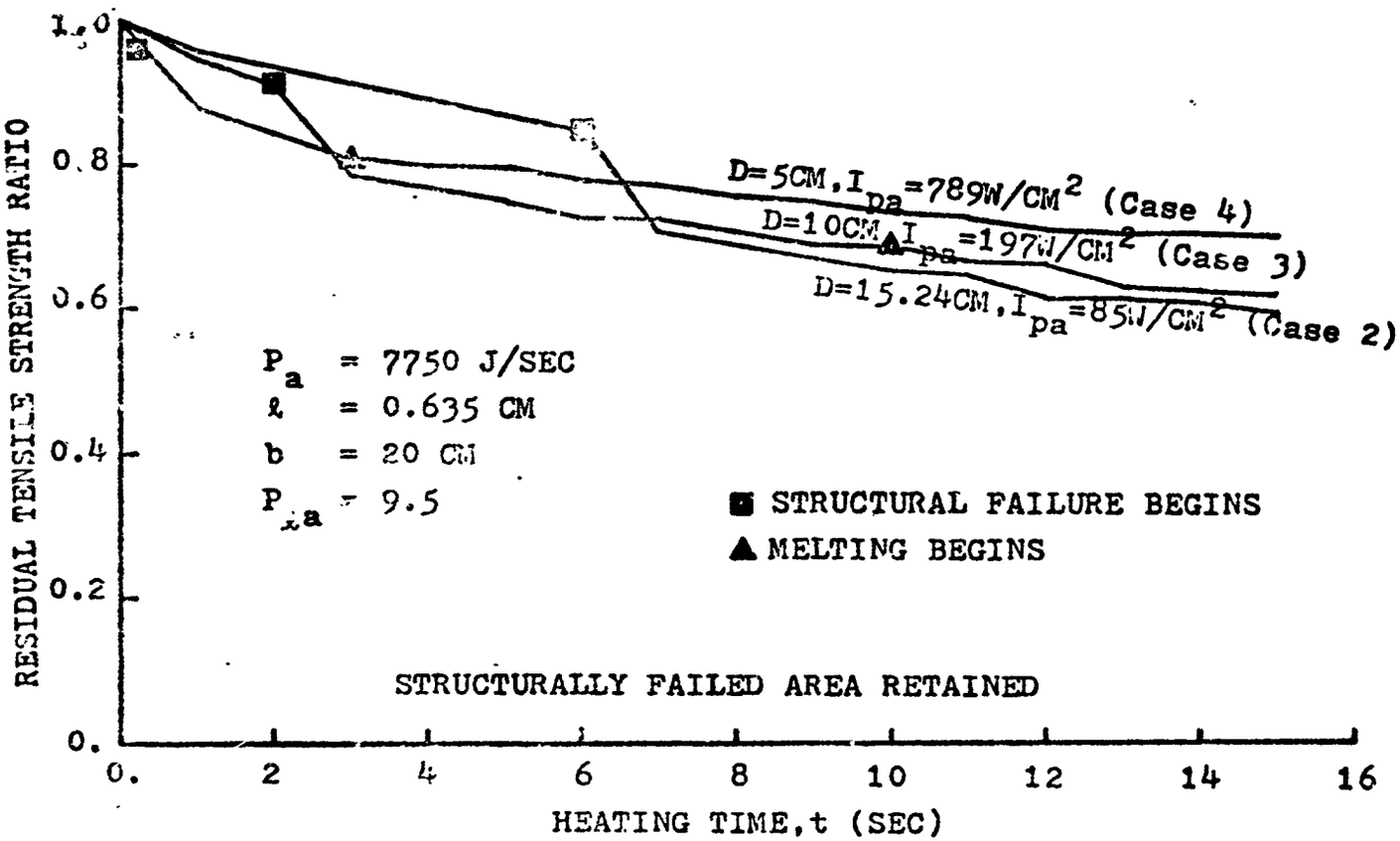

Fig. 15 Effect of Laser Beam Diameter on Residual Tensile Strength

heat flux density is larger resulting in earlier structural failure. As the failed area diameter approaches the beam diameter, the rate of strength reduction becomes increasingly slower because the failed area is the primary factor in determining residual tensile strength. Residual strength continues to decrease until the melted hole approaches the beam size after which heat absorption by the plate ceases.

The larger beam diameter effectively postpones structural failure and melting until a larger area of the plate is heated significantly resulting in strength reduction over a larger portion of the plate. As shown in Fig. 16, the failed area grows more rapidly for the larger beam diameters eventually becoming larger than for the smaller beam diameters.

The effect of beam power on residual strength is shown in Fig. 17. The beam powers selected for this comparison give peak absorbed flux densities corresponding to those for the comparison of beam diameter effects in Fig. 15. The corresponding failed area radii are compared in Fig. 18. Increasing beam power is seen to decrease the time required to achieve structural failure and melting, and to generate larger failed areas (and melted holes) and reduce residual tensile strength at any given time.

Fig. 19 shows the effect of plate thickness on residual strength. The effects are similar to those for beam power with more rapid strength reduction consistently occuring for thinner plates.

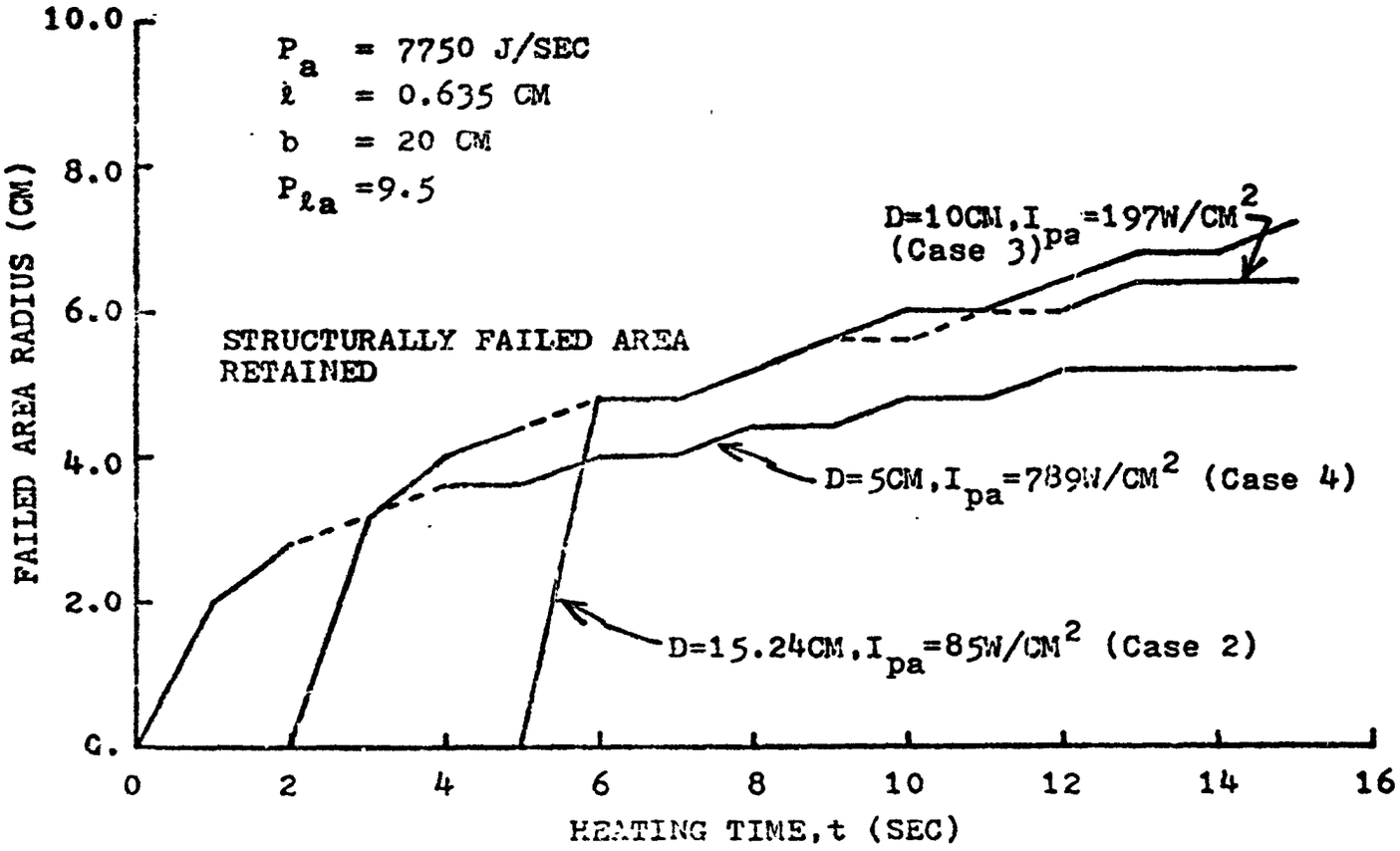

Fig. 16 Effect of Laser Beam Diameter on Melted Hole and Structurally Failed Area Radii

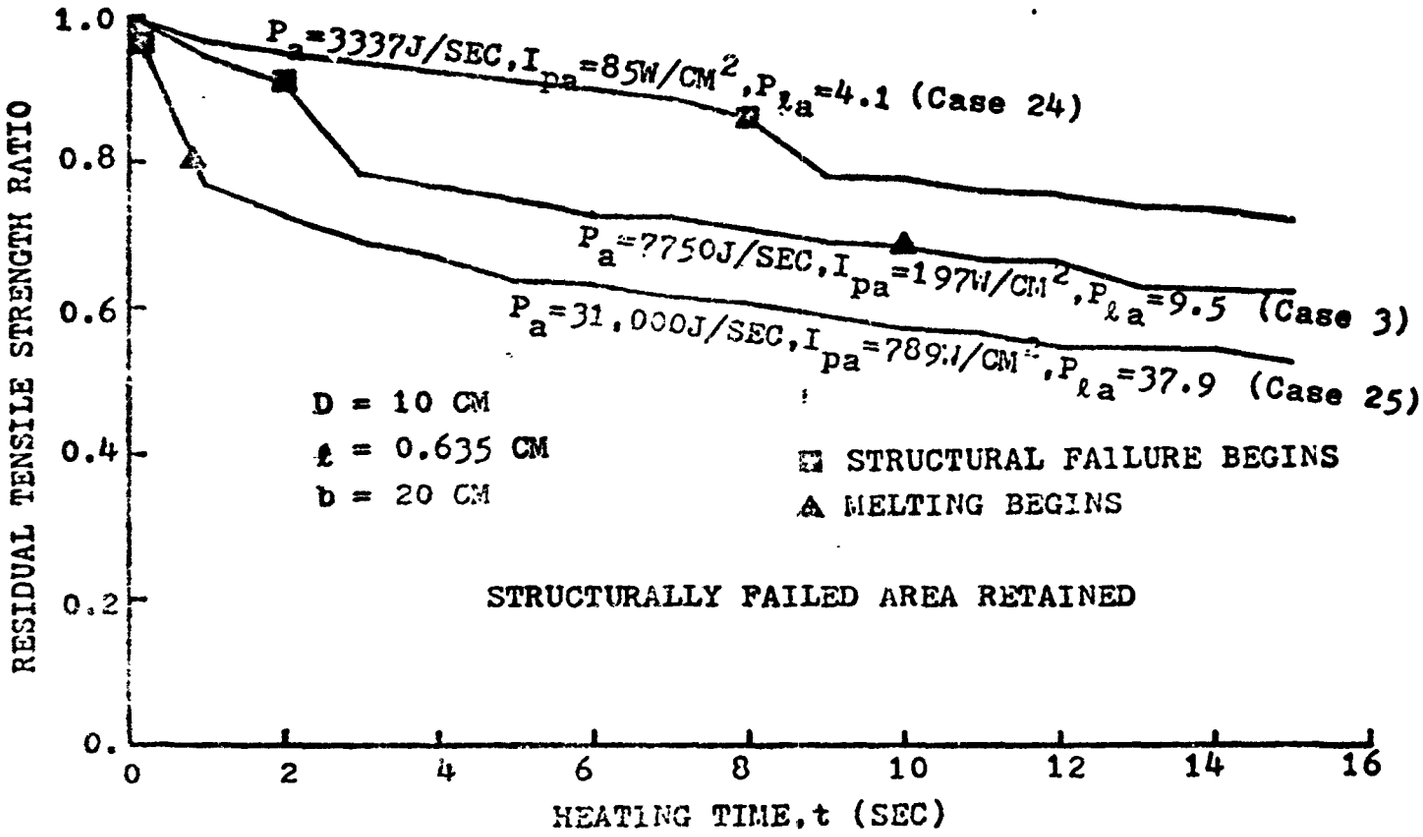

Fig. 17 Effect of Absorbed Power on Residual Tensile Strength

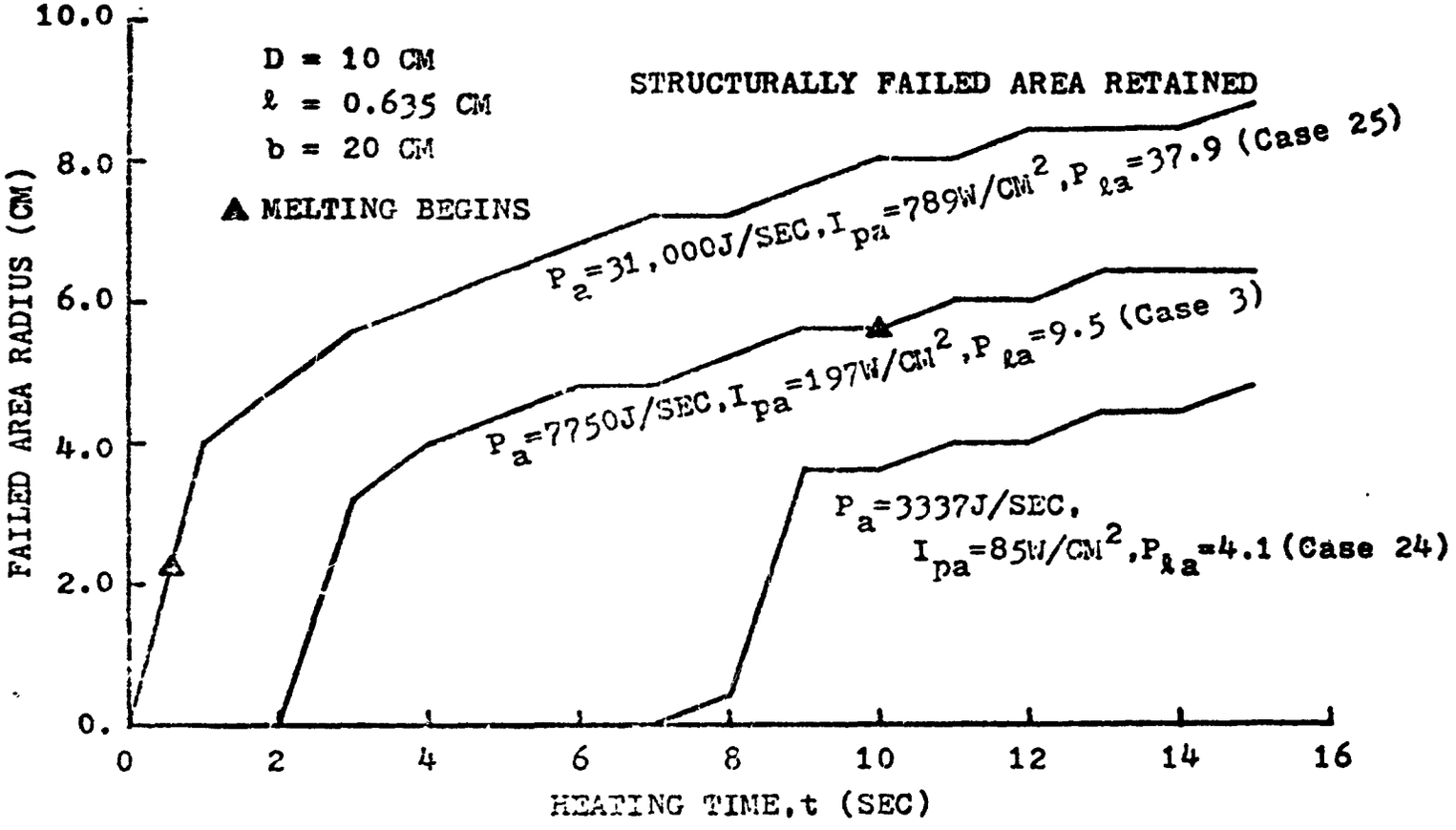

Fig. 18 Effect of Absorbed Power on Melted Hole and Structurally Failed Area Radii

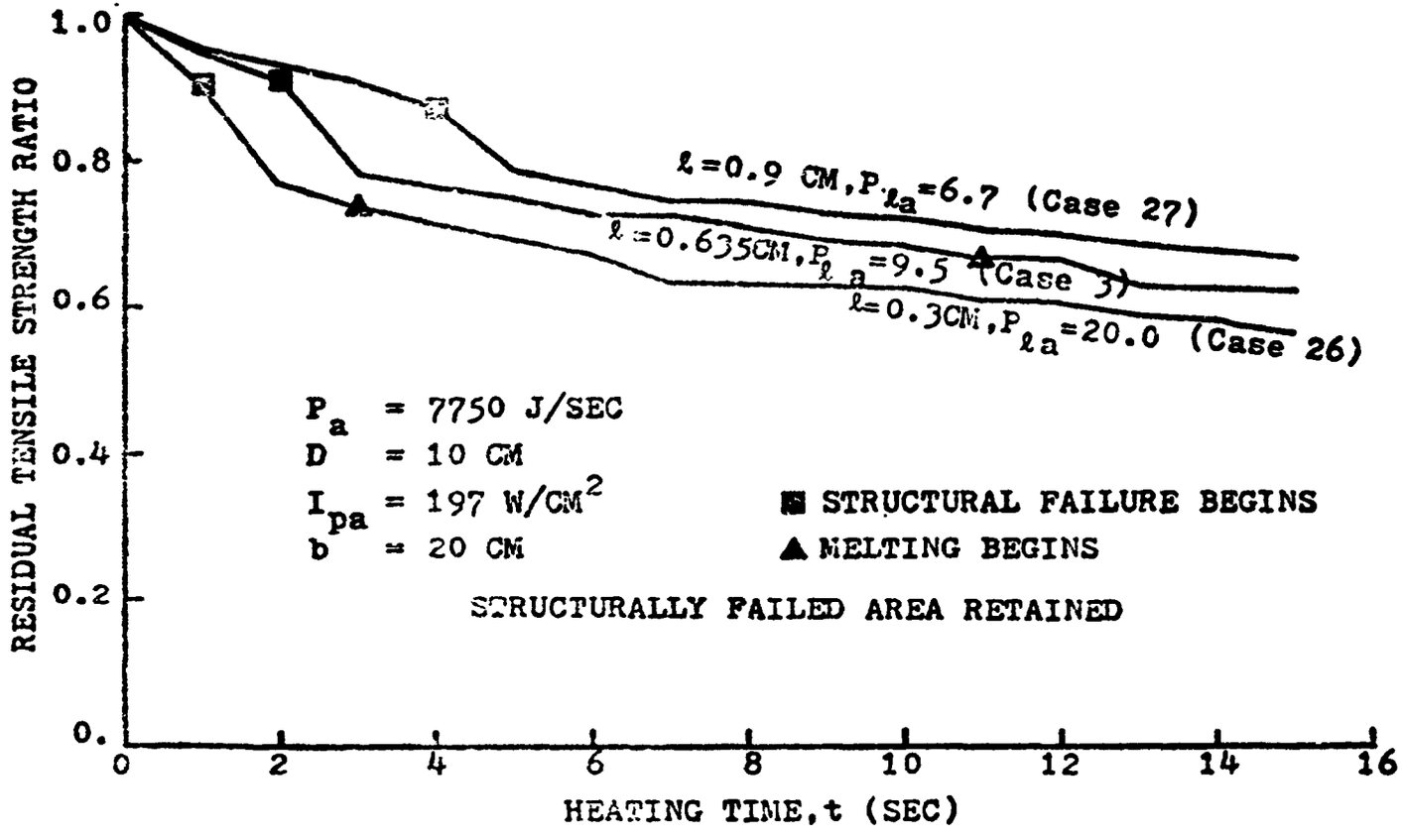

Fig. 19 Effect of Target Plate Thickness on Residual Tensile Strength

One objective of the present study was to determine the relative importance of the thermal stress damage mechanism relative to melting and thermal degradation. From the data presented thus far for the case of one-dimensional radial flux, one major conclusion is that the primary mode of damage (measured in terms of residual strength) is the generation of a structurally failed area by the combined action of thermal stresses and degradation. The relative contributions of each of these mechanisms to structural failure is thus of interest. A qualitative assessment of the relative contributions can be obtained by looking at the peak stresses and temperatures (outside the failed area) as shown in Fig. 20. This plot is typical for all the cases investigated in that once a structur lly failed area is initiated, the tangential compressive stresses remain at relatively high levels while the other stress components are reduced significantly. Fig. 21 and Fig. 22 show that peak tensile stresses remain very small for a wide range of beam powers and diameters. Since both peak tangential compressive stress and maximum temperature (outside failed area) occur at the radius of the failed area, it is concluded that these are the mechanisms which continue to expand the failed area with increasing time. That is, the failed area expands due to compressive yield failure.

Although thermal degradation is not generally a linear function of temperature, for the analytical approximations used in this study (Section VI) and the range of temperatures

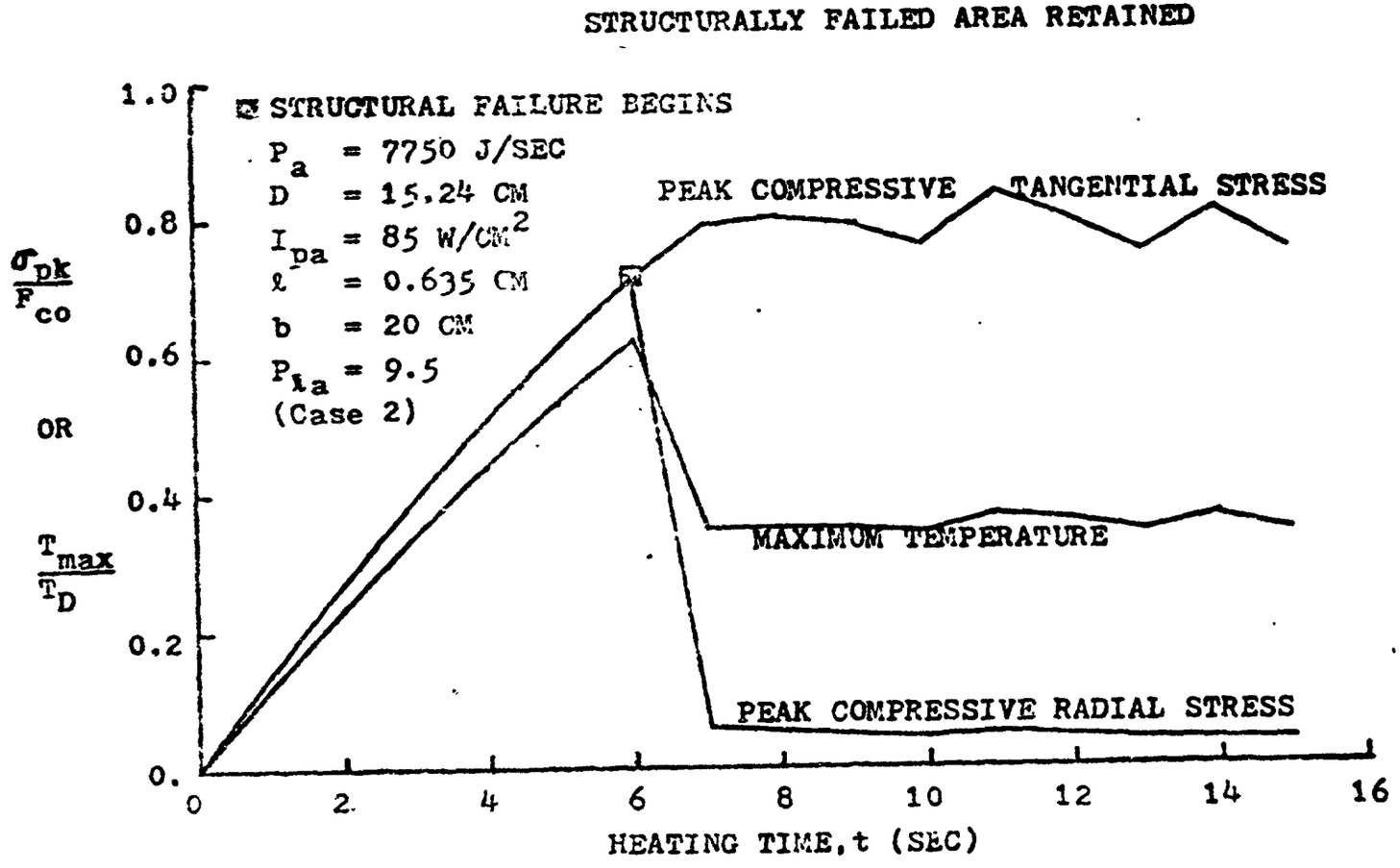

Fig. 20 Comparison of Contributions of Thermal Stresses and Thermal Degradation to Structural Failure

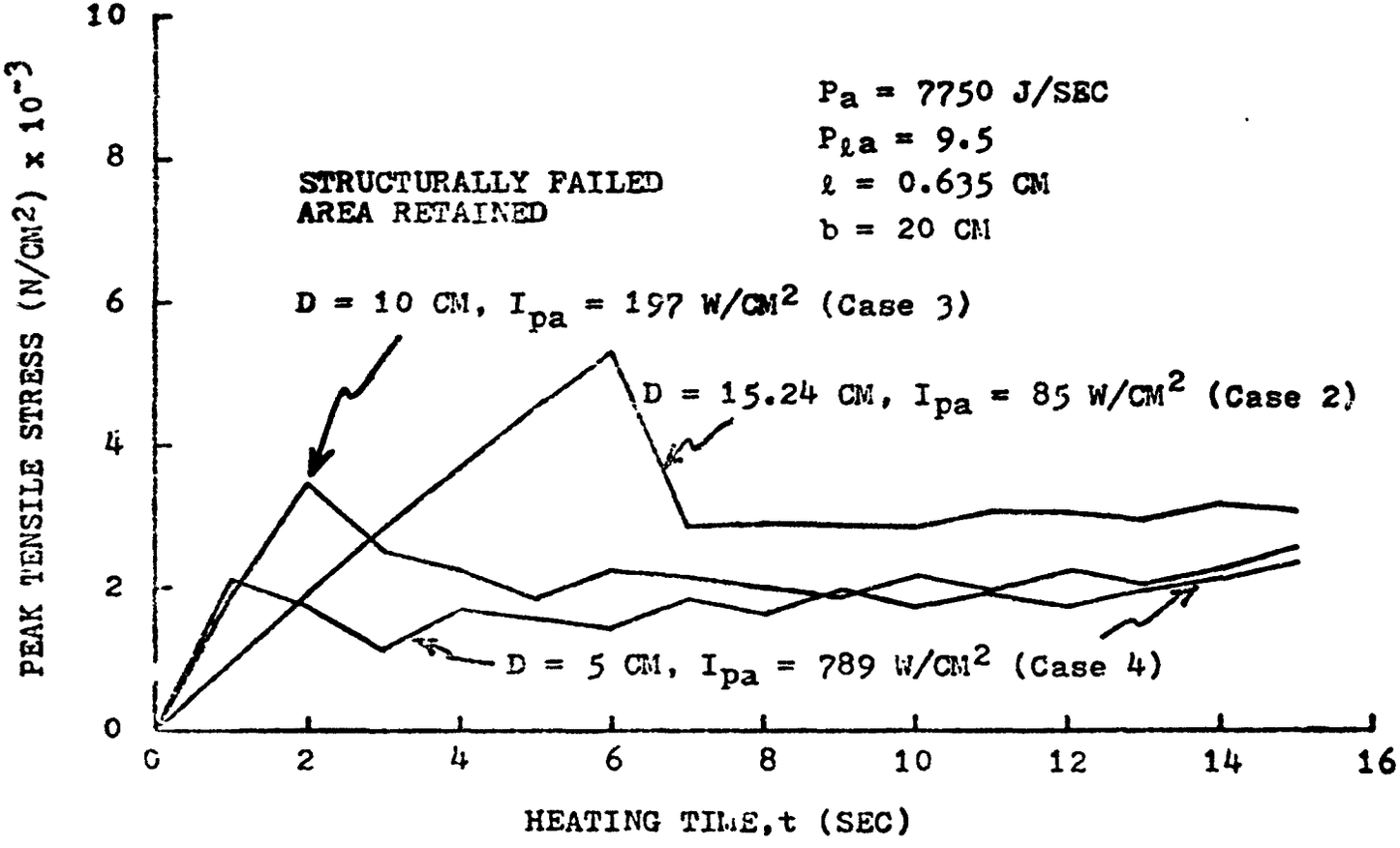

Fig. 21 Peak Tensile Thermal Stresses for a Range of Beam Diameters

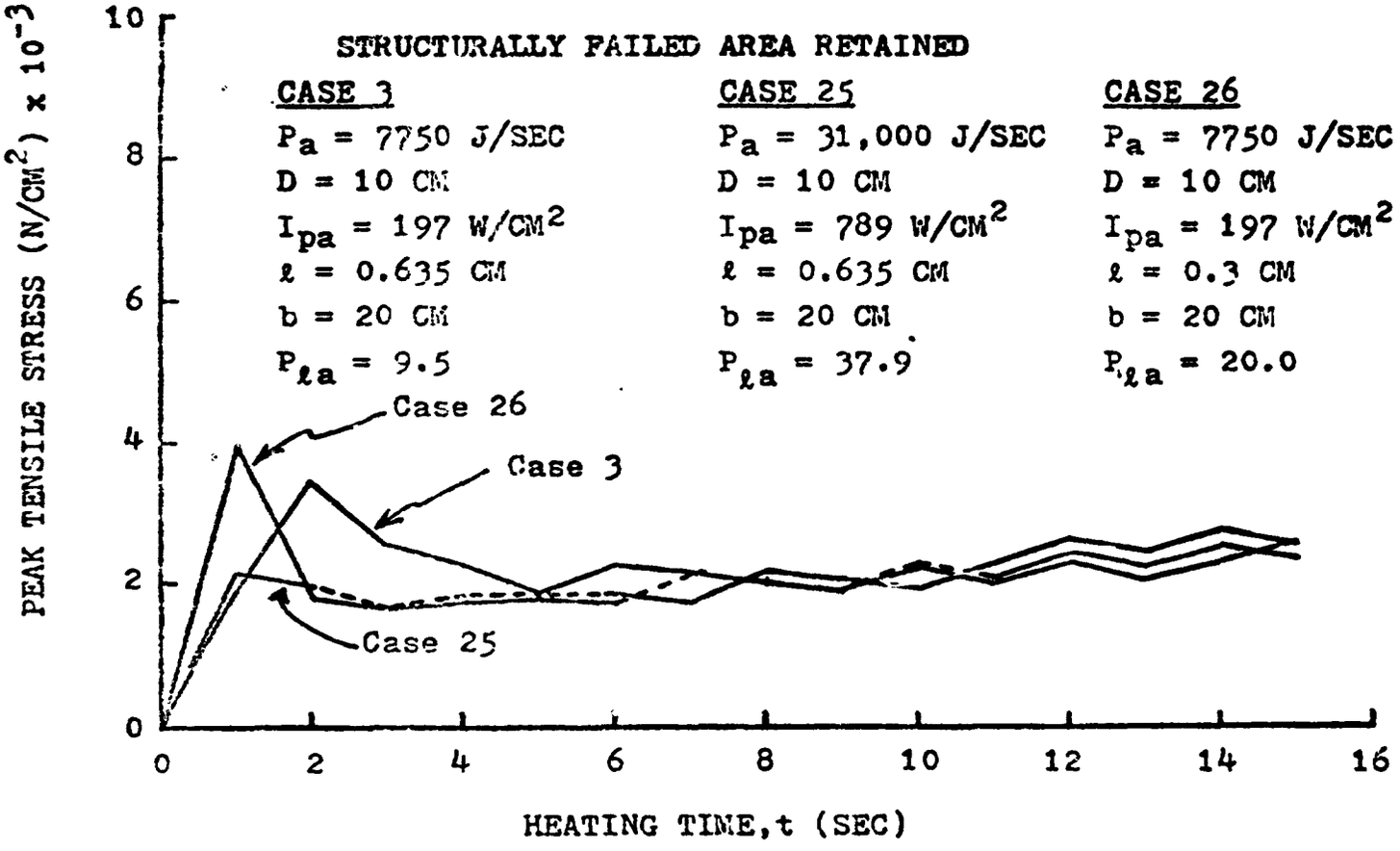

Fig. 22 Peak Tensile Thermal Stresses for a Range of Absorbed Powers

outside the failed area shown in Fig. 20, the relationship is essentially linear. Consequently, the temperature curve in Fig. 20 is a fairly good approximation of the compressive strength reduction due to thermal degradation. The general conclusion is then made that the compressive tangential thermal stresses contribute significantly more to structural failure than does thermal degradation.

A quantitative assessment of the relative contributions to structural failure does not seem feasible. The essential conclusion is that qualitatively, compressive tangential thermal stress at the edge of a failed area is the primary contributor, along with thermal degradation, to the expansion of the damaged or failed area.

From the analysis of the thermal stresses for the one-dimensional radial flux code (reference sample output in Appendix A), it was found that prior to structural failure or melting, thermal stress is a linear function of the beam power and consequently linear in absorbed power, peak absorbed flux density, and peak absorbed fluence through the following relationships.

$$P_a = \alpha_1 Q \tag{103}$$

$$P_a = \frac{\pi}{8} D^2 I_{pa} \tag{104}$$

$$F_{pa} = I_{pa} t \tag{105}$$

where

α_1 = absorptivity

Q = P_i = incident beam power

D = beam diameter

t = heating time

F_{pa} = peak absorbed fluence

I_{pa} = peak absorbed heat flux density

Thermal stresses also were found to be inversely proportional to the target plate thickness. These empirical findings were verified by examination of the algorithms used for temperature, eqn (27), and thermal stresses, eqns (55) and (56). These relationships suggested two dimensionless stress parameters which were studied to see whether they had any particular invariant qualities which might serve to characterize the thermal stress problem.

The parameter $\frac{\sigma \ell}{P_a}$, where σ represents any thermal stress component, expressed in consistent units, has the units of sec/cm^2 which are the inverse units of thermal diffusivity, κ. Hence, the parameter $\frac{\sigma \ell \kappa}{P_a}$ is dimensionless. The parameter $\frac{\sigma \ell}{I_{pa}}$ has the units of seconds. Dividing by the heating time is equivalent to replacing the peak absorbed flux density in the denominator by the peak absorbed fluence, giving another dimensionless parameter $\frac{\sigma \ell}{F_{pa}}$. Fig. 23 compares this parameter, using peak tensile stress, for three beam diameters, as a function of heating time.

The peak absorbed fluence used in Fig. 23 is that for a continuously solid plate without regard to the effect of

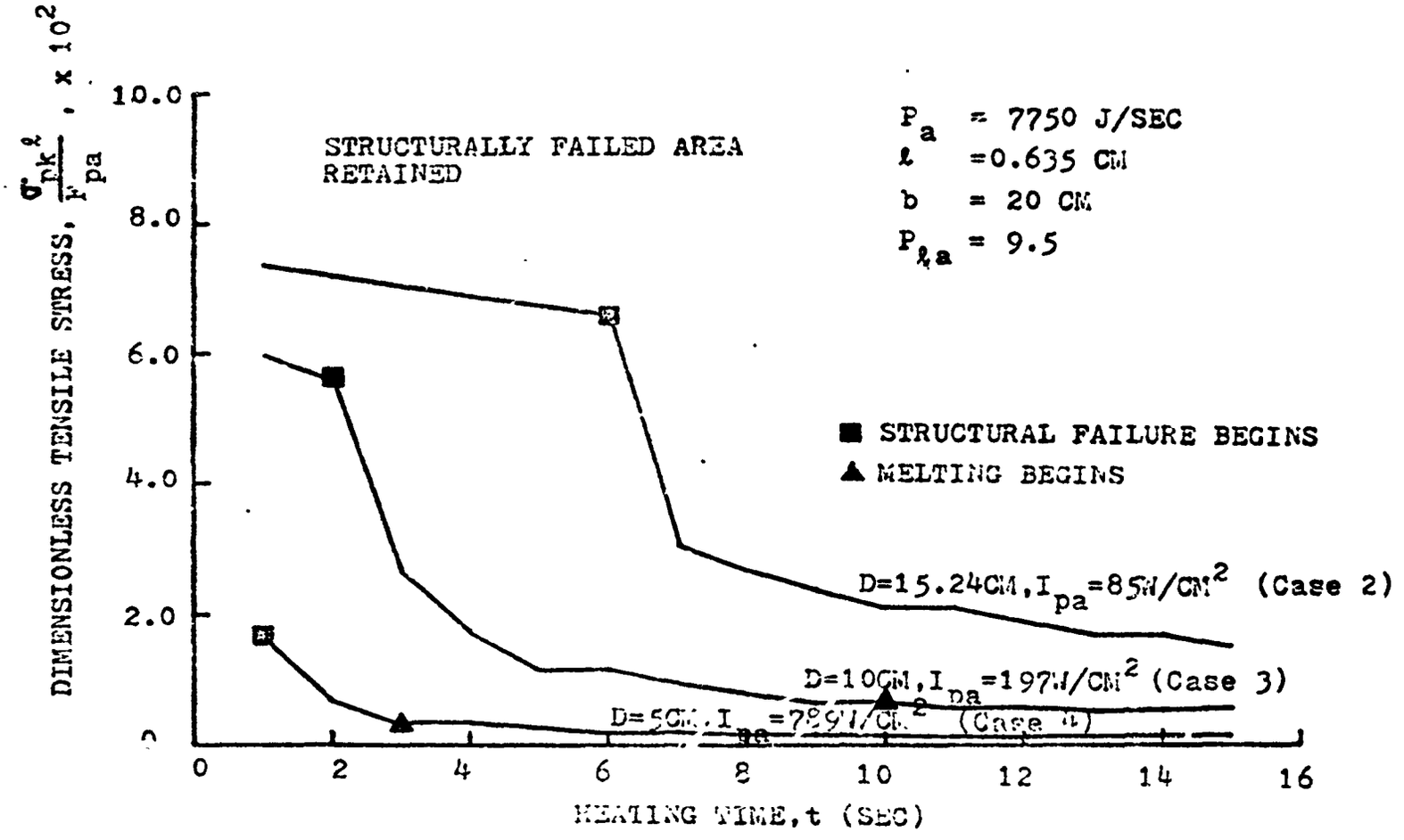

Fig. 23 Dimensionless Thermal Stress Ratio Based on Fluence

the expanding hole in the plate. When this effect is accounted for by using the actual peak absorbed fluence, the results are less orderly than in Fig. 23 due to the step function effect of the hole growth in the numerical model.

Fig. 24 shows the other dimensionless parameter described above for the same conditions of Fig. 23. Comparison of the two plots shows that there is less spread in the data based on $\frac{\sigma \ell \kappa}{P_a}$, and that the relative positions of the curves based on $\frac{\sigma \ell \kappa}{P_a}$ is more indicative of the relative peak tensile stresses, being a linear function of the peak tensile stress (see Fig. 21).

Figure 25 shows the development of peak thermal stresses for a typical case in which the heat conduction is initially axial. The figure shows the theoretical stresses for both one-dimensional axial and radial conductivity models for identical conditions. Radial flux stresses are given for a uniform beam flux distribution. The uniform beam is consistent with the constant flux distribution assumed in the axial conduction model. Fig. 25 shows that the initial transient and subsequent steady state peak stresses for one-dimensional axial flux remain fairly small relative to compressive yield or ultimate tensile strengths (23,) n/cm^2 and 44,820 n/cm^2, respectively).

For the flux density and thickness listed on Fig. 25, the initial conduction is primarily axial through-the-thickness if the beam diameter is at least 5.87 cm. In this case, $P_{\ell a} \geq 70.0$ as determined from eqn (75). Hence,

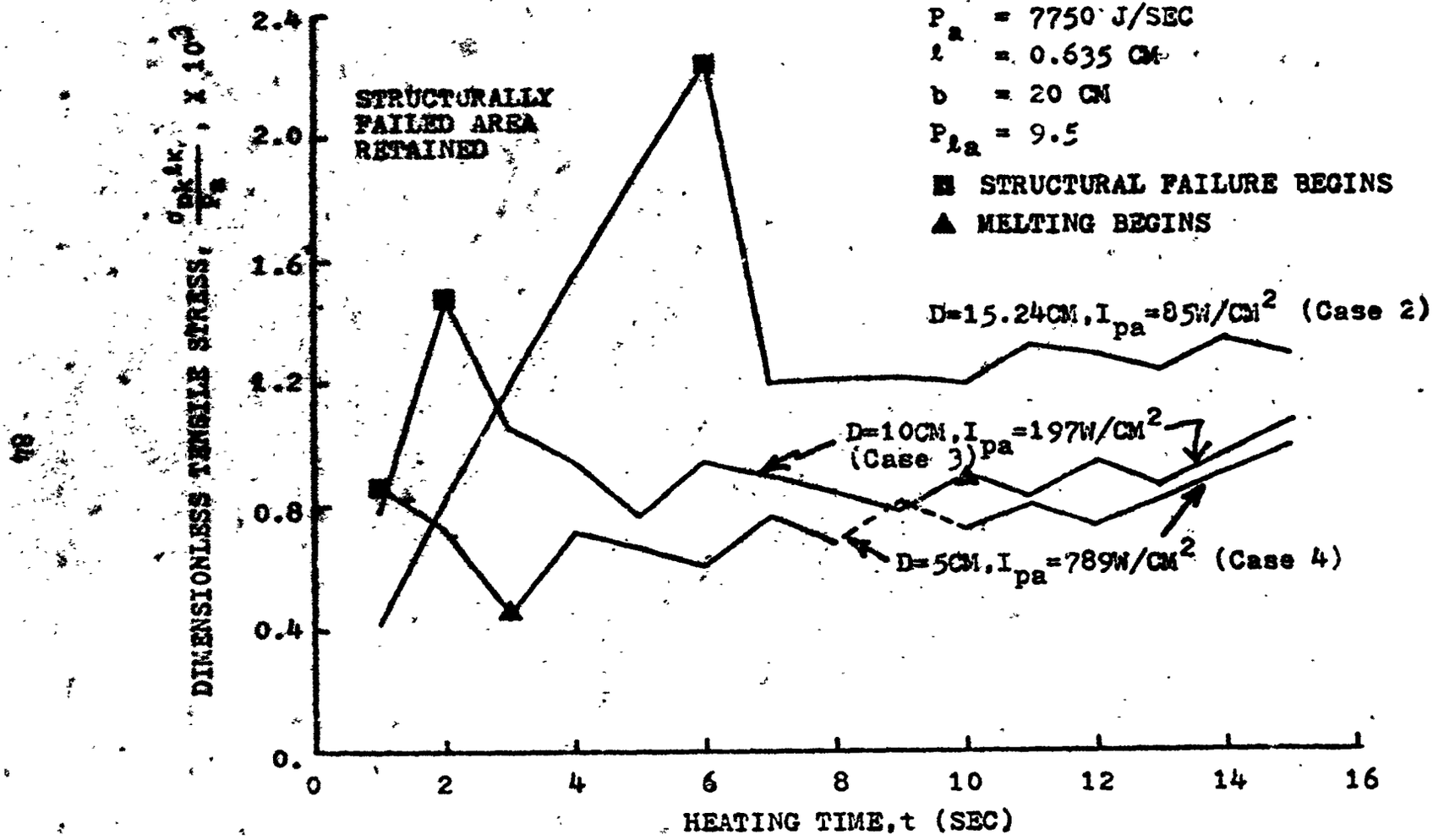

Fig. 24 Dimensionless Thermal Stress Ratio Based on Absorbed Power

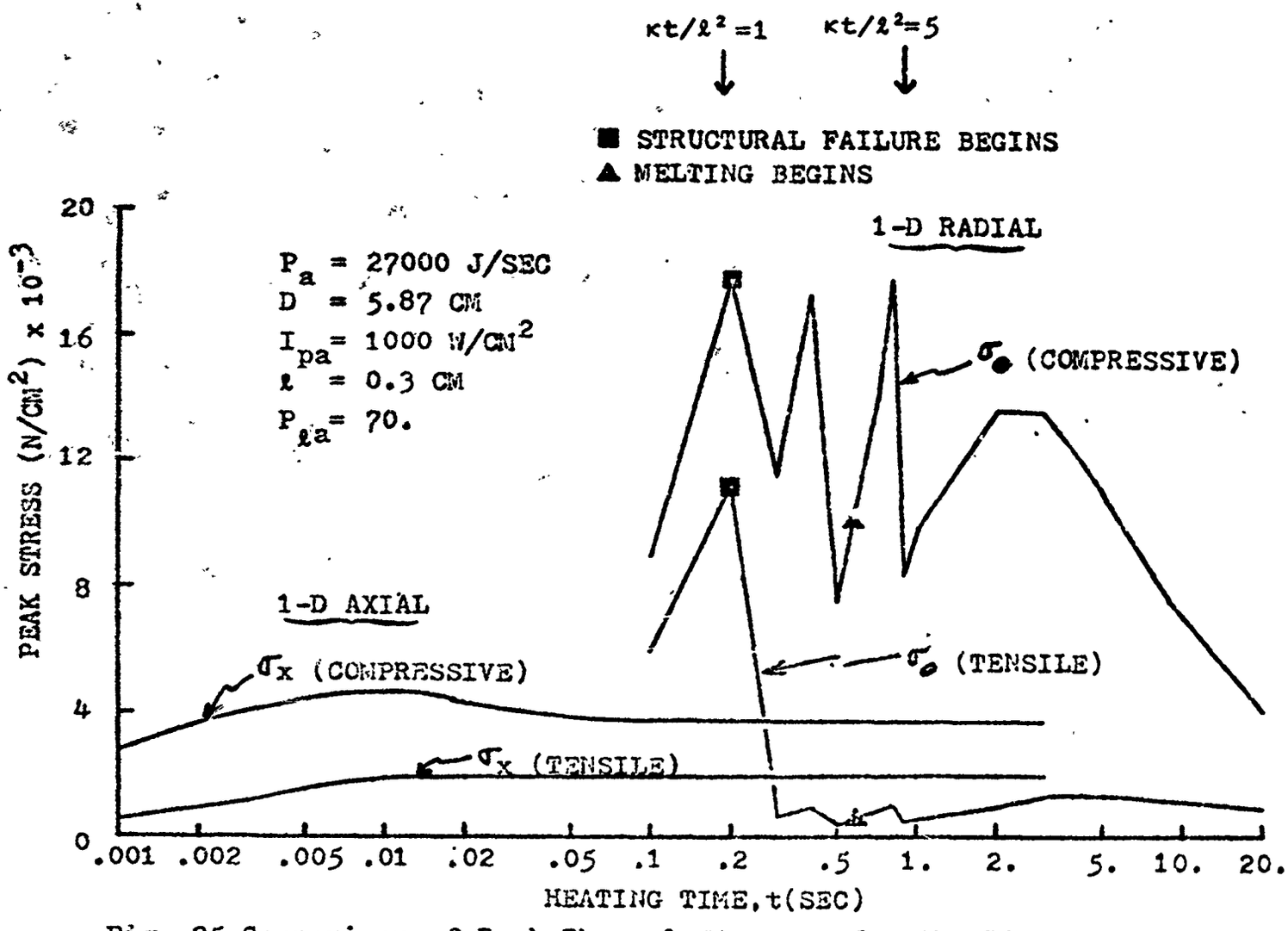

Fig. 25 Comparison of Peak Thermal Stresses for the Limiting One-Dimensional Heat Flux Models

heat flux for this case would remain axial until a hole is melted through the plate. No appreciable radial flux would develop in this time. Consequently, the radial flux results given in Fig. 25 are strictly academic and serve here to indicate the trends in thermal stress development for those cases where the flux vector becomes predominatly radial before melting occurs.

These results illustrate a bound on the radial flux model. If $P_{\ell a} \geq 70$ at the onset of heating, the target plate will melt through without any transition to a radial flux case. Hence, the radial flux model is not generally applicable if, initially, $P_{\ell a} \geq 70$. As noted earlier in this section, if $P_{\ell a} \leq 5$ at the onset of heating, the heat flux vector is primarily radial and remains so as long as heating continues. In intermediate cases ($5 \leq P_{\ell a} \leq 70$), the flux vector would be expected to become increasingly radial at long enough heating times. From eqn (87), the flux vector would be expected to be primarily radial at least by the time $\kappa t/\ell^2$ is about 5. The flux vector becomes primarily radial at ever shorter heating times for decreasing $P_{\ell a}$. The initial flux vector would be expected to be predominantly radial for values of $P_{\ell a}$ near 5 and to be mostly axial for values of $P_{\ell a}$ approaching 70. The axial flux thermal stress model is applicable for all heating times through melting if $P_{\ell a} \geq 70$.

Correlation of dimensionless power per unit thickness, $P_{\ell a}$, with the time to initial structural failure as predict-

ed by the one-dimensional radial flux model was investigated briefly. Fig. 26 presents the results of this correlation, using data, denoted by the circluar data points, that had been developed previously as part of the other analyses conducted.

A definite correlation is apparent which also appears to be a function of the laser beam diameter. The data presented include all of the pre-existing data available which was applicable. That is, no sorting of the data was done to bias the results. As noted previously, most of the data from the radial flux code are for heating conditions with $P_{\ell a} > 5$ which violates the assumed bound on the applicability of the model. Consequently, additional analyses are required to extend the correlations to values of $P_{\ell a} < 5$. The validity of the radial code correlations for $P_{\ell a} > 5$ were qualitatively assessed by plotting corresponding failure times for one-dimensional axial flux ($P_{\ell a} > 70$) on Fig. 26.

For one-dimensional axial flux, the heating time to complete thermal degradation can be expressed as follows by combining eqns (75) and (95) and substituting the 2024-T3 material values.

$$t_D = 0.658 \frac{D^2}{P_{\ell a}} \quad (D \text{ in cm}) \qquad (106)$$

This equation is plotted in Fig. 26 for three diameters corresponding to the radial flux data. The radial and axial

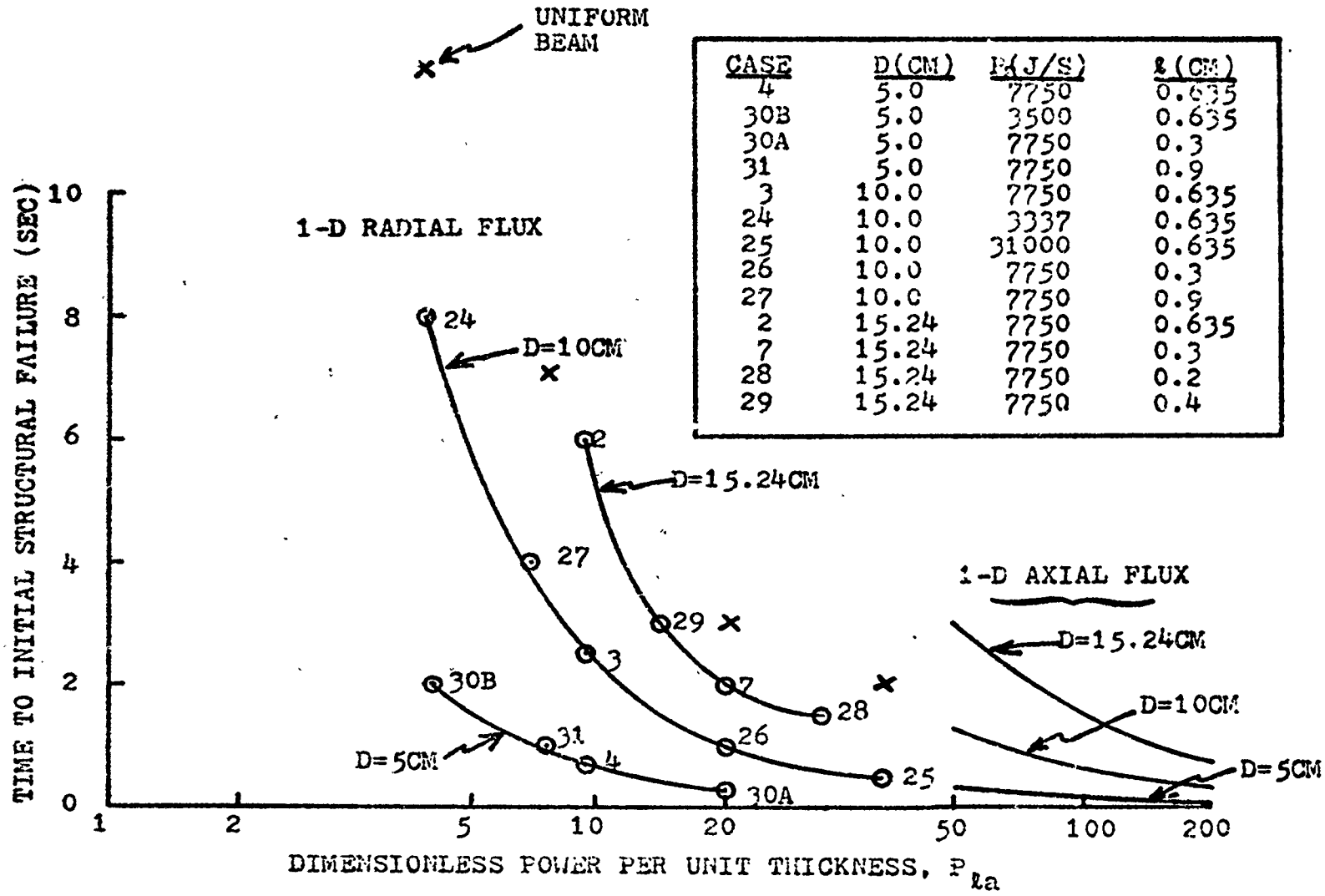

CASE	D(CM)	P(J/S)	ℓ(CM)
4	5.0	7750	0.635
30B	5.0	3500	0.635
30A	5.0	7750	0.3
31	5.0	7750	0.9
3	10.0	7750	0.635
24	10.0	3337	0.635
25	10.0	31000	0.635
26	10.0	7750	0.3
27	10.0	7750	0.9
2	15.24	7750	0.635
7	15.24	7750	0.3
28	15.24	7750	0.2
29	15.24	7750	0.4

Fig. 26 Correlation of Dimensionless Power per Unit Thickness with Initial Structural Failure Heating Time

flux data are not directly comparable because the radial data are based on a Gaussian heat flux density distribution and the axial model assumes a uniform distribution. To make a more consistent comparison, four radial flux code cases with a beam diameter of 10 cm were analyzed for a uniform flux distribution. These results are denoted in Fig. 26 by the x-symbol. The results of this limited comparison indicate that a possibly consistent relationship between failure time and $P_{\ell a}$ may exist over a wide range of $P_{\ell a}$ values. Further study of this relationship is necessary to obtain more definite conclusions.

Correlations of $P_{\ell a}$ with the size of structurally failed damage areas as a function of the laser beam diameter are shown in Fig. 27 for the cases listed in the previous figure. The data plotted are the radii of the structurally failed area at a heating time of 15 seconds. Smooth curves were drawn through the data points.

It was concluded that $P_{\ell a}$ does provide a consistent correlation with the structural damage size. Quantitative definition of this correlation was not established and is a topic requiring additional study. The correlation examined here is actually with the "dimensional" power per unit thickness, P_a/ℓ, since the additional quantities in $P_{\ell a}$ are material properties and only a single material was considered.

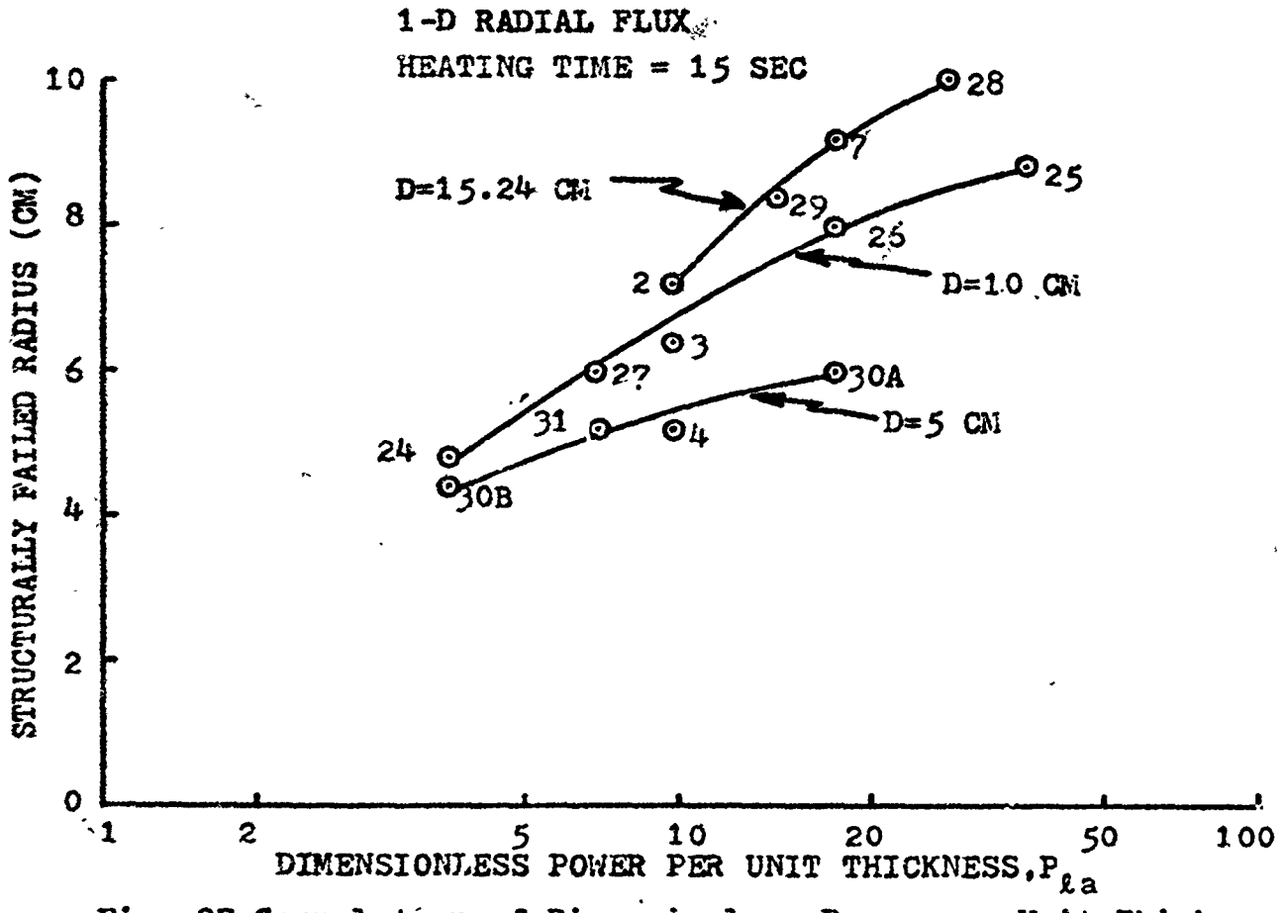

Fig. 27 Correlation of Dimensionless Power per Unit Thickness with Radius of Structurally Failed Area

VIII. Conclusions and Recommendations

Conclusions

For both limiting cases of one-dimensional axial and radial flux, the primary mode of damage is by generating a failed area under the laser beam. For axial flux conditions, the primary damage mechanism is thermal degradation of structural strength, based on the half-hour heating exposure data of (Ref 9). For the range of beam/target parameters considered here (see Section II), thermal stresses are relatively small. For the case of one-dimensional radial flux, the primary damage mode is structural failure due to the combined actions of thermal stresses and thermal degradation. If the structurally failed area is retained in the plate, melting may occur, but never precedes structural failure. Detailed conclusions are given in the following paragraphs.

Axial Flux. For this study, axial flux was defined to exist if the dimensionless power per unit thickness, $P_{\ell a}$, is greater than about 70. The flux was defined to become primarily radial for dimensionless thermal times, $\kappa t/\ell^2$, greater than about 5 since at this time the through-the-thickness temperature variation becomes less than ten percent. Two time regimes were identified as significant in characterizing the thermal stresses for axial flux. The maximum thermal stresses for the beam/target parameters of

interest occur during a transient stage when $\kappa t/\ell^2 < 1$. These maximum stresses become constants when expressed in the following dimensionless form

$$\left(\frac{\sigma_{xx}\kappa}{\phi_0 \ell}\right)_{\substack{\text{peak} \\ \text{tensile}}} = 3.30 \times 10^{-2} @ \kappa t/\ell^2 = 0.1 \qquad (107)$$

$$\left(\frac{\sigma_{xx}\kappa}{\phi_0 \ell}\right)_{\substack{\text{peak} \\ \text{compressive}}} = -7.94 \times 10^{-2} @ \kappa t/\ell^2 = 0.06 \qquad (108)$$

The peak through-the-thickness stresses decrease with increasing time until they reach a steady state value for all $\kappa t/\ell^2 > 1$. For these steady state conditions, the peak thermal stresses are slightly less than the maximum values given in eqns (107) and (108). For the range of beam/target parameters considered in this study, the thermal stresses remain very small relative to target material strength.

Since both melting and thermal degradation are direct functions of temperature, thermal degradation is the initial damage mechanism because the temperature necessary to reduce the material strength to zero is lower than the temperature required for melting. If it is assumed that any material failed by thermal degradation remains in place in the plate, melting will subsequently occur with continued heating. Any material melted was assumed throughout this study to be immediately removed.

For axial flux conditions the damage is essentially restricted to the area under the incident beam spot. Consequently, the damage size would correspond closely to the

beam diameter, for a spatially uniform flux density distribution. For a Gaussian beam, the damage area would be restricted to an area near the beam axis because of the much lower flux density near the beam edges which would tend to develop radial flux. The time required to fail an area equal to the beam spot size is much less than for one-dimensional radial flux.

Radial Flux. The heat conduction in the heated target plate was defined to be essentially one-dimensional radial if $P_{\ell a} < 5$. For cases where $5 < P_{\ell a} < 70$, the flux would be expected to become increasingly radial with increasing heating time. The numerical radial flux code developed as part of this study would be expected to give approximate results for heating conditions with these intermediate values of $P_{\ell a}$ at long enough heating times ($\kappa t/\ell^2 > 5$) and accurate results for $P_{\ell a} < 5$. Temperatures and thermal stresses for the radial code are compared to those from a two-dimensional NASTRAN finite element analysis in Appendix C.

Based on the data from the one-dimensional radial analysis, it was concluded that the primary damage mechanism for radial flux heating conditions is structural failure by thermal stresses and strength degradation in combination. The primary contributor to residual tensile strength reduction is from the reduction in net section load carrying ability resulting from structural failure of a circular portion of the plate. Structural failure is due primarily

to compressive tangential thermal stresses, in combination with thermal degradation. Reductions in residual strength due to thermal degradation and thermal stresses outside the failed area are much less than that due to the failed area.

Thermal degradation contributes less to residual strength reduction outside the failed area than do thermal stresses because significant temperatures are restricted to the immediate vicinity of the failed area while tensile thermal stresses are distributed over most of the unfailed plate area.

Slightly less residual strength reduction occurs if the structurally failed area is assumed to be immediately removed, forming a hole, than for the assumption that the failed area is retained and continues to absorb and conduct heat. If the structurally failed area is retained, subsequent melting produces a hole. Melting does not significantly affect residual tensile strength except for large heat flux densities which produce melting at short heating times. In this case the rapid hole formation retards residual strength reduction because most of the subsequent incident flux passes through the melted hole.

The effect of increasing beam diameter is to retard structural failure and melting, and to increase residual strength reduction at the longer heating times. Increasing beam power and decreasing target plate thickness have the direct effects of promoting earlier structural failure and melting, and increasing residual strength reduction.

The most significant difference in the damage associated with the limiting one-dimensional heat flux cases is in the size of the damage area. Radial flux heating has the potential for producing failed areas larger than the incident beam spot size while axial flux damage is essentially restricted to the area under the beam. Additional damage due to thermal stresses outside any failed area is produced by radial flux in contrast to axial flux heating.

Recommendations

Based on the results of this study, the following recommendations are made.

1. Additional NASTRAN analyses should be conducted to verify the one-dimensional heat conduction limits based on dimensionless power per unit thickness, $P_{\ell a}$.

2. The apparent correlation of damage parameters with $P_{\ell a}$ should be more firmly established by additional studies using the analytical techniques and numerical radial code developed in this study.

3. The realism and accuracy of the TSTRESS radial flux code should be improved by the following improvements.

   a. Include temperature dependent material properties.

   b. More realistic modeling of the thermal degradation of structural strength properties based on laser heating exposure data.

   c. Include heat losses due to surface radiation

and convection.

d. Include melt dynamics and interaction with the incident flux.

4. Additional materials should be studied.

5. Linear elastic fracture mechanics should be applied to improve the realism of the damage tolerance analyses.

6. The effect of target plate size should be analyzed.

7. Plasticity and target pre-loading effects should be studied.

8. The effects of assuming uncoupled quasi-static heat conduction/thermoelasticity theory should be investigated.

Bibliography

1. Wigglesworth, Richard G. "A Numerical Model of Surface Recession Phenomena of Metals Subjected to Laser Radiation in an Aerodynamic Environment." Master's Thesis, Air Force Institute of Technology, Wright-Patterson Air Force Base, Ohio, 1972.

2. McCormick, Caleb W. The NASTRAN User's Manual. NASA SP-222(01). Washington, D.C.: National Aeronautics and Space Administration, May 1973.

3. Ready, John F. Effects of High-Power Laser Radiation. New York: Academic Press, 1971.

4. Carslaw, H. S. and Jaeger, J. C. Conduction of Heat in Solids. Second Edition, London: Oxford University Press, 1959.

5. Boley, Bruno A., and Weiner, Jerome H. Theory of Thermal Stresses. New York: John Wiley & Sons, Inc. 1960.

6. Torvik, Peter J. A Numerical Procedure for Two Dimensional Heating and Melting Calculations, with Applications to Laser Effects. AFIT TR 72-2. Wright-Patterson Air Force Base, Ohio: Air Force Institute of Technology, March 1972.

7. Fung, Y. C. A First Course in Continum Mechanics. Englewood Cliffs, N.J.: Prentice-Hall, Inc. 1969.

8. Torvik, Peter J. Some Further Numerical Studies of Laser Induced Melting and Vaporization. AFIT TR 73-1. Wright-Patterson Air Force Base, Ohio: Air Force Institute of Technology, Jan. 1973.

9. MIL-HDBK-5B. Military Standardization Handbook, Metallic Materials and Elements for Aerospace Vehicle Structures, Volume 1. Washington, D.C.: Department of Defense, 1 Sept. 1971.

10. MARC-CDC Non-linear Finite Element Analysis Program, User Information Manual. Volumes I, II, III. Minneapolis, Minn: Control Data Corporation, Nov.6, 1974.

11. Hurwitz, Myles M. Additions to the NASTRAN User's Manual and Theoretical Manual for a Thermostructural Capability for NASTRAN Using Isoparametric Finite Elements. CMD-1-73. Huntsville, Ala.: George C. Marshall Space Flight Center, Jan. 1973.

12. Wendlandt, B. C. H. Theoretical Studies of the Interaction of High-Power Laser Beams and Metals. Report 547. Maribyrnong, Victoria, Australia: Defence Standards Laboratories, May, 1973.

13. Interaction Study, Vol. IV, Task IV-Structural Degradation by Short Time Heating. AFWL-TR-70-157, Vol. IV. Kirtland Air Force Base, New Mexico: Air Force Weapons Laboratory, Dec. 1970.

14. Hanly, K., Lagedrost, J. and Carmichael, D. C. Mechanical Properties of Structural Materials on Rapid Heating. Draft report. Columbus, Ohio: Battelle Columbus Laboratories, Feb. 24, 1975.

15. Stefansky, T., Triebes, K., Shea, J. Temperature-Induced Degradation of Mechanical Properties Following Instantaneous Heating. AFWL-TR-71-62. Kirtland Air Force Base, New Mexico: Air Force Weapons Laboratory, Sept. 1971.

16. Gilbert, Keith G. and Reinke, R. Rapid Laser Heating of Metals Under Constant Uniaxial Stress. AFWL-TR-72-12. Kirtland Air Force Base, New Mexico: Air Force Weapons Laboratory, May 1972.

17. Moon, Donald P. and Simmons, Ward F. Selected Short-Time Tensile and Creep Data Obtained Under Conditions of Rapid Heating. DMIC Report 130. Columbus, Ohio: Defense Metals Information Center, June 17, 1960.

18. Honeycutt, John H. Rapid Heating and Loading of 70-75-T6 Aluminum Alloy Sheet. Report No. RS-TR-70-6. Redstone Arsenal, Alabama: U.S. Army Missile Command, May 1970.

19. Torvik, Peter J. "Predictions of Melt-Through Times for Laser Heating." AIAA 13th Aerospace Science Meeting, Pasadena, Calif., Jan. 20-22, 1975.

20. Breaux, J. J. "Simple Formulas for CW Laser Burnthrough Times When Radial Heat Conduction is Significant." BRL-1834, Sept. 1975.

21. McClintock, F. A. and Argon, A. S. Mechanical Behavior of Materials. Reading, Mass: Addison-Wesley Publishing Co., 1966.

22. Johnson, R. L. and O'Keefe, J. D. "Laser Burnthrough Time Reduction Due to Tangential Airflow - An Interpolation Formula". AIAA Journal, 12:1106-1109 (August 1974).

23. O'Keefe, J. D. and Johnson, R. L. "Laser Melt Through

Time Reduction due to Aerodynamic Melt Removal." AIAA Journal, 14: 776-780 (June 1976).

24. Ketter, R. L. and Prawel, Jr., S. P. Modern Methods of Engineering Computation. New York: McGraw-Hill Book Company, 1969.

25. Leech, C. M. The Prediction of Thermodynamic Damage of Materials Irradiated by Intense Laser Beams. DREV R-672/72. Quebec, Canada: Defence Research Establishment, November 1972.

26. Hsu, T. R. "Transient Thermal Stresses on a Finite Disk Due to a Continuous Point Heat Source." Journal of Engineering for Industry, 357-365 (May 1970).

27. Boley, Bruno A. "The Determination of Temperature, Stresses, and Deflections in Two-Dimensional Thermoelastic Problems." Journal of Aeronautical Sciences, 67-75 (January 1956).

28. Gatewood, B. E. "Thermal Stresses in Moderately Thick Elastic Plates." Journal of Applied Mechanics, 432-436 (September 1959).

29. Lee, C. W. "Thermal Stresses in a Thick Plate." Journal of Solids and Structures, 6:605-615.

30. Ghosh, A. K. "Review on High-Power-Laser Damage to Materials II." RCA Review, 35:279-319 (June 1974).

31. Camburn, G. Personal Communication. July 1975.

32. Torvik, Peter J. Thermal Response Calculations and Their Role in the Design of Experiments. AFIT TR 73-6. Wright-Patterson Air Force Base, Ohio: Air Force Institute of Technology, December 1973.

APPENDIX A

Numerical Radial Flux Thermal Stress Computer Program (TSTRESS) Listing

```
      PROGRAM TSTRESS(INPUT,OUTPUT)
C  THIS PROGRAM COMPUTES THERMAL STRESSES IN AXISYMMETRICALLY HEATED PLATE
C    FOR 1-D RADIAL HEAT FLUX
C  RHOI=MATERIAL DENSITY(GM/CC)
C  CONDI=MATERIAL THERMAL CONDUCTIVITY(JOULE/SEC CM DEG C)
C  ALPHAI=MATERIAL ABSORPTIVITY
C  CAPPA=THERMAL DIFFUSIVITY(SQ CM/SEC)
C  TMELT=LOWER MELTING TEMPERATURE(DEG C)
C  TUMELT=UPPER MELTING TEMPERATURE(DEG C)
C  HFUSE=HEAT OF FUSION(JOULE/GM)
C  T1=MELT-THROUGH TIME(SEC) FOR 1-D AXIAL HEAT FLUX
C  PA=ABSORBED POWER(JOULES/SEC)
C  ENGABS=ABSORBED ENERGY(JOULES)
C  FLUENCE=ABSORBED ENERGY PER UNIT HEATED AREA(JOULES/SQ CM)
C  FLNCPK=PEAK FLUENCE(JOULES/SQ CM)
C  PLA=DIMENSIONLESS POWER PER UNIT THICKNESS
C  E=MATERIAL MODULUS OF ELASTICITY(NEWTONS/SQ CM)
C  ALPHAT=MATERIAL COEFFICIENT OF THERMAL EXPANSION(PER DEG C)
C  GAUSSIAN BEAM ONLY IF GAUSS = 0., OTHERWISE HAVE UNIFORM BEAM.
C  JTIME=TOTAL NO. TIME INCREMENTS(<300)
C  NTIME=NO. OF PRINTOUTS OF CALCULATIONS(AT EQUAL TIME INCREMENTS)( (< ITIME)
C  TOOFF=TIME OF BEAM SHUTDOWN (SEC)
C  N=NO. OF RADIAL ELEMENTS(CANNOT EXCEED 100)
C  DELR=WIDTH OF RADIAL ELEMENTS(CM)
C  DELT=COMPUTATION TIME INCREMENT(SEC)
C  EL=PLATE THICKNESS(CM)
C  TI=INITIAL PLATE TEMPERATURE(DEG C)
C  B=PLATE RADIUS(CM)
C  D=BEAM DIAMETER(CM)
C  QBEAM=BEAM HEAT FLUX(JOULE/SEC)
C  IPA=PKABSI=PEAK ABSORBED HEAT FLUX DENSITY(JOULE/SEC SQ CM)
C  RMELT=RADIUS OF MELTED HOLE(CM)
C  RFS=RADIUS OF FAILED HOLE DUE TO THERMAL STRESSES ONLY (CM)
C  RFD=RADIUS OF FAILED HOLE DUE TO THERMAL DEGRADATION ONLY (CM)
C  RFDS=RADIUS OF FAILED HOLE DUE TOCOMBINED ACTION OF THERMAL STRESSES &
C     DEGRADATION (CM)
C  RFSC=RADIUS OF FAILED HOLE DUE TO STRESS CONCENTRATION (CM)
C  RFAIL=RADIUS OF FAILED AREA OF PLATE (CM)
C  SIGMAR(I)=RADIAL STRESS COMPONENT AT INNER EDGE OF ELEMENT I (N/SQ CM)
C  SIGMAA(I)=TANGENTIAL STRESS COMPONENT AT INNER EDGE OF ELEMENT I (N/SQ CM)
C  TAUMAX(I)=MAXIMUM SHEAR STRESS COMPONENT AT INNER EDGE OF ELEMENT I (N/SQ CM)
C  ULTENS=ROOM TEMPERATURE ULTIMATE TENSILE STRESS (N/SQ CM)
C  ULTEN1=ELEVATED TEMPERATURE ULTIMATE TENSILE STRESS (N/SQ CM)
C  ULTSHR=ROOM TEMPERATURE ULTIMATE SHEAR STRESS (N/SQ CM)
C  ULTSHR1=ELEVATED TEMPERATURE ULTIMATE SHEAR STRESS (N/SQ CM)
C  COMPYLD=ROOM TEMPERATURE COMPRESSIVE YIELD STRESS (N/SQ CM)
C  COMPYD1=ELEVATED TEMPERATURE COMPRESSIVE YIELD STRESS (N/SQ CM)
C  STRNGTH=AVERAGE ELEVATED TEMPERATURE ULTIMATE TENSILE STRESS (N/SQ CM)
C  P=STRNGTH/ULTENS,
C  RESIDE(I)=STRNGTH
C  PDEG=P
C  SIGAPP=REMOTELY APPLIED TENSILE STRESS (N/SQ CM)
C  RESFAIL=RESIDUAL STRENGTH DUE TO FAILED AREA(N/SQ CM)
C  RESMELT=RESIDUAL TENSILE STRENGTH DUE TO MELTING ONLY (N/SQ CM)
C  RESTRS=RESIDUAL TENSILE STRENGTH DUE TO MELTING AND THERMAL STRESSES(N/SQCM)
C  RESTRSD=RESIDUAL TENSILE STRENGTH DUE TO MELTING,T.STRESSES,&DEGRADATION
C            (N/SQ CM)
```

```
      DIMENSION TEMP(101),SIGMAR(100),SIGMAA(102),TABS(100),TAUMAX(100),
     1R1(102),QSIGR(102),QSIGA(102),QTAU(102),QSREAK(302),QSAPEAK(302),
     1QTPEAK(302),TCALC(302),ASRMAX(302),CAPSIGA(102)
      READ*,RHO1,COND1,CP1,ALP441,E,A_P44T,ULTENS,ULTSHR,TMELT,HFUSE
     1,TUMELT,COMPYLD
      READ*,DELR,N,DELT,EL,QBEAM,TI,JTIME,D,GAUSS,TJOFF,MTIME
      PRINT*," "
      IF(RHO1.EQ.2.70)PRINT*," MATERIAL IS 2024-T3  ALUMINUM"
      PRINT*,"     DENSITY=",RHO1,"GM/CC  THERMAL CONDUCTIVITY=",COND1,"J
     1OULE/SEC-CM-DEG.C  HEAT CAPACITY=",CP1,"JOULE/GM-DEG.C"
      PRINT*,"     ABSORPTIVITY=",ALPHA1,"  MELTING TEMP.=",TMELT,"DEG.C
     1 HEAT OF FUSION=",HFUSE,"JOULE/GM  COEFF. OF THERMAL EXP.=",ALP44T
     1,"PER DEG.C"
      PRINT*,"     UPPER MELTING TEMP.=",TUMELT,"DEG.C"
      PRINT*,"     ULT. TENSILE STRENGTH=",ULTENS,"N/SQ CM  ULT.SHEAR STR
     1ENGTH=",ULTSHR,"N/SQ CM   YOUNGS MODULUS=",E,"N/SQ CM"
      PRINT*,"     COMPRESSIVE YIELD STRENGTH=",COMPYLD "N/SQ CM"
      IF(GAUSS.EQ.0.)GO TO 5
      PRINT*,"  UNIFORM BEAM"
      GO TO 6
    5 PRINT*,"  GAUSSIAN BEAM"
    6 B=N*DELR
      D1=D/2.
      NR=N+1
      PI=2.*ASIN(1.)
      AREA=PI*(D**2.)/4.
      PA=ALPHA1*QBEAM
      PKABSI=R.*PA/(PI*D**2)
      IF(GAUSS.NE.0.)PKABSI=PKABSI/2.
      CAPPA=COND1/(RHO1*CP1)
      CAPPAL2=CAPPA/(EL**2.)
      TI=RHO1*EL*((CP1*(TMELT-TI)+HFUSE)/PKABSI
      PLA=PI*(D**2)/(CAPPA*TI*6.)
      IF(GAUSS.NE.0.)PLA=PLA*2.
      QL=100.*PKABSI/(EL)
      PALKAPA=100.*PA/(CAPPA*EL)
      K4=4
      LTIME=JTIME/MTIME
      PRINT*,"     DELR=",DELR,"CM   N=",N-1," DELT=",DELT,"SEC  L=",EL,"C
     1M  QBEAM=",QBEAM,"JOULES/SQ CM-SEC  TI=",TI,"DEG C  JTIME=",JTIME,
     1"  D=",D,"CM  B=",B,"CM"
      STAB=(RHO1*CP1*DELR**2)/(2.*COND1)
      TEST=0.9*STAB
      IF(DELT.LE.TEST)GO TO 10
      PRINT*,"     DELT REDUCED FROM ",DELT," TO ",TEST," SEC."
      DELT=TEST
   10 PRINT*,"     MTIME=",MTIME," LTIME=",LTIME,"   TOOFF=",TOOFF,"SEC"
      PRINT 7,PKABSI,TI,PLA
    7 FORMAT(4X4HPA=,F9.2,22HJOULES/SQ CM-SEC   TI=,F7.2,10HDEG C   PLA=,
     1F7.2)
      DO 554 IR=1,2
      IF(IR.EQ.1)GO TO 23
      PRINT*," "
      PRINT*,"  RUN ALLOWING HOLE IN PLATE DUE TO MELTING ONLY"
      GO TO 22
   23 PRINT*," "
      PRINT*,"  RUN ALLOWING HOLE IN PLATE DUE TO MELTING OR  STRUCTURAL
     1 FAILURE"
   22 TIME=0.0
    8 PRINT TEMPS AND STRESSES, ONLY WHEN LCOUNT=.TIME
      LCOUNT=1
      TS=0
```

```
120               DO 15 I=1,M
                  R=(I-1)*DELR
                  RAVG=R+DELR/2.
                  IF(GAUSS.NE.0.)GO TO 11
                  IF(RAVG.GT.D)GO TO 12
125               QARS(I)=PKARSI*PI*DELR*(2.*R+DELR)*EXP(-9.*(RAVG/D)**2)
                  GO TO 15
               11 IF(RAVG.GT.D)GO TO 12
                  QARS(I)=PKARSI*PI*DELR*(2.*R+DELR)
                  GO TO 15
130            12 QARS(I)=0.0
               15 TEMP(I)=TI
                  TEMP(M+1)=TI
                  IOFF=(TOOFF/DELT+1)
            C  IOFF=NUMBER OF TIME INCREMENTS UNTIL BEAM SHUT-OFF.
135               IFAIL=0
                  IMELT=0
                  RFD=0.
                  RFS=0.
                  RFDS=0.
140               RMELT=0.
                  RFAIL=0.
                  KRS=0
                  KRDS=0
                  DO 50 IT=1,JTIME
145               TIME=IT*DELT
                  IF(TIME.LE.TOOFF)GO TO 16
                  DO 17 I=1,M
               17 QARS(I)=0.0
               16 IF(IR.EQ.1)IMELT=IFAIL
150               CALL TEMPRAD(QARS,DELR,D,CONDL,M,RADI,CPL,EL,TEMP,DELT,TMELT,TUMEL
                 1T,IMELT)
                  JJ=IMELT+1
                  DO 120 I=JJ,M
                  IF(TEMP(I).LT.TUMELT)GO TO 121
155               RMELT=I*DELR
                  IMELT=I
               120 CONTINUE
               121 CALL STRESSR(E,ALPHAT,B,DELR,SIGMAR,SIGMTA,TEMP,M,TAUMAX,IFAIL)
                  IF(IT.EQ.IOFF)LOCUNT=LTIME
160               IF(LCOUNT.NE.LTIME)GO TO 21
                  TKL2=CAPPAL2*TIME
                  PRINT 24,TIME,TKL2
                24 FORMAT(3X8HTIME=,F5.2,16HSEC   KT/(L**2)=,F10.5)
                  PRINT*,"    R(CM)      TIME(C)      SIGMA R          SIGMA THETA
165               1     TAUMAX       SIGR*L/IPA    SIGA*L/IPA    TAU*L/IPA    SIGA*L*K/PA
                  1"
                  PRINT*,"                                    (N/SQ CM)          (N/SQ CM)
                  1     (N/SQ CM          (SEC)         (SEC)         (SEC)"
                21 DO 70 K=1,KM
170               QSIGR(K)=SIGMAR(K)/QL
                  QSIGA(K)=SIGMA(K)/QL
```

```
      CAPSIGA(K)=SIGMAA(K)/PALKAPA
      QTAU(K)=TAUMAX(K)/QL
      R=(K-1)*DELR
  170 IF(LCOUNT.NE.LTIME)GO TO 30
      PRINT 25,R,TEMP(K),SIGMAR(K),SIGMAA(K),TAUMAX(K),QSIGR(K),QSIGA(K)
     1,QTAU(K),CAPSIGA(K)
   25 FORMAT(4X,F7.3,F10.1,F14.1,F10.1,F10.1,4F13.5)
   30 CONTINUE
  180 20 CALL RADFAIL(TEMP,RFD,RFS,RFDS,NR,DELR,SIGMAR,SIGMAA,TAUMAX,ULTEMS
     1,COMPYLD,ULTSHR,IFAIL,KRS,CRPS)
      IF(RMELT.GT.RFDS)GO TO 123
      IF(RFDS.GT.RFAIL)RFAIL=RFDS
      GO TO 124
  185 123 IF(RMELT.GT.RFAIL)RFAIL=RMELT
  124 IFAIL=RFAIL/DELR
      RCHECK=IFAIL*DELR
      IF(RCHECK.LT.RFAIL)IFAIL=IFAIL+1
      IF(LCOUNT.NE.LTIME)GO TO 90
  190 SUMTEMP=0.0
      SUMSIGA=0.0
      SUMTAU=0.0
      DO 35 I=1,N
      SUMTEMP=SUMTEMP+TEMP(I)
  195 SUMSIGA=SUMSIGA+SIGMAA(I)
   35 SUMTAU=SUMTAU+TAUMAX(I)
      AVGTEMP=SUMTEMP/N
      AVGSIGA=SUMSIGA/N
      AVGTAU=SUMTAU/N
  200 PRINT 36,AVGTEMP,AVGSIGA,AVGTAU
   36 FORMAT(4X,8HAVERAGES,F9.1,14X,2F10.1)
   90 CALL SORT(QSIGR,KM,QSRMAX,QSRMIN,DELR,RRMAX,RRMIN)
      CALL SORT(QSIGA,KM,QSAMAX,QSAMIN,DELR,ARMAX,ARMIN)
      CALL SORT(QTAU,KM,QTMAX,QTMIN,DELR,TRMAX,TRMIN)
  205 IF(LCOUNT.NE.LTIME)GO TO 65
      LCOUNT=0
      PRINT 37,QSRMAX,QSAMAX,QTMAX
      PRINT 38,QSRMIN,QSAMIN,QTMIN
   38 FORMAT(4X,13HMINIMUM VALUE,54X,3F13.5)
  210 37 FORMAT(4X,13HMAXIMUM VALUE,54X,3F13.5)
      PRINT 101,RRMAX,ARMAX,TRMAX
      PRINT 102,RRMIN,ARMIN,TRMIN
  101 FORMAT(4X16HR AT MAX. STRESS,51X,3F13.3)
  102 FORMAT(4X16HR AT MIN. STRESS,51X,3F13.3)
  215 PRINT 130,RMELT
  130 FORMAT(4X,6HRMELT=,F7.2)
      PRINT 135,RFD,RFS,RFDS,RFAIL
  135 FORMAT(4X,4HRFD=,F7.2/4X,4HRFS=,F7.2/4X,5HRFDS=,F7.2/4X,6HRFAIL=,F
     17.2)
  220 IF(KRDS.EQ.0)GO TO 46
      IF(KRS.EQ.0)GO TO 31
      IF(KRS.EQ.3)GO TO 33
      IF(KRS.EQ.2)GO TO 32
      PRINT*,"    RFS:COMPRESSIVE YIELD"
  225 GO TO 31
   32 PRINT*,"    RFS:TENSILE ULTIMATE"
      GO TO 31
   33 PRINT*,"    RFS:SHEAR ULTIMATE"
```

```
      31 IF(KRDS.EQ.3)GO TO 46
  230    IF(KRDS.EQ.2)GO TO 47
         PRINT*,"    RFDS:TENSILE ULTIMATE"
         GO TO 46
      47 PRINT*,"    RFDS:COMPRESSIVE YIELD"
         GO TO 46
  235 48 PRINT*,"    RFDS:SHEAR ULTIMATE"
      45 IF(IR.EQ.1)GO TO 49
         IF(RFDS.EQ.0.)GO TO 49
         DO 140 IX=1,11
         SIGAPP=ULTENS*(1.-(IX-1)/5.)/3.
  240    CALL RANSC(N,DELR,RFDS,SIGAPP,ULTENS,0,RFSC)
         PRINT 145,SIGAPP,RFSC
  145 FORMAT(4X,7HSIGAPP=,F10.1,5X,5HRFSC=,F7.2)
  140 CONTINUE
      49 CALL STRONG(TEMP,DELR,N,0,STRNGTH,*,IFAIL)
  245    PHELT=(1-RMELT/B)
         RESMELT=PHELT*ULTENS
         PRINT 48,STRNGTH,P
      48 FORMAT(4X7HRESDEG=,F10.0,10H N/SQ CM     PDEG=,F6.3)
         PO=(1.-RFAIL/B)
  250    RESFAIL=PO*ULTENS
         PRINT 45,RESFAIL,PO
      45 FORMAT(4X8HRESFAIL=,F10.0,10H N/SQ CM     PO=,F6.3)
      42 PRINT 55,RESMELT,PHELT
      55 FORMAT(4X,8HRESMELT=,F10.0,10H N/SQ CM     PMELT=,F6.3)
  255    CALL RESTRNG(SIGMAA,0,N,J,ULTENS,IFAIL,DELR,RESTRSS,PSTRSS,RESTRS
        12,PSTRS2,TEMP)
         PRINT 60,RESTRSS,PSTRSS,RESTRS2,PSTRS2
      60 FORMAT(4X,8HRESTRSS=,F10.0,21H N/SQ CM     PSTRSS=,F6.3/4X,8HREST
        1RS2=,F10.0,20H N/SQ CM     PSTRS2=,F6.3)
  260    ENGABS=PA*TIME
         FLUENCE=ENGABS/AREA
         PRINT 103,ENGABS,FLUENCE
  103 FORMAT(4X16HABSORBED ENERGY=,F11.3,6HJOULES,5X17HABSORBED FLUENCE=
        1,F11.3,12HJOULES/SQ CM)
  265    FLUCPK=PKABSI*TIME
         PRINT 104,FLNCPK
  104 FORMAT(4X22HPEAK ABSORBED FLUENCE=,F11.3,12HJOULES/SQ CM)
      65 ASRMAX(IS)=ARMAX
         TCALC(IS)=TIME
  270    QSRPEAK(IS)=QSRMIN
         QSAPEAK(IS)=QSAMAX
         IF((ABS(QTMAX)).GT.(ABS(QTRIN)))GO TO 39
         QTPEAK(IS)=QTMIN
         GO TO 41
  275 39 QTPEAK(IS)=QTMAX
      41 IS=IS+1
         LCOUNT=LCOUNT+1
      50 CONTINUE
         IS=IS-1
  280    ASRMAX(1)=0.
         TCALC(1)=0.
         QSRPEAK(1)=0.
         QSAPEAK(1)=0.
         QTPEAK(1)=0.
  285    IF((IR.EQ.2).AND.(TEMP(I).NE.0.))GO TO 200
  995 CONTINUE
  200 STOP
         END
```

```
      SUBROUTINE TEMPRAD(QABS,DELR,O,COND1,M,RHO1,CP1,EL,TEMP,DELT,TMELT
     1,TUMELT,IFAIL)
C  THIS SUBROUTINE COMPUTES 1-D RADIAL HEAT FLUX TEMPERATURE DISTRIBUTION
      DIMENSION QIN(101),QABS(100),TEMP(101),COND(101),RHO(100),CP(100)
      COND(M+1)=0.0
      QIN(1)=0.0
      J=IFAIL+1
      PI=2.*ASIN(1.)
      DO 4 I=1,M
      CP(I)=CP1
      RHO(I)=RHO1
      IF(I.LE.IFAIL)GO TO 3
      COND(I)=COND1
      IF(TEMP(I).LT.TMELT)GO TO 4
      IF(TEMP(I).GT.TUMELT)GO TO 3
      CP(I)=CP1+(HFUSE/(TUMELT-TMELT))
      GO TO 4
    3 COND(I)=0.0
      TEMP(I)=0.
      QIN(I)=0.
    4 CONTINUE
      QIN(J)=0.
      DO 5 I=J,M
      R=(I-1)*DELR
      QIN(I+1)=COND(I)*(TEMP(I)-TEMP(I+1))*2.*PI*(R+DELR)*EL/DELR
    5 CONTINUE
      DO 10 I=J,M
      TEMP(I)=TEMP(I)+DELT*(QIN(I)+QABS(I)-QIN(I+1))/(CP(I)*RHO(I)*PI*
     1EL*(2.*I-1)*DELR**2)
   10 CONTINUE
      RETURN
      END
```

```
      SUBROUTINE STRESSR(E,ALPHAT,A,DELR,SIGMAR,SIGMAA,TEMP,M,TAUMAX,IFA
     1IL)
C     THIS SUBROUTINE COMPUTES 3-COMPONENT STRESSES FOR 1-D RADIAL TEMP-
C       ERATURE DISTRIBUTION
      DIMENSION SIGMAR(100),SIGMAA(100),R(101),TEMP(101),TAUMAX(100)
      EALPH=E*ALPHAT
      RFAIL=IFAIL*DELR
      RFAIL2=RFAIL**2.
      B2A2=(B**2.)-RFAIL2
      DO 20 I=1,M
   20 R(I)=(I-1)*DELR
      R(M+1)=A
      J=IFAIL+1
      J1=J+1
      SUM=0.0
      SUMT=0.0
      DO 23 I=J1,M
   23 SUM=SUM+2.*R(I)*TEMP(I)
      SUMT=SUM+R(M+1)*TEMP(M+1)
      IF(J.EQ.1)GO TO 24
      SUMT=SUMT+R(J)*TEMP(J)
   24 AB=(DELR/2.)*SUMT
      IF(J.GT.1)GO TO 26
      X2=AB/(B**2.)
      SIGMAR(1)=EALPH*(X2-TEMP(1)/2.)
      SIGMAA(1)=SIGMAR(1)
      TAUMAX(1)=SIGMAR(1)/2.
   26 DO 25 I=J,M
      IF(I.EQ.1)GO TO 25
      IF(I.EQ.J)GO TO 33
      SUM=0.0
      SUMM=0.0
      I1=I-1
      IF(I.GT.2)GO TO 29
      ARR=((DELR**2)*(TEMP(1)/6.+TEMP(2)/3.)
      GO TO 31
   29 IF(I.GT.J1)GO TO 28
      GO TO 34
   33 ARR=0.
      GO TO 31
   28 DO 30 K=J1,I1
   30 SUMM=SUMM+2.*R(K)*TEMP(K)
   34 SUMT=SUMM+R(I)*TEMP(I)
      IF(J1.EQ.2)GO TO 32
      SUMT=SUMT+R(J)*TEMP(J)
   32 ARR=(DELR/2.)*SUMT
   31 R2=R(I)**2.
      C1=(R2+RFAIL2)/(B2A2*R2)
      C2=(R2-RFAIL2)/(B2A2*R2)
      X=C1*AB
      X1=C2*ARR
      Y=ARR/R2
      SIGMAR(I)=EALPH*(X1-Y)
      SIGMAA(I)=EALPH*(X+Y-TEMP(I))
      A=ABS(SIGMAR(I)-SIGMAA(I))
      IF(A.GT.ABS(SIGMAR(I)))GO TO 35
      IF(ABS(SIGMAR(I)).GT.ABS(SIGMAA(I)))GO TO 40
      GO TO 45
   35 IF(A.GT.ABS(SIGMAA(I)))GO TO 60
   45 TAUMAX(I)=SIGMAA(I)/2.
      GO TO 25
   40 TAUMAX(I)=SIGMAR(I)/2.
      GO TO 25
   60 TAUMAX(I)=(SIGMAR(I)-SIGMAA(I))/2.
   25 CONTINUE
      IF(J.LE.1)GO TO 70
      DO 65 I=1,IFAIL
      SIGMAR(I)=0.
      SIGMAA(I)=0.
   65 TAUMAX(I)=0.
   70 RETURN
      END
```

```
      SUBROUTINE STRONG(TEMP,DELR,M,B,STRNGTH,R,IFAIL)
C  COMPUTES RESIDUAL TENSILE STRENGTH DUE TO THERMAL DEGRADATION (PLUS MELTING).
C  APPLIES TO 2024-T3 ALUMINUM ONLY.
C  RSTAR=R AT WHICH TEMP. BECOMES GREATER THAN 200 DEG. C
      DIMENSION TEMP(101)
      SUM1=0.
      SUM2=0.
      SUM3=0.
      SUM4=0.
      L=IFAIL+2
      RF=IFAIL*DELR
      IF(TEMP(L-1).LT.200.)GO TO 105
      DO 115 I=L,M
      IF(TEMP(I).LT.200.)GO TO 110
  115 SUM1=SUM1+2.*TEMP(I)
  110 SUM2=SUM1+TEMP(L-1)-TEMP(I-1)
      ISTAR=I+1
      RSTAR=(I-1)*DELR
      GO TO 120
  105 ISTAR=L
      RSTAR=IFAIL*DELR
  120 DO 100 J=ISTAR,M
  100 SUM3=SUM3+2.*TEMP(J)
      N=M+1
      K=ISTAR-1
      SUM4=SUM3+TEMP(K)+TEMP(N)
      RF01=SUM2*DELR/2.
      R101=SUM4*DELR/2.
      STRNGTH=((B-0.25*RSTAR-0.75*RF)*44828.+200.*((RSTAR-RF)*200.-RF01)
     1-55.*R101)/B
      R=STRNGTH/44828.
      RETURN
      END
```

```
      SUBROUTINE RADSC(M,DELR,RFS,SIGAPP,ULTENS,B,RFSC)
C  THIS SUBROUTINE COMPUTES RADIUS OF FAILED AREA DUE TO STRESS CONCENTRATION.
      RFSC=RFS
      IF(RFS.LT.DELR)GO TO 15
      J=(RFS/DELR)
      DO 5 I=J,M
      R=I*DELR
      ETA=(RFS/R)**2.
      SIGSC=(1.+ETA/2.+3.*((ETA)**2.)/2.)*SIGAPP
      IF(SIGSC.GE.ULTENS)RFSC=R
      IF(RFSC.GE.B)GO TO 10
    5 CONTINUE
      GO TO 15
   10 PRINT*,"    PLATE FAILED-STRESS CONCENTRATION"
   15 RETURN
      END
```

```
      SUBROUTINE RESTRNG(SIGMAA,N,M,ULTENS,IFAIL,DELR,RESTRSS,PSTRSS,
     1RESTRS2,PSTRS2,TEMP)
C  THIS SUBROUTINE COMPUTES VARIOUS RESIDUAL TENSILE STRENGTHS.
C  APPLIES ONLY TO 2024-T3 ALUMINUM
      DIMENSION SIGMAA(102),ULT(100),TEMP(101)
      SUM1=0.
      RFAIL=IFAIL*DELR
      97=RFAIL
      94=RFAIL
      95=0.
      DO 4 I=1,M
      IF(SIGMAA(I).LE.0.)GO TO  4
      95=(I-1)*DELR
      IF(95.GT.94)GOTO 5
      95=94
      GO TO 10
    4 CONTINUE
    5 95=95
   10 I6=96/DELR+2
      I7=97/DELR+2
      M=M-1
      DO 15 I=I6,M
   15 SUM1=SUM1+2.*SIGMAA(I)
      SUM=SUM1+SIGMAA(I6-1)+SIGMAA(M)
      AVGTENS=SUM*DELR/(2.*(96-95))
      RESTRSS=ULTENS*(1-94/96)-AVGTENS*(1-96/96)
      PSTRSS=RESTRSS/ULTENS
      SUM1=0.
      K=I7+1
      DO 30 I=K,M
      IF(TEMP(I).LT.200.)GO TO 20
      IF(TEMP(I).GT.  0.)GO TO 25
      ULT(I)=33610.-(TEMP(I)-200.)*200.
      GO TO 30
   20 ULT(I)=44820.-TEMP(I)*55.
      GO TO 30
   25 ULT(I)=0.
   30 CONTINUE
      DO 35 I=I7,M
   35 SUM1=SUM1+2.*ULT(I)
      SUM=SUM1+ULT(K)+ULT(M)
      ULTEMP=SUM*DELR/(2.*(96-97))
      RESTRS2=ULTEMP*(1-97/96)-AVGTENS*(1-96/96)
      IF(RESTRS2.LT.0.)RESTRS2=0.
      PSTRS2=RESTRS2/ULTENS
      RETURN
      END
```

```
      SUBROUTINE RADFAIL(TEMP,RFD,RFS,RFDS,NR,DELR,SIGMAR,SIGMAA,TAUMAX,
     1ULTENS,COMPYLD,ULTSHR,IFAIL,KRS,KRDS)
C THIS SUBROUTINE DETERMINES RESPECTIVE RADII OF FAILED PLATE AREA DUE TO
C      THERMAL DEGRADATION ALONE,THERMAL STRESSES ALONE,AND IN COMBINATION.
C  APPLIES TO 2024-T3 ALUMINUM ONLY.
      DIMENSION TEMP(101),SIGMAR(100),SIGMAA(102),TAUMAX(100)
      R1=0.
      R2=0.
      R3=0.
      R4=0.
      RT=0.
      RC=0.
      RC2=0.
      RS=0.
      KK=KRS
      KV=KRDS
      J=IFAIL+1
      DO 5 I=J,NR
      IF(TEMP(I).LT.370.)GO TO 10
      RFD=I*DELR
    5 CONTINUE
   10 DO 15 I=J,NR
      IF(SIGMAR(I).LT.COMPYLD)R1=I*DELR
      IF(SIGMAA(I).GT.ULTENS)R2=I*DELR
      IF(ABS(TAUMAX(I)).GT.ULTSHR)R3=I*DELR
      IF(SIGMAA(I).LT.COMPYLD)R5=I*DELR
   15 CONTINUE
      IF(R1.GE.R5)GO TO 18
      R1=R5
   18 CALL RFMAX(R1,R2,R3,R4,KRS)
      IF(R4.GT.RFS)GO TO 16
      KRS=KK
      GO TO 17
   16 RFS=R4
   17 DO 75 I=J,NR
      IF(TEMP(I).LT.288.)GO TO 20
      IF(TEMP(I).GT.370.)GO TO 25
      ULTEN1=33610.-(TEMP(I)-288.)*288.
      GO TO 30
   20 ULTEN1=44820.-TEMP(I)*55.
      GO TO 30
   25 ULTEN1=0.
   30 IF(SIGMAA(I).GE.ULTEN1)RT=I*DELR
      IF(TEMP(I).LT.232.)GO TO 35
      IF(TEMP(I).GT.370.)GO TO 40
      COMPYD1=-(17850.-(TEMP(I)-232.)*1.8.)
      GO TO 50
   35 COMPYD1=-(23440.-(TEMP(I))*25.)
      GO TO 50
   40 COMPYD1=0.
      GO TO 50
   50 IF(SIGMAR(I).LE.COMPYD1)RC=I*DELR
      IF(SIGMAA(I).LE.COMPYD1)RC2=I*DELR
      IF(RC.GE.RC2)GO TO 51
      RC=RC2
   51 IF(TEMP(I).LT.218.)GO TO 55
      IF(TEMP(I).GT.370.)GO TO 60
      ULTSHR1=19240.-(TEMP(I)-218.)*132.
      GO TO 70
   55 ULTSHR1=25610.-(TEMP(I))*29.
      GO TO 70
   60 ULTSHR1=0.
      GO TO 70
   70 IF(ABS(TAUMAX(I)).GE.ULTSHR1)RS=I*DELR
   75 CONTINUE
      CALL RFMAX(RT,R3,RS,RM,KRDS)
      IF(RM.GT.RFDS)GO TO 80
      KRDS=KV
      GO TO 85
   80 RFDS=RM
   85 RETURN
      END
```

```
      SUBROUTINE RMAX(R1,R2,R3,RMAX,KR)
C  THIS SUBROUTINE DETERMINES THE GREATEST(RMAX) OF THREE POSITIVE QUANTITIES
      IF(R1.GE.R2)GO TO 5
      IF(R3.GE.R2)GO TO 10
      RMAX=R2
      KR=2
      GO TO 20
   10 RMAX=R3
    5 IF(R1.GE.R3)GO TO 15
      KR=3
      GO TO 20
   15 RMAX=R1
      KR=1
   20 RETURN
      END



      SUBROUTINE SORT(A,K,AMAX,AMIN,DR,R2,R1)
C  THIS SUBROUTINE COMPUTES MAXIMUM & MINIMUM VALUES OF QUANTITY "A".
      DIMENSION A(102)
      DO 2 I=1,K
      IF(A(I).EQ.0.)GO TO 2
      GO TO 3
    2 CONTINUE
    3 J=I+2
      IF(A(I+1).GT.A(I))GO TO 5
      AMAX=A(I)
      R2=(I-1)*DR
      AMIN=A(I+1)
      R1=I*DR
      GO TO 10
    5 AMAX=A(I+1)
      R2=I*DR
      AMIN=A(I)
      R1=(I-1)*DR
   10 DO 100 I=J,K
      IF(A(I).GT.AMAX)GO TO 20
      IF(A(I).LT.AMIN)GO TO 15
      GO TO 100
   15 AMIN=A(I)
      R1=(I-1)*DR
      GO TO 100
   20 AMAX=A(I)
      R2=(I-1)*DR
  100 CONTINUE
      RETURN
      END
```

SAMPLE OUTPUT

```
MATERIAL IS 2024-T3  ALUMINUM
  DENSITY=2.7834/CC  THERMAL CONDUCTIVITY=1.5JOULE/SEC-CM-DEG.C  HEAT CAPACITY=1.88JOULE/GM-DEG.C
  ABSORPTIVITY=.5  MELTING TEMP.=502.DEG.C  HEAT OF FUSION=375.JOULES/GM  COEFF. OF THERMAL EXP.=.000023PER DEG.C
  UPPER MELTING TEMP.=539.DEG.C
  ULT. TENSILE STRENGTH=44828.N/SQ CM  ULT.SHEAR STRENGTH=25518.N/SQ CM  YOUNGS MODULUS=6900000.N/SQ CM
  COMPRESSIVE YIELD STRENGTH=-23446.N/SQ CM
GAUSSIAN BEAM
  DELR=.025CM  N=58  DELT=.01SEC  L=.175CM  QBEAM=15986.JOULES/SQ CM-SEC  TI=0.DEG C  JTIME=150  B=9.CM  B=26.CM
  MTIME=15 LTIME=10  TQUEN=20.SEC
 IPA=  75%.41JOULES/SQ CM-SEC  TI=  2.92SEC  PLA=  9.67

RUN ALLOWING HOLE IN PLATE DUE TO MELTING OR STRUCTURAL FAILURE
TIME=  .15SEC  KT/(L**2)=  .12764
```

R(CM)	TEMP(C)	SIGMA R (N/SQ CM)	SIGMA THETA (N/SQ CM)	TAUMAX (N/SQ CM)	SIGR*L/IPA (SEC)	SIGA*L/IPA (SEC)	TAU*L/IPA (SEC)	SIGA*L**K/PA
9.000	48.9	-3224.2	-3224.2	-1512.1	-.02594	-.02594	-.01297	-.00176
.408	37.8	-3819.8	-2813.7	-1309.5	-.02428	-.02203	-.01214	-.00119
.800	30.3	-2551.8	-2128.1	-1325.5	-.02172	-.01705	-.01856	-.00089
1.200	22.5	-2296.2	-1231.5	-1149.1	-.01847	-.00998	-.00924	-.00752
1.600	15.1	-1916.7	-437.3	-358.3	-.01542	-.00352	-.00771	-.00010
2.000	9.2	-1556.5	141.9	-949.1	-.01252	.00114	-.00593	.00006
2.400	5.1	-1242.5	482.8	-952.5	-.00999	.00388	-.00594	.00020
2.800	2.5	-984.3	827.4	-906.1	-.00792	.00505	-.00549	.00025
3.200	1.1	-782.2	644.1	-713.2	-.00629	.00518	-.00574	.00027
3.600	.5	-626.5	593.2	-610.9	-.00504	.00479	-.00491	.00025
4.000	.2	-503.2	523.1	-513.6	-.00409	.00421	-.00415	.00022
4.400	.1	-417.9	451.2	-434.5	-.00336	.00363	-.00350	.00019
4.800	.0	-348.2	388.9	-368.1	-.00280	.00312	-.00296	.00016
5.200	.0	-293.6	335.3	-314.8	-.00236	.00270	-.00253	.00014
5.600	.0	-250.3	292.9	-271.6	-.00201	.00236	-.00218	.00012
6.000	.0	-215.3	257.9	-236.6	-.00173	.00207	-.00190	.00011
16.000	0.0	-12.0	54.6	-33.3	-.00010	.00044	-.00027	.00002
16.400	0.0	-10.4	53.0	-31.7	-.00008	.00043	-.00025	.00002
16.800	0.0	-8.9	51.5	-30.2	-.00007	.00041	-.00024	.00002
17.200	0.0	-7.5	50.1	-28.8	-.00006	.00040	-.00023	.00002
17.600	0.0	-6.2	48.8	-27.5	-.00005	.00039	-.00022	.00002
18.000	0.0	-5.0	47.5	-26.3	-.00004	.00038	-.00021	.00002
18.400	0.0	-3.9	46.4	-25.2	-.00003	.00037	-.00020	.00002
18.800	0.0	-2.9	45.4	-24.1	-.00002	.00037	-.00019	.00002
19.200	0.0	-1.8	44.4	-23.1	-.00001	.00036	-.00019	.00002
19.600	0.0	-.9	43.5	-22.2	-.00001	.00035	-.00018	.00002
AVERAGES	3.3		-40.1	-297.9				
MAXIMUM VALUE					-.00001	.00518	-.00018	
MINIMUM VALUE					-.02594	-.02594	-.01237	
R AT MAX. STRESS					19.600	3.209	19.600	
R AT MIN. STRESS					0.000	0.000	0.000	

```
PMELT=   0.00
PFD=   0.00
PFS=   0.00
PFNS=   1.00
PFAIL=   0.00
PESDES=   44552. N/SQ CM     PDES=  .996
PESFAIL=   44928. N/SQ CM     PD=  1.000
PESMELT=   44928. N/SQ CM     PMELT=  1.000
PESTRSS=   44659. N/SQ CM     PSTRSS=  .997
PESTRS2=   43514. N/SQ CM     PSTRS2=  .973
ABSORBED ENERGY=   775.008JOULES     ABSORBED FLUENCE=   39.478JOULES/SQ CM
PEAK ABSORBED FLUENCE=   78.941JOULES/SQ CM
```

SAMPLE OUTPUT - AFTER MELTING HAS BEGUN

TIME= .71 SEC KT/(L**2)= .99209

R(CM)	TEMP(C)	SIGMA R (N/SQ CM)	SIGMA THETA (N/SQ CM)	TAUMAX (N/SQ CM)	SIGR*L/IPA (SEC)	SIGA*L/IPA (SEC)	TAU*L/IPA (SEC)	SIGA*L**K/PA
0.000	0.0	0.0	0.0	0.0	0.00000	0.00000	0.00000	0.00000
.400	0.0	0.0	0.0	0.0	0.00000	0.00000	0.00000	0.00000
.800	0.0	0.0	0.0	0.0	0.00000	0.00000	0.00000	0.00000
1.200	0.0	0.0	0.0	0.0	0.00000	0.00000	0.00000	0.00000
1.600	188.5	0.0	-15883.5	-7901.0	0.00000	-.12712	-.06356	-.00665
2.000	67.9	-2728.6	-8378.7	-4134.3	-.01073	-.06584	-.03342	-.00350
2.400	41.1	-2006.9	-3487.5	-1743.7	-.02322	-.02803	-.01401	-.00147
2.800	22.9	-2760.3	-731.8	-1398.1	-.02220	-.00588	-.01118	-.00031
3.200	11.8	-2412.6	679.5	-1546.2	-.01941	.00547	-.01244	.00029
3.600	5.7	-2833.7	1275.9	-1956.3	-.01636	.01020	-.01332	.00054
4.000	2.5	-1594.1	1439.1	-1366.1	-.01363	.01157	-.01250	.00061
4.400	1.0	-1411.6	1395.3	-1401.0	-.01135	.01116	-.01127	.00059
4.800	.4	-1183.6	1264.8	-1224.2	-.00952	.01017	-.00968	.00053
5.200	.1	-1048.9	1124.3	-1062.6	-.00805	.00904	-.00855	.00047
5.600	.0	-953.9	992.3	-973.1	-.00687	.00798	-.00743	.00042
6.000	.0	-734.8	879.1	-806.5	-.00591	.00705	-.00648	.00037
18.000	.0	-17.0	162.4	-89.7	-.00014	.00131	-.00072	.00007
18.400	.0	-13.2	158.5	-85.9	-.00011	.00128	-.00069	.00007
18.800	.0	-9.5	154.9	-82.3	-.00008	.00125	-.00066	.00007
19.200	.0	-6.2	151.6	-79.0	-.00005	.00122	-.00063	.00006
19.600	.0	-3.0	148.4	-75.7	-.00002	.00119	-.00061	.00006
AVERAGES	9.1		-175.3	-688.8				
MAXIMUM VALUE					-.00002	.01197	-.00061	
MINIMUM VALUE					-.02322	-.12712	-.06356	
R AT MAX. STRESS					19.600	0.000	19.600	
R AT MIN. STRESS					2.400	1.600	1.600	

SMELT= 8.98
RFD= 4.88
RFS= 1.78
RFSS= 1.59
RFAIL= 1.68
RFSICOMPRESSIVE YIELD
RFSICOMPRESSIVE YIELD

SIGAPP=	14940.0	RFSC=	1.60
SIGAPP=	17928.0	RFSC=	1.60
SIGAPP=	20915.0	RFSC=	1.60
SIGAPP=	23904.0	RFSC=	2.00
SIGAPP=	25892.0	RFSC=	2.00
SIGAPP=	29880.0	RFSC=	2.40
SIGAPP=	32868.0	RFSC=	2.40
SIGAPP=	35856.0	RFSC=	2.80
SIGAPP=	38844.0	RFSC=	3.60
SIGAPP=	41832.0	RFSC=	4.50

PLATE FAILED-STRESS CONCENTRATION
SIGAPP= 44820.0 RFSC= 20.00
RESSED= 41819. N/SQ CM PDSS= .915
RESFAIL= 41234. N/SQ CM PD= .920
RESMELT= 44928. N/SQ CM PMELT= 1.000
RESTRSS= 40951. N/SQ CM PSTRSS= .911
RESTRS2= 39731. N/SQ CM PSTRS2= .886
ABSORBED ENERGY= 9429.898JOULES ABSORBED FLUENCE= 276.293JOULES/SQ CM
PEAK ABSORBED FLUENCE= 552.586JOULES/SQ CM

APPENDIX B

Algorithms used in Program TSTRESS

Numerical Integration Algorithm

Numerical integration is applied in subroutines STRESSR, STRONG, and RESTRNG to compute thermal stresses and various residual strengths. In all cases, the trapezoidal rule is used (Ref 24:229), which gives

$$\int_a^b y\,dx = \frac{h}{2}\left[y_a + 2y_{a+1} + 2y_{a+2} + \cdots + 2y_{a+n-1} + y_{a+n}\right] \qquad (109)$$

where

a,b = integration limits

y = f(x)

h = segment length used to divide the interval, $a \leq x \leq b$

n = (b-a)/h = number of segments into which interval is divided

In FORTRAN code, a typical integration routine would be as follows.

```
      SUM = 0.
      DO  50  I = J,M
   50 SUM = SUM + 2.*Y(I)
      SUMM = SUM + Y(J-1) + Y(M+1)
      AB = SUMM * H/2.
```

Numerical Computation of Thermal Stresses near r = 0.

For a solid plate, the thermal stresses are given by eqns (57) and (58). At the plate center where r = 0, these eqns become indeterminant. Hence, seperate algorithms are

necessary to compute thermal stresses near r = 0. Assuming finite temperatures, and applying l'Hopital's rule to eqns (57) and (58) gives the following.

$$\sigma_{rr}(0) = \sigma_{\theta\theta}(0) = \alpha E \frac{1}{b^2}\left[\int_0^b Trdr - \frac{1}{2}T(0)\right] \qquad (110)$$

This equation is numerically integrated in subroutine STRESSR to obtain stresses at r = 0.

It was also found that a special algorithm was required for computing stresses at the first radial increment away from r = 0 because eqns (57) and (58) are still erroneous for small values of r. The following term in these equations becomes erroneously large for very small values of r.

$$\frac{1}{r^2}\int_0^r Trdr$$

To evaluate this integral at the first radial increment, replace the upper limit with r = ΔR, where ΔR = radial element width. Assuming a linear temperature distribution between r = 0 and r = ΔR,

$$T(r) = T(0)\,[1-Pr] \qquad (111)$$

where

T(0) = temperature at r = 0

P = constant (slope of temperature distribution)

Define

$$ARR = \int_0^{\Delta R} rTdr = T(0) \int_0^{\Delta R} r(1-Pr)dr \qquad (112)$$

The value of P is found as follows.

$$T(1) = T(0)\ [1-P(\Delta R)] \qquad (113)$$

where

T(1) = temperature at r = ΔR

$$P = \frac{1}{\Delta R}\left[1-\frac{T(1)}{T(0)}\right] \qquad (114)$$

Substituting into eqn (112) and integrating gives

$$ARR = (\Delta R)^2[T(0)/6+T(1)/3] \qquad (115)$$

This algorithm is used in computing thermal stresses at the outer radius of the first radial element for a solid disk.

Radius of Melted Hole (RMELT)

An element is considered to be melted (transformed from the solid to the liquid phase) when the temperature of that element reaches the upper melting temperature (TUMELT) which is 638°C for 2024-T3 aluminum. The phase change is accounted for as described in Section VI. The assumption is made that the melt is removed instantaneously upon reach-

ing the upper melting temperature. Since the axially symmetric beam is considered to be located over the center of a flat plate, melting produces a circular hole in the plate which progressively grows radially with continued application of heat flux. The hole growth ceases when the hole becomes so large that any remaining irradiated plate area absorbs insufficient heat flux to produce further melting. The radius of the melted hole is given by

$$RMELT = I*DELR \tag{116}$$

where

I = element number of outermost element which has been heated to upper melting temperature (638°C)

DELR = element radial width

Radius of Failed Area due to Thermal Degradation (RFD)

This quantity is computed in Subroutine RADFAIL (lines 18 to 21). It is postulated that a failed area, centered at the coincident beam and plate centers, is generated or expanded whenever any of the three structural strength properties is reduced to zero, as defined by Figures 2 through 4. As noted in Section VI, all three strength properties of an element are taken to be zero if the temperature of that element is greated than 370°C (for 2024-T3 aluminum). Hence, the radius of a failed area due to thermal degradation is considered to be dependent on temperature only and

is developed in a manner analagous to that of a hole due to melting (RMELT). That is, the area radius is given by

$$RFD = I*DELR \qquad (117)$$

where

I = element number of outermost element which has been heated to zero structural strength temperature (370°C)

Radius of Failed Area due to Thermal Stresses (RFS)

This quantity is computed in Subroutine RADFAIL (lines 22 to 34) and is based on the postulate that a beam axis centered failed area is generated in the heated plate if any of the three thermal stress components exceeds its respective room temperature strength criterion. This parameter is used as a measure of the failed area that would be produced by thermal stresses independent of the action of structural strength thermal degradation. The thermal stresses of each element are compared to room temperature ultimate tensile strength, compressive yield strength, and ultimate shear strength. If any of these criteria are exceeded at any element, the plate material is considered to have zero strength at the element. A failed area radius is then defined by the outermost radial element which has reached a failure strength level.

Radius of Failed Area due to Combined Action of Thermal Stresses and Degradation (RFDS)

This quantity is computed in Subroutine RADFAIL (lines 35 to 70) and is based on the postulate that a radial element is reduced to zero strength if any of the three stress components exceeds its respective elevated temperature structural strength as defined in Section VI. The radius of a failed area due to the combined action of thermal stresses and thermal degradation of structural strength is determined by the outer radius of the outermost element which has one or more stress components greated than its failure strength.

Actual Radius of Failed Area (RFAIL)

Two options concerning plate failure zones are provided in Program TSTRESS. Although structurally failed areas are defined by RFS, RFD, and RFDS, it is conceivable that these failed circular areas might either remain in place in the plate or be immediately removed by some source such as aerodynamic pressure. In either case it is postulated that any melted zone (RMELT) is immediately removed. Hence, one option considered (defined by IR = 1, line 108 of TSTRESS) is that of allowing a hole to be formed by either of the mechanisms defined by RMELT and RFDS. That is, the actual hole radius (RFAIL) would be the larger of the above radii, in which case immediate removal of this zone is assumed regardless of the failure mechanism. The second option (defined by IR = 2) removes the failed area only if the failure

mechanism is melting. That is the actual hole radius is always equal to RMELT, in which case laser beam heat flux continues to be absorbed by the plate area within a structurally failed circle and outside the melted hole. As shown in the sample output of TSTRESS, Appendix A, for either of the above options, all of the above failed radii are listed. Following the failed radii listing are listings of the stress components which caused failure due to thermal stresses alone, and due to combined thermal stresses/degradation.

Failed Hole due to Stress Concentration (RFSC)

Following the above listings in the sample output, Appendix A, is a table of failed hole radius due to stress concentration (RFSC) as a function of the remotely applied tensile stress (SIGAPP) in the plane of the plate. The initial hole radius is taken as that due to structural failure. It is assumed that failure due to melting is associated with high temperatures at the edge of the hole which tend to soften the material to the extent that stress concentrations are negligible. For a plate in uniaxial tension, the ratio of local tensile stress to the remotely applied tensile stress is (Ref 21:399)

$$\frac{\sigma_\theta}{\sigma_\infty} = 1 + \frac{1}{2}\eta + \frac{3}{2}\eta^2 \qquad (118)$$

where

$$\eta = a^2/r^2$$

a = hole radius = RFSC

σ_∞ = remotely applied tensile stress = SIGAPP

σ_θ = local tensile stress @r

If σ_θ exceeds room temperature ultimate tensile strength, the failed radius (RFSC) is computed. Computations are made for several values of remotely applied stress (SIGAPP). These calculations are made in Subroutine RADSC and in TSTRESS at lines 238 to 240.

Residual Tensile Strength Due to Thermal Degradation (RESDEG)

The uniformly distributed, remotely applied tensile force required to fail a solid plate in tension, considering only the effects of thermal degradation of ultimate tensile strength is given by (Ref 31)

$$\int_{-b}^{b}\int_{0}^{\ell}\sigma(t)\,dzdx = \int_{-b}^{b}\int_{0}^{\ell}\{\sigma_o+M[T(x,t)-T_o]\}dzdx \qquad (119)$$

where

$\sigma(t)$ = STRNGTH = RESDEG = residual tensile strength due to thermal degradation

$\sigma_o = F_{to}$ = original unheated tensile strength

M = slope of thermal degradation plot of ultimate tensile strength vs. temperature

$T(x,t)$ = local temperature of plate at distance x from plate center

T_0 = temperature corresponding to σ_o

$2b = 2B$ = plate width

ℓ = plate thickness

Performing the indicated integrations on the left side and integrating with respect to z on the right side gives

$$\sigma(t) = \frac{1}{2b} \int_{-b}^{b} \{\sigma_o + M[T(x,t) - T_o]\}\, dx \qquad (120)$$

Due to axial symmetry, this is equivalent to

$$\sigma(t) = \frac{1}{b} \int_{0}^{b} \{\sigma_o + M[T(x,t) - T_o]\}\, dx \qquad (121)$$

As discussed in Section VI, the thermal degradation curve was approximated by two straight lines. Eqn (121) then becomes

$$\sigma(t) = \frac{1}{b} \left\{ \int_{0}^{b^*} \{\sigma_{o_2} + M_2[T(x,t) - T_{o_2}]\}\, dx + \int_{b^*}^{b} \{\sigma_{o_1} + M_1[T(x,t) - T_{o_1}]\}\, dx \right\} \qquad (122)$$

where b^* = value of x where $T(b^*,t) = T_{o_2}$

T_{o_2} = temperature at intersection of the two straight line approximations

M_2 = slope of degradation curve for $370°C > T(x,t) > T_{o_2}$

M_1 = slope of degradation curve for $T_{o_1} < T(x,t) < T_{o_2}$

$T_{o_1} = T_o$

$\sigma_{o_1} = \sigma_o = F_{to}$

σ_{o_2} = ultimate tensile strength at T_{o_2}

Allowance for a failed area at the plate center is accounted

for by beginning the integration at the edge of this area.

$$\sigma(t) = \frac{1}{b}\left\{\int_{b_f}^{b^*}[\sigma_{O2}+M_2T(x,c)-M_2T_{O2}]dx + \int_{b^*}^{b}[\sigma_{O1}+M_1T(x,t)-M_1T_{O1}]\quad dx\right\} \tag{123}$$

where b_f = BF = radius of failed area

The following approximations also are made:

$$\sigma_{O2} \simeq 0.75\ \sigma_{O1}$$
$$T_{O1} \simeq 0°C$$

This results in the form of the algorithm used in subroutine STRONG.

$$\sigma(t) = \frac{1}{b}\left\{(b-0.25b^*-0.75b_f)\sigma_{O1} -M_2[T_{O2}(b^*-b_f)-\int_{b_f}^{b^*}T(x,t)dx] +M_1\int_{b^*}^{b}T(x,t)dx\right\} \tag{124}$$

where $M_2 = -200\ \frac{n/cm^2}{°C}$ for 2024-T3 aluminum

$M_1 = -55\ \frac{n/cm^2}{°C}$

$\sigma_{O1} = F_{to} = 44{,}820\ n/cm^2$

$T_{O2} = 200°C$

The proportion of the original unheated ultimate tensile

strength is then computed as

$$PDEG = P = STRNGTH/\sigma_{01} \tag{125}$$

Residual Tensile Strength Due to Melting (RESMELT)

This quantity is a direct function of the reduction in plate cross-sectional area due to melting of a hole, and is computed in the main program (lines 245-246) as follows

$$PMELT = (1-RMELT/B) \tag{126}$$

$$RESMELT = PMELT*ULTENS \tag{127}$$

where

PMELT = proportion of original unheated ultimate tensile strength remaining

RMELT = radius of melted hole

B = plate radius

ULTENS = F_{to} = original unheated ultimate tensile strength

RESMELT = residual tensile strength due to effect of melted hole only

Residual Strength Due to Thermal Stresses (RESTRSS)

The tensile load carrying capacity of the rectangular plate at any time t, considering only the effects of thermal stresses and a failed area at the plate center, is

$$P = P_{tu} - \sigma_a [2\ell(b-b_4)] - P_{tu} \frac{b_4}{b} \tag{128}$$

where

P_{tu} = room temperature ultimate tensile load strength

σ_a = thermal tensile stress averaged over area of applied load

ℓ = plate thickness

b = plate radius or width/2

b_4 = radius of failed area

b_5 = radius at which tensile stress (σ_θ) becomes greater than zero

b_6 = the greater of b_4 or b_5

Dividing by the original plate cross-sectional area, $2b\ell$, gives the residual tensile strength due to thermal stresses only.

$$\sigma = F_{to}\left(1-\frac{b_4}{b}\right) - \sigma_a\left(1-\frac{b_6}{b}\right) \qquad (129)$$

where

F_{to} = ULTENS = room temperature ultimate tensile strength

σ = RESTRSS = residual tensile strength due to thermal stresses only

Dividing by F_{to} gives the proportion of the original tensile strength remaining.

PSTRSS = RESTRSS/ULTENS

The average tensile stress is computed by numerical integration of

$$\sigma_a = \text{AVGTENS} = \frac{1}{b-b_6} \int_{b_6}^{b} \sigma_\theta dr \qquad (130)$$

Residual Tensile Strength Due to the Combined Actions of Melting, Thermal Stresses, and Thermal Degradation (RESTRS2)

This algorithm is similar to that for thermal stresses except that the elevated temperature ultimate tensile strength, averaged over the net section area, replaces the room temperature ultimate strength.

$$\sigma = F_{tu}\left(1-\frac{b_7}{b}\right) - \sigma_a\left(1-\frac{b_6}{b}\right) \qquad (131)$$

where

σ = RESTRS2 = residual tensile strength due to melting, thermal stresses and thermal degradation

F_{tu} = ULTEMP = elevated temperature ultimate tensile strength averaged over net section area

$b_7 = b_4$ = B7 = radius of failed area

ULTEMP is computed by numerical integration of the thermal degradation equations from Section VI for ultimate tensile strength.

$$\text{ULTEMP} = \frac{1}{b-b_7} \int_{b_7}^{b} F_{tu} dr \qquad (132)$$

where

F_{tu} = ULT(I) = elevated temperature ultimate tensile strength

The proportion of room temperature ultimate strength is

$$PSTRS2 = RESTRS2/ULTENS \quad (133)$$

Residual Tensile Strength Due to Failed Area (RESFAIL)

The above measures of residual strengths contain the effects of a reduction in net section load-carrying area due to melting or structural failure. The effect of the structurally failed area on residual tensile strength is computed in the main program (lines 249-250) as follows.

$$PO = (1-RFAIL/R) \quad (134)$$

$$RESFAIL = PO*ULTENS \quad (135)$$

where

PO = proportion of room temperature ultimate tensile strength remaining

APPENDIX C

NASTRAN Validation of Program TSTRESS

NASTRAN Validation of Program TSTRESS

To validate the one-dimensional radial heat conduction program, temperature and thermal stress distributions were compared with those from a two-dimensional finite element analysis using NASTRAN (Ref 2). The NASTRAN finite element model consisted of a segment of a solid cylinder as shown in Fig. 28. The wedge shaped segment was divided into 15 radial elements and 5 depth elements. The radial width of the elements varied from a fine mesh under the laser beam to a relatively broad mesh at the outer radii. The element thicknesses were constant, each being 1/5 of the plate thickness.

The wedge segment is sufficient to model the problem of interest because of the axial symmetry of the heat flux input which implies that the problem is independent of the radial coordinate. The wedge angle was chosen to be 15 degrees to provide reasonable aspect ratios (width/length) for the finite elements. The radius of the wedge was taken as 15 cm to be consistent with the one-dimensional numerical radial flux model. In general, this study was restricted to large plate diameter/beam diameter ratios to minimize the effect of this parameter on the results. Also, as in the numerical radial model, no heat losses were considered in the NASTRAN analysis.

The heat flux input to the surface elements under the beam radius was approximated by using the flux density value at the radial midpoint of each surface element. For a

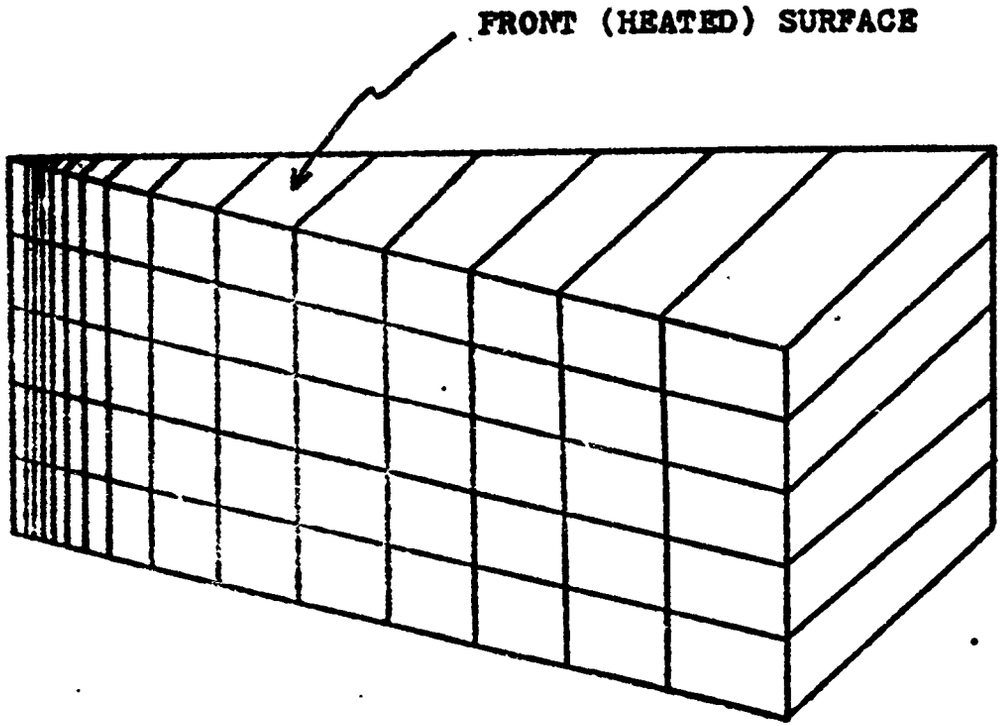

Fig. 28 Two-Dimensional Finite Element Model

Gaussian beam, the heat flux density distribution is given by eqn (9) as

$$I(r) = I_{pa} e^{-2r^2/a^2}$$

where

$$a = 2\sigma = \text{beam radius}$$

This is the same approximation used for the heat flux input to the one-dimensional model. However, the one-dimensional model has constant width (radial) elements sized to achieve a compromise between accuracy and computational efficiency. This was initially accomplished by analyzing the effect of reducing element width on computer time, and on temperature and thermal stress values. An element width of 0.3 cm was selected as a reasonable compromise based on the judgment that larger widths gave significantly different temperatures and thermal stresses while smaller widths produced very small differences in temperatures and thermal stresses but rapidly increased computational cost.

Figures 29 and 30 show comparisons of thermal stresses between the one-dimensional radial model and the NASTRAN two-dimensional finite element results. Such comparisons were made for four different input conditions involving two different heat flux densities and two plate thicknesses. Only one beam diameter was considered, 3 cm. The results presented in Figures 29 and 30 are typical. The NASTRAN

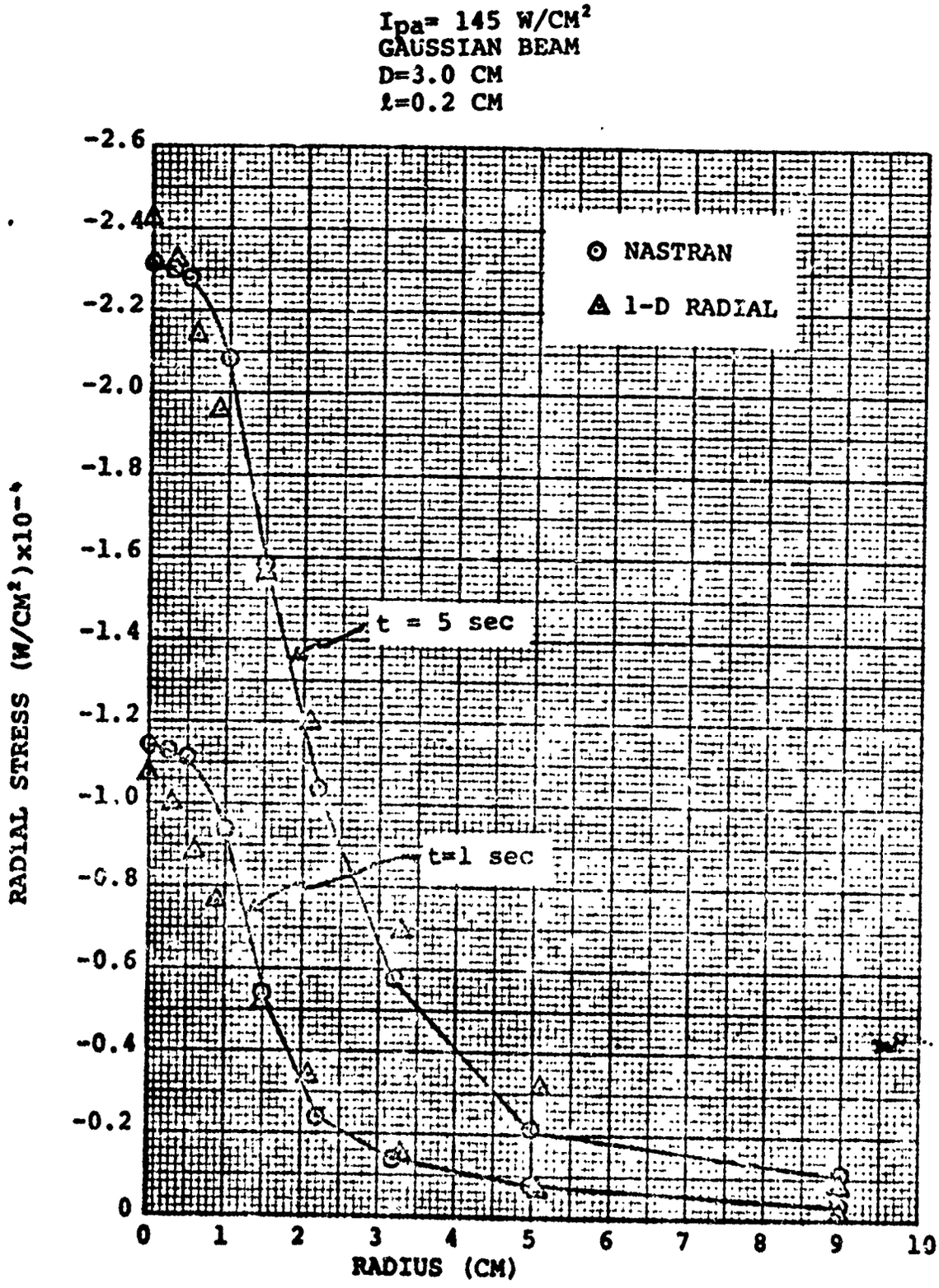

Fig. 29 Radial Thermal Stress Comparison, NASTRAN and 1-D Radial Heat Flux Model

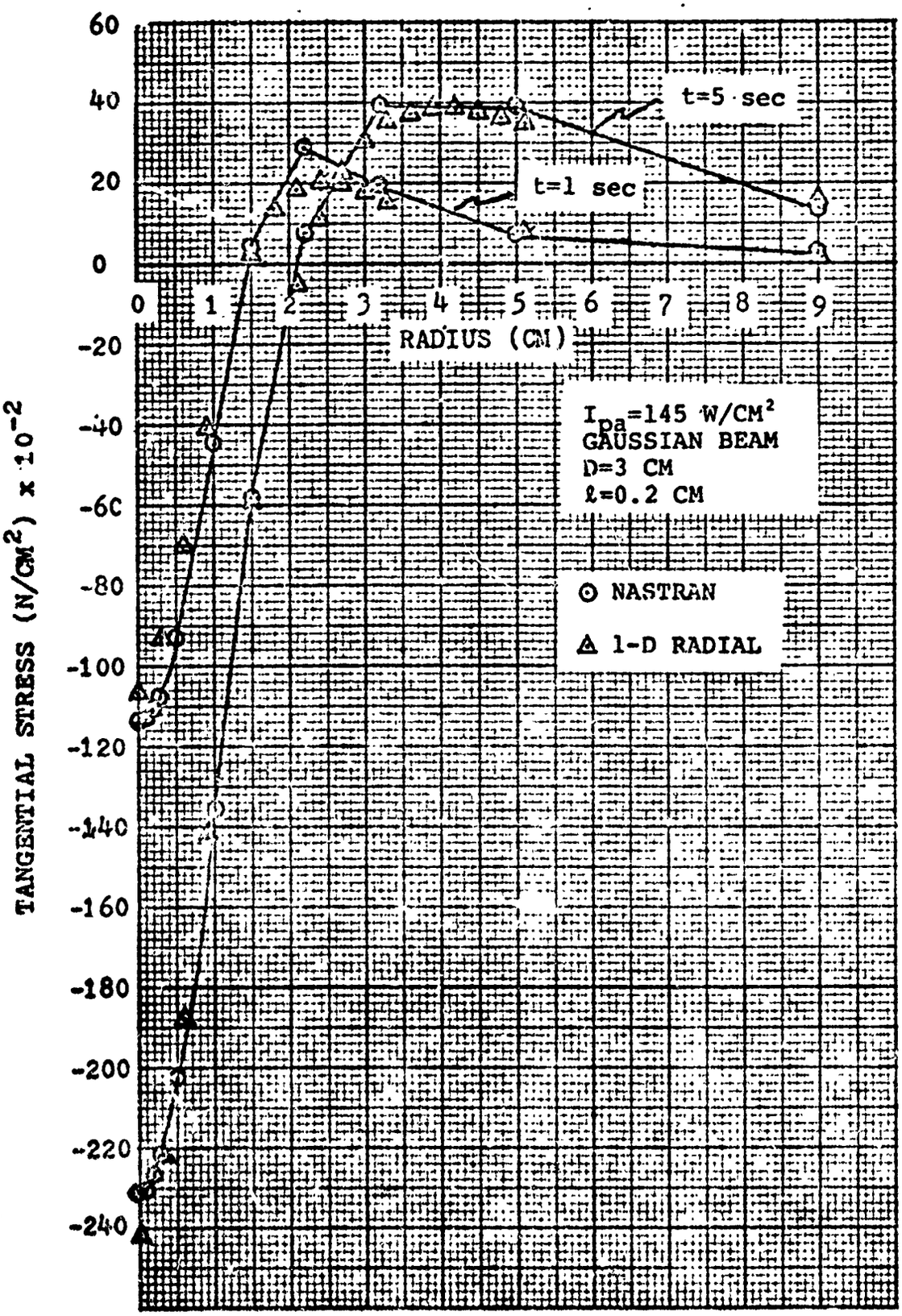

Fig. 30 Tangential Thermal Stress Comparison

stresses are at the heated, or front, surface. For the conditions listed in the figures, the heat conduction is primarily radial as determined by comparing front and back surface temperatures and stresses as partially listed in Table I. The relatively small front-to-back differences in the temperatures indicate that the axial heat flux vector component is small since the heat conduction is directly proportional to the spatial thermal gradient (reference eqn (21)).

Two conclusions drawn from Fig. 29 are that the one-dimensional radial flux model does not give zero slopes in the stress distributions at r = 0, and that the radial flux model stresses appear to increase (become more negative) relative to the NASTRAN stresses with increasing time. These trends also are exhibited in Fig. 30. Zero slope at r = 0 is required by the axial symmetry of the problem.

In order to evaluate the significance of these trends, the temperature distributions were compared in greater detail as shown in Fig 31. Solid curves were fitted through the NASTRAN data, and the one-dimensional radial flux model data for the same conditions are represented by the triangle symbol. The same trends exist in the temperature comparisons as noted for the previous stress comparisons.

The expanded radius scale allows all of the NASTRAN grid point values to be plotted. In Figures 29 and 30 several of the grid point values near r = 0 were not plotted in order to clarify the plot. Since the temperature comparisons showed similar results to the stress comparisons, the

Table I, NASTRAN Front and Back Surface Temperatures and Stresses at Selected Radii (for conditions listed in Fig. 30)

Radius (cm)	t = 1.0 sec.						t = 5.0 sec.					
	Temp.(°C)		σ_r(n/cm^2)		σ_θ (n/cm^2)		Temp.(°C)		σ_r(n/cm^2)		σ_θ (n/cm^2)	
	Front	Back	Front	Back	Front	Back	Front	Back	Front	Back	Front	Back
0.	142.0	133.	-1.15×10^4	-0.998×10^4	-1.15×10^4	-0.998×10^4	296.8	287.2	-2.32×10^4	-2.15×10^4	-2.32×10^4	-2.15×10^4
2.2	7.40	7.51	-2.39×10^3	-2.34×10^3	2.88×10^3	2.85×10^3	73.1	73.1	-1.04×10^4	-1.03×10^4	7.63×10^2	7.27×10^2
9.	0	0	-2.58×10^2	-2.58×10^2	2.33×10^2	2.31×10^2	0	0	-1.05×10^3	-1.05×10^3	1.34×10^3	1.33×10^3

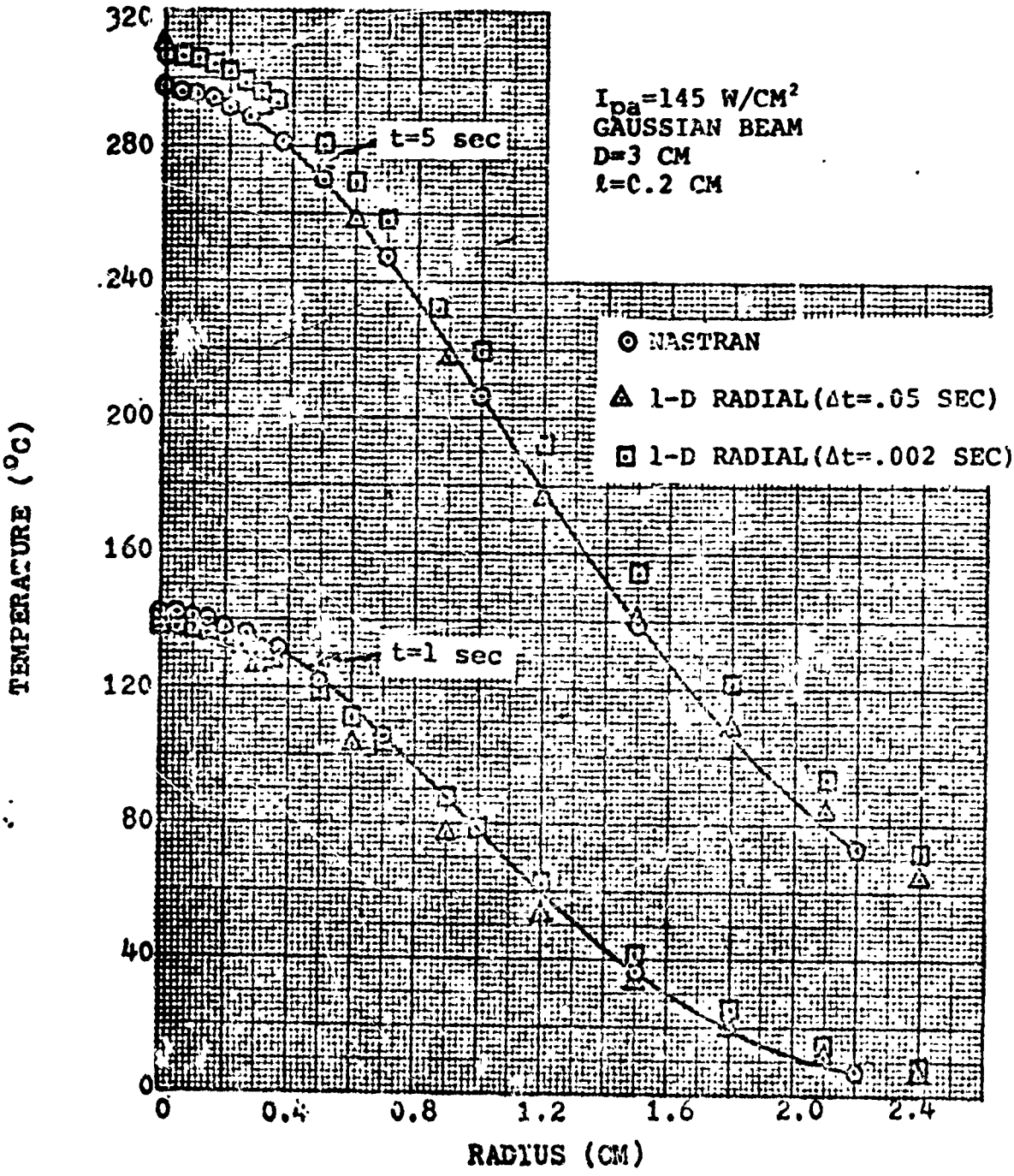

Fig. 31 Temperature Distribution Comparison

possibility that the differences noted are due to the differences in element size was investigated. As shown by the data in Fig. 31, the resolution of the NASTRAN finite element model was much finer near the beam axis (r=0) than that of the constant width element radial flux model. For the data presented thus far, the computational time increment was 0.05 sec. in both the NASTRAN analysis and the one-dimensional radial flux results. In order to reduce the element size in the one-dimensional radial model to that of the NASTRAN model under the beam, the heat conduction stability criterion of eqn (28) requires a consequent reduction in computational time increment. These combined reductions result in a very large increase in computer time cost (on the order of a factor of 20).

The element size for the one-dimensional radial model was reduced to 0.05 cm, requiring that the time increment be reduced to 0.002 sec, and the results are represented in Fig. 31 by the square symbols. Comparison with the previous radial model data in the same figure shows that the smaller element size does develop a flatter slope near r = 0. Hence, it is concluded that the apparent lack of zero slopes in the one-dimensional radial model data is due to the relatively coarse spatial resolution used to achieve a compromise with computer run time.

The trend for the one-dimensional radial model values to increase with time relative to the NASTRAN values is still evident. The one-dimensional radial model with in-

creased resolution is seen to give slightly reduced values ar r = 0 while those at the larger radii are increased especially for the longer heating time. This result is believed to be least partially attributable to plate diameter effect. The one-dimensional radial model code was developed with a one-dimensional array storage limit of 100 spaces which was judged to be a reasonable upper limit on the number of radial elements to be applied. For the analysis plotted in Fig. 31 with element widths of 0.05 cm, this limited the plate radius to 5 cm. Recalling that the NASTRAN data are for a plate radius of 15 cm, it is reasoned that the effect of the insulated (no heat losses) plate edge is being felt and causing temperatures to increase at the larger radii. If this is the case it would be expected that this effect would cause the outer radii temperatures relative to those from NASTRAN to increase with time. It would be expected that this effect would propagate to smaller radii with increasing time.

The data in Fig. 31 are consistent with the expected effects of reducing the plate/beam diameter ratio, although it is not certain whether this effect is significant enough to be causing the one-dimensional radial 5 second heating time values to exceed the NASTRAN values near r = 0.

Fig. 32 presents additional comparisons of temperature distributions for a plate thickness of 0.3 cm. In this case the heat flux vector contains a slightly larger axial component than for the 0.2 cm thick plate at corresponding heat-

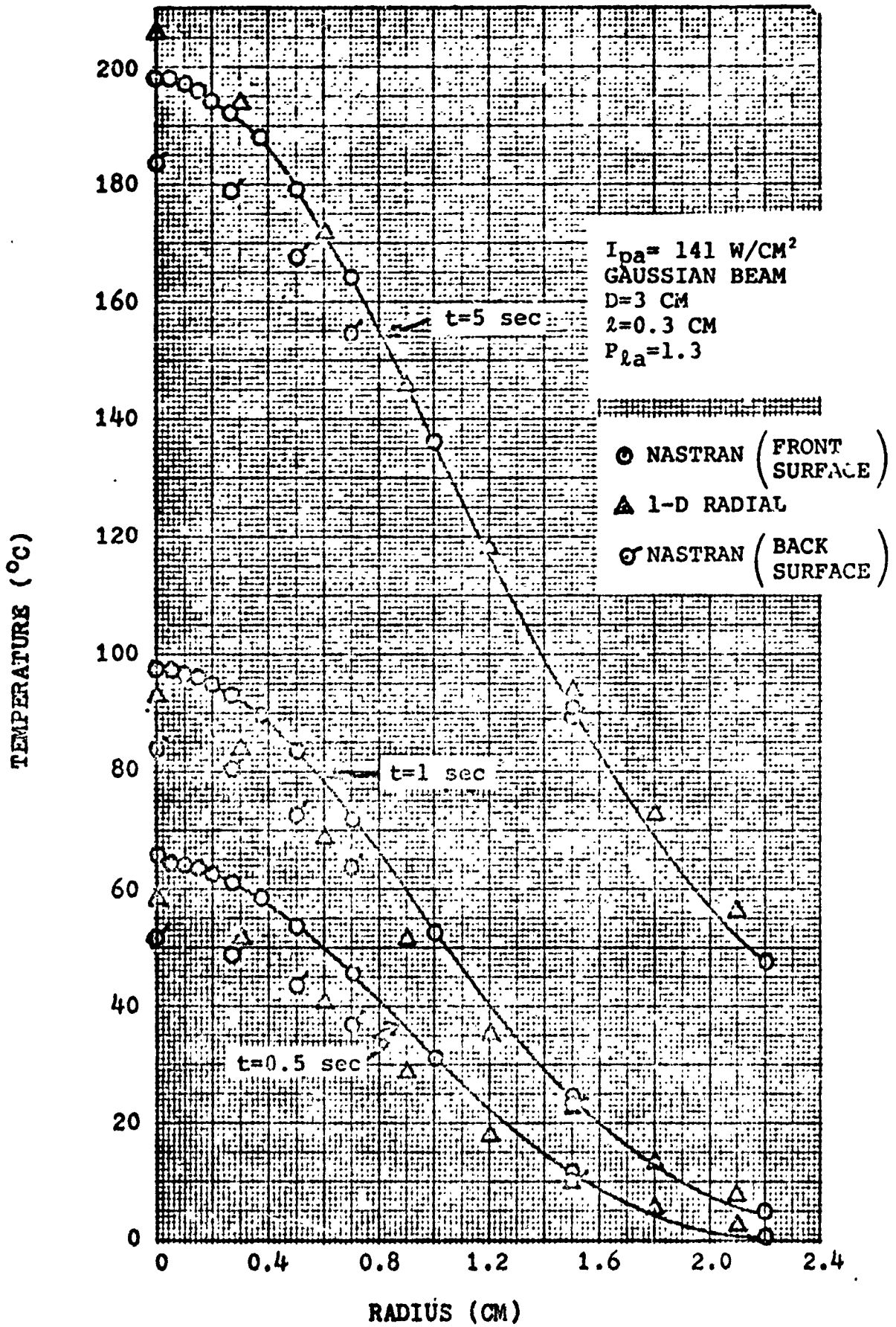

Fig. 32 Temperature Distribution Comparison, ℓ = 0.3 cm

ing times. This is indicated by the comparison of the front and back surface temperatures from the NASTRAN analysis as shown in Fig. 32.

Comparison of the NASTRAN front surface and radial flux temperatures shows the same trends as noted in Fig. 31 for the thinner plate. The effect of reducing the radial model element width from 0.3 cm to 0.05 cm also was evaluated for the thicker plate as shown in Fig. 33. Again the results are similar to those of Fig. 31 and no additional insight is provided on the possible cause of the increase with time of the radial model temperatures near r = 0 relative to those from the NASTRAN analysis.

Based on the preceding comparisons, it is concluded that the one-dimensional radial flux numerical model produces temperature distributions which are generally within 10 percent of those from the two-dimensional NASTRAN analysis. Peak compressive stresses also are in close agreement between the two analyses. Tensile stress distributions are in reasonable agreement although conclusions regarding peak tensile stresses are not definite due to inadequate resolution in the NASTRAN finite element model at the larger radii (see Fig. 30). Improved evaluation of the radial flux model could be obtained by modifying the radial flux code to increase the maximum number of elements from 100 to 300 which would eliminate the plate size effect introduced by decreasing the element width to 0.05 cm. Also the NASTRAN finite element model (Fig. 28) should have additional radial ele-

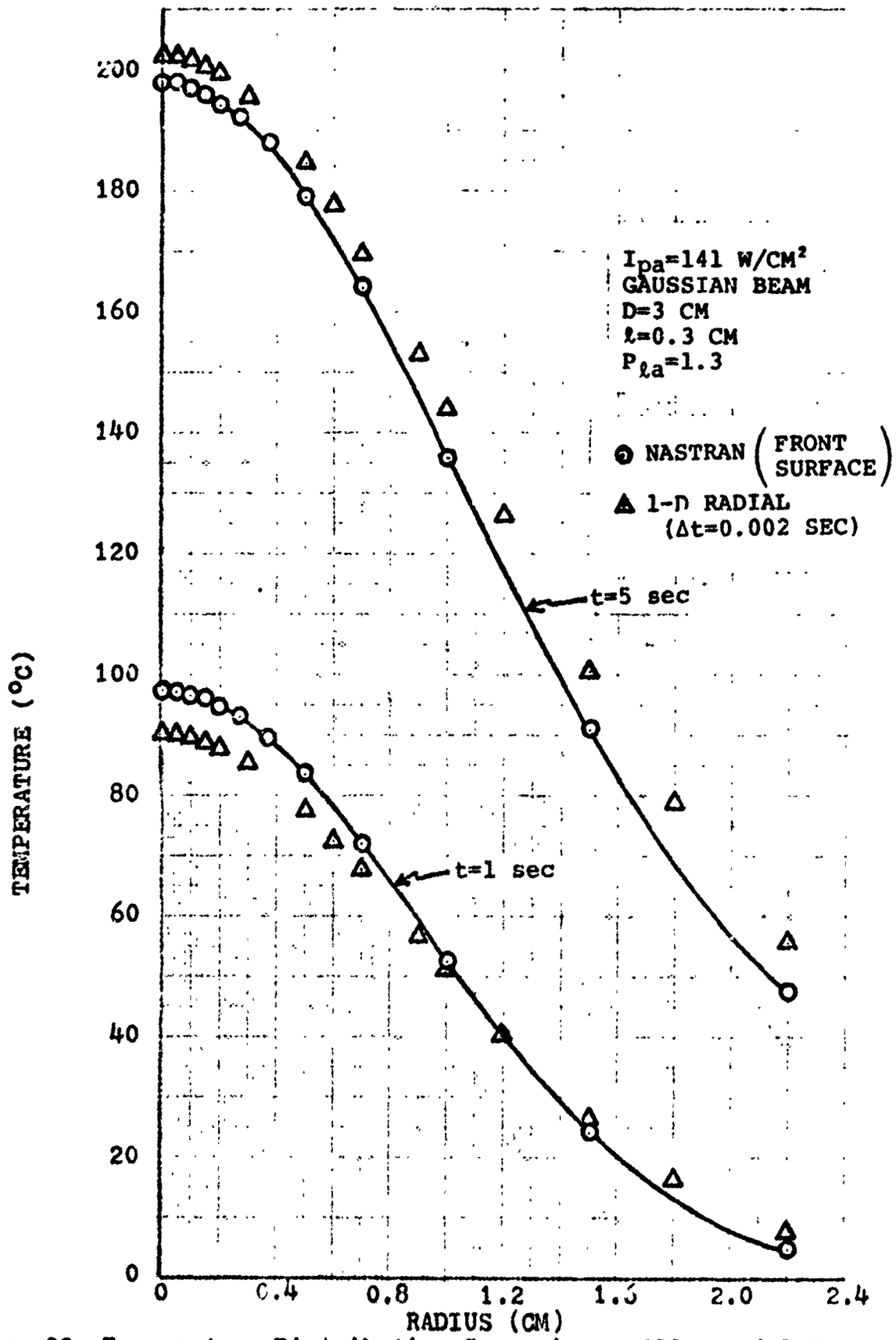

Fig. 33 Temperature Distribution Comparison; Effect of 1-D Radial Heat Flux Model Element Size

ments added to improve the resolution in the areas where peak tensile stresses occur; and NASTRAN data should be generated for longer heating times than 5 seconds to better evaluate the possible trend for the radial model temperatures to increase with time relative to the NASTRAN temperatures.

UNCLASSIFIED

SECURITY CLASSIFICATION OF THIS PAGE (When Data Entered)

REPORT DOCUMENTATION PAGE	READ INSTRUCTIONS BEFORE COMPLETING FORM
1. REPORT NUMBER: GAE/MC/75-4	2. GOVT ACCESSION NO. / 3. RECIPIENT'S CATALOG NUMBER
4. TITLE (and Subtitle): THERMAL STRESSES AS A LASER HEATING DAMAGE MECHANISM	5. TYPE OF REPORT & PERIOD COVERED: MS Thesis
	6. PERFORMING ORG. REPORT NUMBER
7. AUTHOR(s): Jan N. Garrison	8. CONTRACT OR GRANT NUMBER(s)
9. PERFORMING ORGANIZATION NAME AND ADDRESS: Air Force Institute of Technology, AFIT/ENB, Wright-Patterson AFB, Ohio 45433	10. PROGRAM ELEMENT, PROJECT, TASK AREA & WORK UNIT NUMBERS
11. CONTROLLING OFFICE NAME AND ADDRESS: (See 9. above)	12. REPORT DATE: November 1976
	13. NUMBER OF PAGES: 156
14. MONITORING AGENCY NAME & ADDRESS(if different from Controlling Office)	15. SECURITY CLASS. (of this report): Unclassified
	15a. DECLASSIFICATION/DOWNGRADING SCHEDULE

16. DISTRIBUTION STATEMENT (of this Report)

Approved for public release; distribution unlimited

17. DISTRIBUTION STATEMENT (of the abstract entered in Block 20, if different from Report)

18. SUPPLEMENTARY NOTES

Approved for public release; IAW AFR 190-17

Jerral F. Guess, Captain, USAF
Director of Information

19. KEY WORDS (Continue on reverse side if necessary and identify by block number)

Laser Heating Effects
Thermal Stresses
Numerical Model

20. ABSTRACT (Continue on reverse side if necessary and identify by block number)

The relative significance of thermal stresses as a laser heating damage mechanism is assessed by comparison with the damage mechanisms of melting and thermal degradation of structural strength properties. The limiting cases of one-dimensional axial and one-dimensional radial heat flux in a thin target plate whose plane is normal to the axis of a stationary, axially symmetric heat source, are investigated. A one-dimensional radial heat conduction numerical model of the

DD FORM 1 JAN 73 1473 EDITION OF 1 NOV 65 IS OBSOLETE

UNCLASSIFIED

SECURITY CLASSIFICATION OF THIS PAGE (When Data Entered)

linear thermoelastic stress field including the effects of melting and structural failure is developed. Residual tensile strength and damage size are presented as functions of the laser beam and target plate parameters.